INVESTIGATION OF MICRORNAS ON GENOMIC INSTABILITY REGIONS IN BREAST CANCER

ŞADAN DUYGU SELÇUKLU

NOVEMBER 2007

INVESTIGATION OF MICRORNAS ON GENOMIC INSTABILITY REGIONS IN BREAST CANCER

A THESIS SUBMITTED TO
THE GRADUATE SCHOOL OF NATURAL AND APPLIED SCIENCES
OF
MIDDLE EAST TECHNICAL UNIVERSITY

BY
ŞADAN DUYGU SELÇUKLU

IN PARTIAL FULFILLMENT OF THE REQUIREMENTS
FOR
THE DEGREE OF MASTER OF SCIENCE
IN
BIOLOGY

NOVEMBER 2007

Approval of the Thesis

INVESTIGATION OF MICRORNAS ON GENOMIC INSTABILITY REGIONS IN BREAST CANCER

Submitted by **Ş. DUYGU SELÇUKLU** in partial fulfillment of the requirements for the degree of **Master of Science in Biology Department, Middle East Technical University** by,

Prof. Dr. Canan Özgen _____
Dean, Graduate School of **Natural and Applied Sciences**

Prof. Dr. Zeki Kaya _____
Head of the Department, **Biology**

Assist. Prof. Dr. A. Elif Erson _____
Supervisor, **Biology Dept., METU**

Assoc. Prof. Dr. Cengiz Yakıcıer _____
Co-Supervisor, **Molecular Biology and Genetic Dept., Bilkent University**

Examining Committee Members

Prof. Dr. Hüseyin Avni Öktem _____
Biology Dept., METU

Prof. Dr. Gülay Özcengiz _____
Biology Dept., METU

Assist. Prof. Dr. Ayşe Elif Erson _____
Biology Dept., METU

Assoc. Prof. Dr. Cengiz Yakıcıer _____
Molecular Biology and Genetic Dept., Bilkent University

Dr. Sreeparna Banerjee _____
Biology Dept., METU

Date: 13/11/2007

I hereby declare that all information in this document has been obtained and presented in accordance with academic rules and ethical conduct. I also declare that, as required by these rules and conduct, I have fully cited and referenced all material and results that are not original to this work

Name, Last name: Ş.Duygu Selçuklu

Signature :

ABSTRACT

INVESTIGATION OF MICRORNAS ON GENOMIC INSTABILITY REGIONS IN BREAST CANCER

Selçuklu, Ş.Duygu
M.Sc., Department of Biology
Supervisor: Assist. Prof. Dr. Ayşe Elif Erson

November 2007, 119 pages

Genomic instability is commonly seen in breast cancers. To date, various chromosomal or segmental loss or amplification regions have been detected in primary tumors and cell lines. Hence, an intensive search for potent tumor suppressors or oncogenes located in these regions continues.

MicroRNAs (miRNAs) are ~18-24 nt long non-coding RNAs that regulate protein expression either by target mRNA cleavage or translational repression. We hypothesized that miRNAs located in genomic instability regions in breast cancer cells may contribute to the initiation or maintenance of breast tumors. Here, we investigated genomic levels of miRNAs on frequent loss or gain regions of breast cancer cells. First, using bioinformatics resources we mapped known miRNAs and candidate miRNAs to reported genomic instability regions. Our extensive searches resulted with more than 30 known miRNAs and 35 candidate

miRNAs. To further confirm loss or amplification of miRNA genes on these chromosomal regions in breast cancer cells, we designed specific primers for the known pre-miRNA DNA regions and performed semi-quantitative PCR in 20 breast cancer cell lines, 2 immortalized mammary cell lines, and 2 control samples. Densitometry results suggested that a striking 61 % (22/36) of selected miRNAs showed either loss or amplification in at least 3 different breast cancer cell lines. Interestingly most of these alterations were found to be amplifications even in regions reported to harbor losses in breast tumors. Genomic fold change results of these microRNAs provide a biologically relevant starting point for further expression and functional experiments of microRNAs in breast cancer studies. Genomic fold change analysis followed expression analysis of two significant microRNAs (hsa-miR-21 and hsa-miR-383) was done by qRT-PCR method.

Our data provide a wide screen of genomic instability of 36 microRNA genes in 20 breast cancer cells and normal samples detected by semi-quantitative duplex PCR method as well as expression analysis of two microRNAs. To this date, such an extensive data on genomic status of microRNA genes in breast cancer cells did not exist. Therefore, our results are the first comprehensive investigation of many microRNA genes on genomic instability regions in breast cancers and provide further clues to the potential involvement of these microRNAs in breast tumorigenesis MicroRNA genomic instability may affect their expression and therefore their targets' expressions. Understanding how these microRNAs regulate their targets and contribute to the neoplastic events will also contribute to the field by using this information for future diagnostic and threaupetical applications.

Key words: Breast cancer, genomic instability, microRNAs

ÖZ

MEME KANSERİNDE GENOMİK İNSTABİLİTE BÖLGELERİNDEKİ "MİKRO-RNA"LARIN ARAŞTIRILMASI

Selçuklu, Ş.Duygu
Yüksek Lisans, Biyoloji Bölümü
Tez yöneticisi: Yrd. Doç. Dr. Ayşe Elif Erson

Kasım 2007, 119 sayfa

Genomik instabilite meme kanserinde sıklıkla görülür. Bugüne kadar primer tümörlerde ve kanser hücre hatlarında bir çok kromozomal veya bölgesel kopya sayısı değişikliği gösteren bölge belirlenmiştir. Bu sebeple, bu bölgelerdeki potansiyel tumor baskılayıcı genler veya onkogenler araştırılmaktadır.

MikroRNAlar ~18-24 nt uzunluğunda protein kodlamayan RNAlardır. Protein ekspresyonunu hedef mRNAlarin kesilmesi veya translasyonun engellenmesi ile düzenlerler. Bu çalışmanın hipotezi, meme kanseri hücrelerindeki sıklıkla görülen genomik instabilite bölgelerinde bulunan mikroRNAların tümörigenez mekanizmasındaki etki edebilecekleri veya katkıda bulunabilecekleridir. Bu çalışmada, meme kanserinde sıklıkla görülen kopya sayısı değişikliği gösteren bölgelerde bulunan mikroRNA genlerinin genomik düzensizlikleri araştırılmıştır. İlk olarak, biyoinformatik kaynaklar kullanılarak bugüne kadar belirlenmiş, sıklıkla görülen genomik instabilite bölgelerinden 18

tane seçildi ve bu bölgelerde bulunan 30 dan fazla ve 35 aday mikroRNA genleri belirlendi. Belirlenen mikroRNA genlerindeki kopya sayısı değişikliklerini doğrulamak için öncül mikroRNA'lara spesifik primerler dizayn edildi ve "yarı-nicel PCR" yöntemi ile 20 meme kanseri hücre hattı DNAsında, 2 ölümsüz hücre hattı DNAsında ve 2 normal kontrol DNA örneğinde kopya sayısı analizleri yapıldı. Densitometre ölçüm sonuçlarına göre dikkat çekici bir şekilde mikroRNAların % 61 'inde (22/36) en az 3 farklı hücre hattında kopya sayısı değişikliği (delesyon veya amplifikasyon) gösterdiği bulundu. İlginç olarak bu değişikliklerin çoğu literatürde delesyon olarak geçen bazı bölgelerdeki mikroRNAların amplifikasyonu olarak bulundu. Belirlenen kopya sayıları, biyolojik olarak anlamlı bir başlangıç noktası olarak kullanılabilir ve meme kanserinde mikroRNA ekspresyon düzeyi ve fonksiyonel çalışmalar açısından adayların seçilmesinde önemlidir Kopya sayısı analizlerini takiben seçilen iki mikroRNA geninin (hsa-miR-21 ve hsa-miR-383) qRT-PCR yöntemi ile ekspresyon analizi yapıldı.

Bu çalışmanın sonuçları, 20 meme kanseri hücre hattında ve normal örneklerde 36 mikroRNA geninin yarı-nicel PCR yöntemi ile genomik instabilite düzeylerinin kapsamlı taramasını sunmaktadır. Bugüne kadar meme kanseri hücre hatları ile bu kadar geniş çaplı bir tarama yapılmamıştır ve sunduğumuz sonuçlar bir çok mikroRNAnın meme kanserinde kapsamlı araştırılmasını içermektedir ve meme kanseri mekanizmasında potansiyel olarak rolü olabilecek adayların belirlenmesi açısından önemli ipuçları sunmaktadır. MikroRNAların genomik instabilitesi ekspresyon düzeylerine etki edebilir, bu da hedef genlerin ekspresyonunu etkileyecektir. MikroRNAların bu genleri nasil düzenlediklerinin belirlenmesi tümörigenez mekanizmasına katkıda bulunacak, teşhis ve tedavi amaçlı uygulamalarda bu bilgiler kullanılabilecektir.

Anahtar kelimeler: meme kanseri, genomik instabilite, mikroRNA

To my Family

ACKNOWLEDGEMENTS

I am most grateful to my Supervisor Assist.Prof.Dr.Elif Erson for her endless support and encouragements throughout this study. It's impossible to express my feelings about how lucky I am to be a part of her team. I am deeply thankful to her for changing my direction to be a good scientist, without her I would lost my way.

I am sincerely thankful to my Co-supervisor Assist.Prof.Dr.Cengiz Yakıcıer from Bilkent Universtiy for sharing his invaluable ideas and wisdom leading me to work on microRNAs. I would like to thank all staff in department of Molecular biology and Genetics in Bilkent University for letting me to complete a part of my experiments.

I would like to thank all my jury members; Prof. Dr. Gülay Özcengiz, Prof. Dr. Hüseyin Avni Öktem and Dr. Sreeparna Banerjee for their invaluable comments and advices and contributions to my thesis.

I would like to express my grateful thanks to my lab buddy Serkan Tuna for his great contribution to PCR experiments and densitometry analyses and his hard work. Besides these, I am thankful to him for his friendship, patience and motivation. I'm glad to work with him in the same project.

Many thanks to my dear lab mates Begüm Akman, Shiva Akhavan, Aysegul Sapmaz for their invaluable helps all the time and sharing all those tough and fun times, and my other lab mates Kevser Gençalp, Aycan Apak, Rukiye Yüce, Ferhunde Ayşin and Murat Kavruk for their friendship. It's impossible to find this kind of team anywhere else.

I would like to thank Biochemistry department staff, University College Cork, Ireland for providing me the cancer cell lines. Also, I would like to thank Prof. E.Petty, University of Michigan, US fro providing breast cancer cell line DNAs.

I would like to express my special thanks to Dr. Charles Spillane for welcoming me to his laboratory in University College Cork, Ireland as an exchange student to complete a part of my experiments. He treated me as a part of his team and I'm grateful to him for his advices and encouragements for this study and for my future academic life. I'd like to express my deepest thanks to Katherine Schouest for her support during my experiments and contributions to my thesis. Also I'd like to thank Prasad Kovvuru, Rachel Clifton and Grace Martin in Spillane lab for their valuable helps during my research in University College Cork.

I would like to thank my best friends Özge Aydın and Umut Özbek for their true friendship forever and being a part of my best years.

I would like to express my deepest gratitude to a special person in my life, Mert Ayaroğlu, for sharing my tears and joy, his endless patience and helping me for overcoming all kinds of challenges.

Finally I would like to thank my dear parents, my father, Soner Selçuklu and my mother, Hanife Selçuklu for being inspiration throughout my life. They always supported my dreams and aspirations. They thought me never ever giving up. I'm grateful to them for believing in me

This work was supported by METU BAP-2006-07-02-0001 and TUBA_GEBIP.

TABLE OF CONTENTS

LIST OF TABLES

LIST OF FIGURES

LIST OF ABBREVIATIONS

BLAST	Basic Local Alignment Search Tool
bp	Base Pairs
cDNA	Complementary Deoxyribonucleic Acid
CGH	Comparative Genomic Hybridization
Ct	Cycle Threshold
DEPC	Diethyl Pyrocarbonate
DMEM	Dulbecco's minimum Essential Medium
DMSO	Dimethyl Sulfoxide
DNA	Deoxyribonucleic Acid
DNase I	Deoxyribonuclease I
Dntp	Deoxyribonucleotide Triphosphate
DTT	Dithiothreitol
EDTA	Ethylenediaminetetraacetic Acid
FASTA	Fast Aye
FISH	Fluorescence *in situ* Hybridization
g	Centrifuge gravity force
GAPDH	Glyceraldehyde 3-Phosphate Dehydrogenase
HD	Homozygous Deletion
NCBI	National Center for Biotechnology Information
LOH	Loss of Heterozygosity
miRNA	microRNA
mRNA	Messenger RNA
PCR	Polymerase Chain Reaction
PBS	Phosphate Buffered Saline
Pri-miRNA	Primary microRNA

Pre-miRNA	Precursor microRNA
RISC	RNA-induced Silencing Complex
RNA	Ribonucleic Acid
RNase	Ribonuclease
RNU6B	Small Nuclear U6B
rpm	Revolution Per Minute
RT-PCR	Reverse Transcription Polymerase Chain Reaction
siRNA	Small Interfering RNA
SKY	Spectral Karyotyping
SNP	Single Nucleotide Polymorphism
stRNA	Small Temporal RNA
Taq	*Thermus aquaticus*
TBE	Tris-Boric acid-EDTA
UCSC	University of California, Santa Cruz
UTR	Untranslated Region

CHAPTER 1

INTRODUCTION

1.1 Cancer and Genetic Alterations

Cancer remains as one of the leading causes of death worldwide. Several studies predict that by 2020, the number of cancer cases will increase to more than 15 million, with cancer-related deaths increasing to 12 million world-wide [2]. Cancer is a complex genetic disorder, and cancer cells usually harbor various genetic alterations and demonstrate uncontrolled cell proliferation [3], [4], [5]. Continuous cell proliferation leads to further accumulation of mutations in important genes such as *PTEN*, *RAS,* or *TP53* which may also predispose cells to neoplastic transformation [6], [7].

According to some studies, not all but most cancers have common six "acquired capabilities": (a) ability to grow in the absence of stimulatory signals, (b) avoiding apoptosis, (c) resistance to anti-growth signals, (d) ability to invade other tissues, (e) angiogenesis, and (f) continuous replication potential as summarized in Figure 1.1. For example, loss of function of tumor suppressor genes such as TP53 allows genomic instability to generate selectively advantageous cells and enables them to continue to acquire other capabilities [8].

In terms of genetic content, most epithelial human cancers show complex karyotypes with high genomic instability [9] with chromosomal losses, gains, or translocations [10]. Genomic instability is a chromosomal state that the cell gains or loses whole chromosomes or specific regions of chromosomes. Genomic

instability may also increase the risk of new mutations or it may manifest itself due to mutations in certain genes. Therefore, it's still not clear that if genomic instability is a cause or consequence of cancer [11], [12].

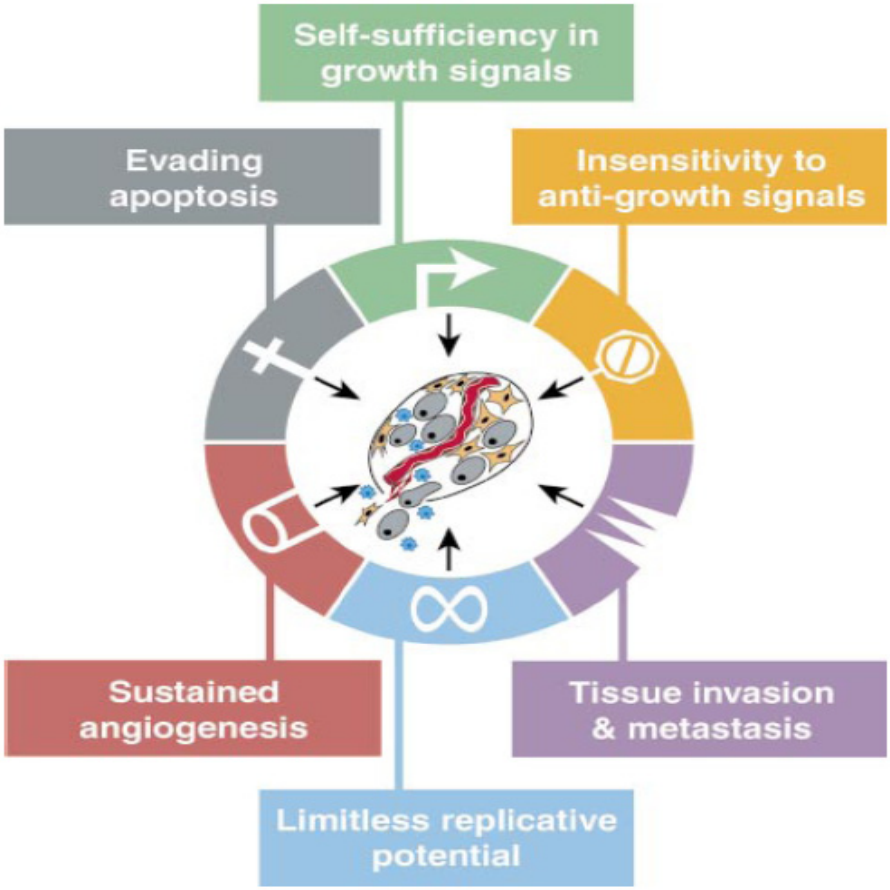

Figure 1.1: Features of cancerous state.
(Figure taken from Hanahan *et al*, 2000).

Translocations, changes in gene copy numbers such as deletions or amplifications, may cause inactivation of tumor suppressors or activation of oncogenes, respectively which may contribute to cancer progression [11], [13], [14].

Loss of heterozygosity (LOH) and homozygous deletions (HD) may indicate the presence of tumor suppressor genes on a specific chromosomal band [15]. Although LOH and HD are frequent alterations in cancers such as lung cancer, only a few tumor suppressor genes have been identified: *TP53*, *RB*, *p16*, *PTEN*, and *FHIT* [13], [14]. Identification of homozygous deletions is a good way to start searching for novel tumor suppressor genes [13] as the candidate gene is lost and, thus, functionally inactive unlike LOH regions. In a microarray study of homozygous deletions in human cancer genomes, 281 homozygous deletions were identified in 636 cancer cell lines including deletions of some known tumor suppressor genes and fragile sites but some were "unexplained" regions which many of them were found to be in intergenic DNA regions [16]. Similarly, amplification regions may indicate the regions harboring oncogenes as some amplification regions were shown to harbor oncogenes such as *MYC* and *ERBB2* [14].

1.2 Common Genomic Instability Regions in Breast Cancer

Breast cancer is the most common cancer type among women in the developing world. It is the leading cause of cancer mortality in women with 411,000 annual deaths representing 14% of female cancer deaths worldwide [17].

Comparative genomic hybridization (CGH) studies on many chromosomal regions in breast cancer cells show genomic instability regions such as HD or LOH in 3p21, 5q33, 8p21, 11q, and 13q and amplifications in 8p23, 11q, and 17q [14]. Among these, 3p deletions (LUCA and AP20 regions) have been identified in 80% of breast carcinomas as well as small-cell lung carcinoma, renal carcinoma, cervix, kidney, and head and neck carcinomas [18], [19]. For instance, 3p21.3 has been identified as a frequent homozygous deletion region in lung and breast cancers [18], [20]. This region is known to harbor some candidate tumor

suppressor genes such as *PL6*, *NPRL2*, *101F6,* and *FUS1* [21]. Another region, 8p, has been shown to be one of the most common allelic loss regions in many human cancers including breast (and bladder, prostate, non-small cell lung, larnygeal, hepatocellular, medulloblastoma, pancreatic, biliary and colorectal carcinomas) [22], [23], [24]. On the contrary, a segmental region of 8p11-12 was shown to be amplified in breast cancer cell lines harboring *FGFR1* as a candidate oncogene [25]. Another frequent deletion region, 11q23-24, in breast, ovarian and lung cancers has been shown to harbor a candidate tumor suppressor gene (BCSC-1) [26].

Cancer cell lines are good sources to model tumor genomes for identification of cancer related genes as it is not easy to work with tumor samples, grow or treat them with chemicals. Cell lines provide useful data on DNA copy number changes for meaningful biological interpretation of neoplastic events. Cancer cell lines show complex karyotypes such as a common model breast cancer cell line MCF7 (See Figure 1.2). It is described as having multiple rearrangements, almost a "triploid cell line", and translocations were found in almost all chromosomes, except chromosome 4, and deletions were detected on chromosomes 3 and 13 [27]. Another model breast cancer cell line, T47D, shows translocations in chromosomes 1, 3, 4, 5, 6, 7, 8, 9, 10, 12, 13, 14, 15, 16, 17, 20 and X and deletions in chromosomes 3, 10, 11, 12 and 18 [27], karyotype is shown in Figure.1.3.

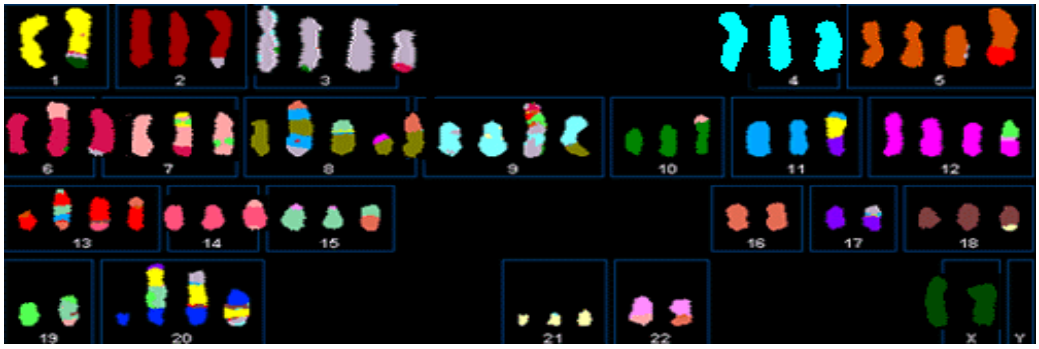

Figure 1.2: MCF7 SKY (Spectral Karyotyping) karyotype
(Figure taken from Davidson *et al*, 2000, http://www.path.cam.ac.uk/)

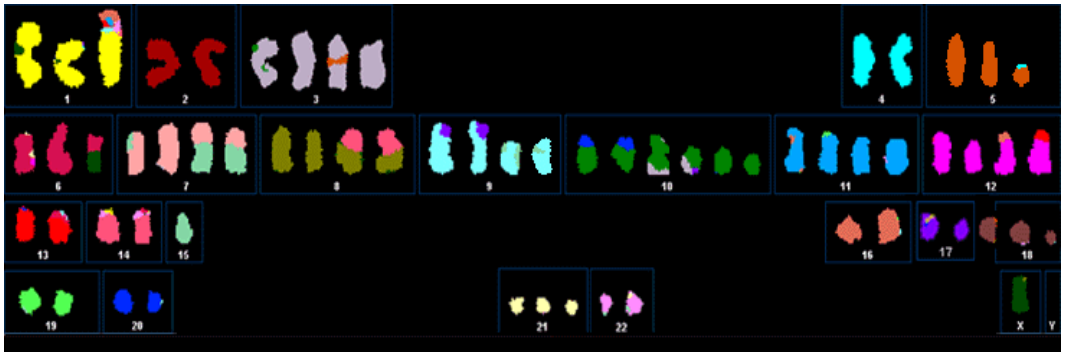

Figure 1.3: T47D SKY karyotype
(Figure taken from Davidson *et al*, 2000, http://www.path.cam.ac.uk/)

Array comparative genomic hybridization (CGH) studies on genomic alterations in breast cancer cell lines show many genomic alterations revealing potential oncogenes and tumor suppressors. For example, the MCF7 cell line shows common losses in 8p, 11q14-pter, 13q21-qter, X, 1p13, 8p14, 17q23, and 20q13 and gains in 11q13, 17q21-qter, 20q, 3q13, 8p, 11q23, 11q14, and 13q14. A detailed summary of these regions is listed in Figure 1.4 and Figure 1.5. [5], [10], [28].

Cell line	Losses	Gains[a]
BT-474	1p10–p31, p10–p14, 5q10–q23, 6q23–qter, 8p, 9p, 21q10–q21, Xq	1q22–q25, 1q42–qter, 3q13.3–qter, 5p, 7pter–q22, 7q33–qter, 8q21–qter, 9q33–qter, 10q25-qter, 11q13-q14, 12q, 14q10–q21, 15q10–q21, 17q (**17q10–q23**), 18p, 19, **20q**, Xp
BT-549	2, 10q25–qter, 11p, Xp	1p31–pter, 8, 9p, 9q34, 11q13, 17p, 20q
CAMA-1	1p22–p32, 6q, 8p21–pter, 11q14–qter, 12p, X	1p21–qter, 5q31–qter, 6p, 7q32–qter, 8q, 9q, 16, 17q21, 17q24–qter, 22q10–q12.1
DU4475	5q14–q23, 6q10–q22, 11q23–qter, 18	1q, 7, 10pter–q22
MCF7	1p21–p22, 4p15–qter, 8p, 9p21–pter, 11p, 11q14–qter, 13q21–qter, 18q12–qter, X	1q, 3p13–p14, 7q21–q31, 8q21–qter, 9q22–qter, 11q13, 12q24–qter, 14q, 15q23–qter, **17q21–qter**, 19, 20q (**20q12–qter**)
MDA-MB-134	2q, 8p22–pter, 11q21–qter, 13q, 16q, 17p, 18p	8p12–qter (**8p10–p12**), **11q13**, 11p14–pter
MDA-MB-157	3p10–p21, 8p21–pter, 12p, 13q10–q22, 18q	1p32–pter, 1q32–qter, 2p, 2q31–qter, 3p22–pter, 5p, 5q31–qter, 6p, 7, 8q, 9q, 10p12–pter, 11q13, 13q31–qter, 14q32–qter, 17, 18p, 19, 20, 21q22–qter, X
MDA-MB-361	8p21–pter, 9p21–pter, 11p, 11q21–q22, 21q10–q21, Xq	1q32–qter, 5p, 6p, 8p21–qter, 9q32–qter, 10q23–qter, 12, 15q23–qter, 16, 17q, 20q
MDA-MB-436	1p13–p21, 2q22–q24, 3q24–q27, 4q21–q28, 4q32–q34, 5q14–q23, 6p12–q14, 8p10–p12, 8q21–q22, 9p13–p21, 11q22–q23, 12q10–q23, 13q13–q31, 14q13–q24, 18p, 18q21–qr, 20p10–p12	1p31–pter, 1q, 2p23–pter, 2p13–q21, 3p24–pter, 4p15–pter, 5p, 5q31–qter, 6q2–3qter, 7, 8p21–pter, 8q23–qter, 9q, 11q10q13, 12p12–pter, 13q32–qter, 15q10–q24, 16p, 17p12–pter, 19p13–pter, 19q13.3–qter, 20q13.1–qter
MPE600	9q, 11q14–qter, 16q	**1q**, 11q13, 13q10–q14, 13q32–qter, 16p, 17q, 20q12–qter
SK-BR-3	2q22–q34, 3p12–q13, 4p, 4q26–qter, 5pter–q23, 6q10–q22, 10q24, 18, Xq	1p31–pter, 1q10–q42, 3p21–pter, 3q26–qter, 5q31–qter, 6p21–pter, 7, **8q12–qter** 9q32–qter, 10q22, 11q13, 12q23–qter, 13q32–qter, 14q24–qter, 16p, 17q10–q21, 17q23–qter, 19q, 20 (**20q12–qter**), 22q12–qter
T-47D	1p10–p31, 2q22–q33, 3p10–p13, 4p15.1–qter, 6q10–q22, 7q31, 9p, 13q, 18q, X	1p31–pter, 1q, 3p21–pter, 3q13.3–qter, 5q31–qter, 6p, 7pter–q21, 8q23–qter, 9q22–qter, 11p13–qter, 12q, 14q12–q21, 15q21–qter, 16p, 16q22–qter, 17q, 19p13.1–pter, 20q, 22q
UACC-812		1q21–q41, 7pter–q21, 8q, 12q, 13q21–q33, 17q, 20q, 21q22
UACC-893	2q34–qter, 3p, 4pter–q24, 5q, 8p, 10q23–qter, 11p14–pter, 11q23–qter, 13q14–q31, 17p, 18q10–q21, 20p, Xp	1p32–pter, 1q, 2p16–pter, 6p, 6q25–qter, 7p, 8q, 10pter–q22, **11q13–q14**, 14q10–q21, 15q24–qr, 17q, 20q
ZR-75-1	1p21–p31, 2, 6pter–q22, 11q14–qter, 20p, 21q, X	1q (**1q25–qter**), 4q31–qter, 7p, 8p21–q21, 11q13, 12pter–q15, 15q10–q24, 16 (**16p**) 17q21–qter, 18, 20q, 22q10–q13.1

Figure 1.4: Genomic instability regions in breast cancer cell lines [10].
(Figure taken from Kytola *et al*, 2000).

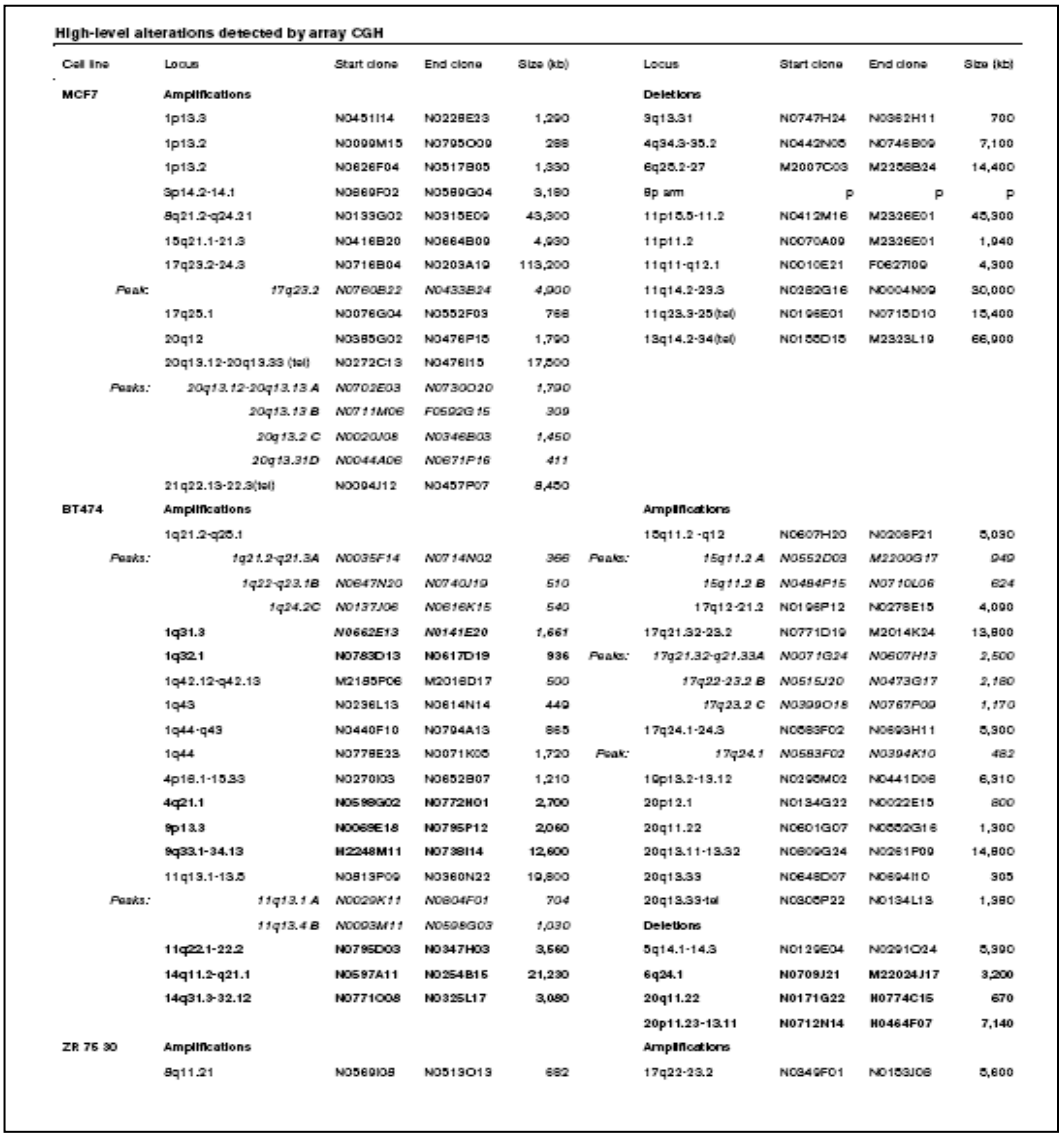

High-level alterations detected by array CGH

Cell line	Locus	Start clone	End clone	Size (kb)		Locus	Start clone	End clone	Size (kb)
MCF7	**Amplifications**					**Deletions**			
	1p13.3	N0451I14	N0228E23	1,290		3q13.31	N0747H24	N0362H11	700
	1p13.2	N0099M15	N0795O09	288		4q34.3-35.2	N0442N05	N0746B09	7,100
	1p13.2	N0626F04	N0517B05	1,330		6q25.2-27	M2007C03	M2256B24	14,400
	3p14.2-14.1	N0869F02	N0589G04	3,180		8p arm	p	p	p
	8q21.2-q24.21	N0133G02	N0315E09	43,300		11p15.5-11.2	N0412M16	M2326E01	45,300
	15q21.1-21.3	N0416B20	N0664B09	4,930		11p11.2	N0070A09	M2326E01	1,940
	17q23.2-24.3	N0716B04	N0203A19	113,200		11q11-q12.1	N0010E21	F0627I09	4,300
	Peak: 17q23.2	*N0760B22*	*N0433B24*	*4,900*		11q14.2-23.3	N0282G16	N0004N09	30,000
	17q25.1	N0076G04	N0552F03	768		11q23.3-25(tel)	N0196E01	N0715D10	15,400
	20q12	N0385G02	N0476P15	1,790		13q14.2-34(tel)	N0155D15	M2323L19	66,900
	20q13.12-20q13.33 (tel)	N0272C13	N0476I15	17,500					
	Peaks: 20q13.12-20q13.13 A	*N0702E03*	*N0730O20*	*1,790*					
	20q13.13 B	*N0711M06*	*F0592G15*	*309*					
	20q13.2 C	*N0020J08*	*N0346B03*	*1,450*					
	20q13.31D	*N0044A06*	*N0671P16*	*411*					
	21q22.13-22.3(tel)	N0094J12	N0457P07	8,450					
BT474	**Amplifications**					**Amplifications**			
	1q21.2-q25.1					15q11.2 -q12	N0607H20	N0208P21	5,090
	Peaks: 1q21.2-q21.3A	*N0035F14*	*N0714N02*	*366*	*Peaks:*	*15q11.2 A*	*N0552D03*	*M2200G17*	*949*
	1q22-q23.1B	*N0647N20*	*N0740J19*	*510*		*15q11.2 B*	*N0484P15*	*N0710L06*	*624*
	1q24.2C	*N0137J06*	*N0616K15*	*540*		17q12-21.2	N0196P12	N0278E15	4,090
	1q31.3	*N0662E13*	*N0141E20*	*1,661*		17q21.32-23.2	N0771D19	M2014K24	13,800
	1q32.1	**N0783D13**	**N0617D19**	**936**	*Peaks:*	*17q21.32-q21.33A*	*N0071G24*	*N0607H13*	*2,500*
	1q42.12-q42.13	M2185P06	M2016D17	500		*17q22-23.2 B*	*N0515J20*	*N0473G17*	*2,180*
	1q43	N0236L13	N0614N14	449		*17q23.2 C*	*N0399O15*	*N0767P09*	*1,170*
	1q44-q43	N0440F10	N0794A13	865		17q24.1-24.3	N0583F02	N0693H11	5,300
	1q44	N0778E23	N0071K05	1,720	*Peak:*	*17q24.1*	*N0583F02*	*N0394K10*	*482*
	4p16.1-15.33	N0270I03	N0652B07	1,210		19p13.2-13.12	N0295M02	N0441D08	6,310
	4q21.1	**N0589G02**	**N0772H01**	**2,700**		20p12.1	N0134G22	N0022E15	800
	8p13.3	**N0068E18**	**N0795P12**	**2,060**		20q11.22	N0601G07	N0552G16	1,300
	9q33.1-34.13	**M2248M11**	**N0738I14**	**12,600**		20q13.11-13.32	N0609G24	N0261P09	14,800
	11q13.1-13.5	N0813P09	N0360N22	19,800		20q13.33	N0648D07	N0694I10	905
	Peaks: 11q13.1 A	*N0029K11*	*N0804F01*	*704*		20q13.33-tel	N0305P22	N0134L13	1,380
	11q13.4 B	*N0093M11*	*N0598G03*	*1,030*		**Deletions**			
	11q22.1-22.2	**N0795D03**	**N0347H03**	**3,560**		5q14.1-14.3	N0129E04	N0291O24	5,390
	14q11.2-q21.1	**N0597A11**	**N0254B15**	**21,230**		**6q24.1**	**N0709J21**	**M2204J17**	**3,200**
	14q31.3-32.12	**N0771O08**	**N0325L17**	**3,080**		**20q11.22**	**N0171G22**	**N0774C15**	**670**
						20p11.23-13.11	**N0712N14**	**N0464F07**	**7,140**
ZR 75 30	**Amplifications**					**Amplifications**			
	8q11.21	N0569I08	N0513O13	682		17q22-23.2	N0849F01	N0153J06	5,600

Figure 1.5: Genomic instability regions and calculated copy numbers in breast cancer cell lines by CGH [28]. (Figure taken from Shadeo *et al*, 2006)

In a microarray study of copy number changes in breast cancer cell lines several regions were found to be amplified (Xq21.1, 19p13.3) or homozygously deleted (13q31.3, 11q14.1, 20q13.2, listed in Figure 1.6 [29].

Amplification regions

Cell line or tumor	Size range[b] (Mb)	Cytoband[c]	Candidate gene[d]	Inferred copy number[e]	Measured copy number[f]
H1395	0.06–0.47	8q24.12	*NOV*	9	43.23
H1395	0–0.73	8q24.21	*MYC*	7	37.45
H1395	0–0.62	20q11.23-q13.11		9	60.63
H2171	1.72–2.63	8q12.1-q12.3		9	33.80
H2171	1.08–2.08	8q24.13-q24.21	*MYC*	12	43.57
H2171	1.67–2.11	11q14.1-q14.2		7	14.52
H2171	1.86–3.21	12p11.23-p11.22		9	23.14
HCC1143	0.46–6.3	11q13.1-11q13.4	*CCND1*	7	25.44
HCC1143	1.98–3	12q14.3-q15	*DYRK2*	9	10.05
HCC1599	4.5–5.76	19q12-q13.12	*CCNE1*	7	13.48
HCC2218	0.13–0.99	17q11.2		11	32.90
HCC2218	1.69–2.82	17q25.1		9	22.97
BT-474	2.07–4.64	17q12-q21.2	*ERBB2*	9	35.27
BT-474	2.74–5.12	20q13.2-q13.31	*BCAS1*	14	36.91
UACC-812	1.88–4.7	13q14.2-q14.3		7	5.15
UACC-812	7.29–8.59	13q21.31-q21.33		7	14.86
UACC-812	3.33–4.1	13q22.2-q31.1		7	8.64
UACC-812	2.73–3.24	13q31.3		10	21.97
MCF7	2.84–3.74	3p14.2-p14.1		9	23.90
MCF7	0.78–2.46	20q13.2-20q13.31	*BCAS1*	13	35.89
10372 (tumor)	5.91–6.21	12q12-q13.11		7	9.85

Homozygous deletion regions

Cell line or tumor	Size range[b] (Mb)	Cytoband[c]	Candidate gene[d]	Inferred copy number[e]	Measured copy number[f]
NCI-H1648	0.21–0.5	3p14.2	*FHIT*	0	0.00012
NCI-H1648	0.39–0.68	9p21.3	*P16*	0	0.00021
NCI-H1648	1.88–4.5	Xq21.31-Xq21.33		0	0.00090
NCI-H2141	0.26–0.83	10p12.1		0	0.015
HCC1187	0.05–1.01	14q23.2		0	0.0069
HCC1599	4.06–4.16	4q35.1-q35.2		0	0.00028
HCC1937	0.76–2.04	10q21.3		0	0.0012
HCC38	2.48–5.86	3p12.3-p12.2		0	0.00019
HCC38	10.05–10.72	9p21.3-p21.1	*P16*	0	0.00063
HCC1395	0.43–2.03	6q16.1		0	0.00033
HCC1395	2.88–4.43	6q16.3-q21		0	0.000081
HCC1395	0.12–1.6	11p13-p12		0	0.000083
HCC1395	7.99–10.37	13q14.3-q21.2		0	0.0013
HCC1395	0.74–2.53	Xq21.1-q21.2		0	0.000083
MCF7	0.22–0.4	3q13.31		0	0.12
10372	0.84–1.01	1p13.1-p12		0	2.31
10372	1.83–6.04	19p13.3		0	1.21

Figure 1.6: Amplification and Homozygous deletion regions in breast cancer cell lines by SNP Microarrays.
(Figure taken from Zhao *et al*, 2004)

1.3 MicroRNAs

MicroRNAs (miRNAs) were first discovered in 1993 by Victor Ambros and his colleagues while studying developmental timing in *Caenorhabditis elegans.* They found that a gene, *lin-4,* which doesn't code for a protein but a small RNA that controls timing of *C. elegans* larval development [30], [31]. This small RNA is complementary to the 3'UTR region of *lin-14* messenger RNA (mRNA) which is a developmental repressor of LIN-14 protein; *lin-4* binds to *lin-14* mRNA and represses translation [31]. *Lin-4* is known to be the first microRNA discovered and *let-7*, the second identified microRNA, was later found to act as *lin-4* in the same way by binding to the 3' UTR complementary regions of genes such as *lin-14*. They were first named as small temporal RNAs (stRNAs) [32] because of their role in development. However, other labs soon discovered many small RNAs that are not developmentally regulated but specific in certain cell types in *Drosophila*, human, and *C. elegans* and then they were named as microRNAs [33].

By 2007, more than 400 microRNAs have been identified in eukaryotes [34], [35] and more than 2000 miRNAs in vertebrates, flies, nematodes, plants, and viruses [36]. The predicted number of microRNAs is about 1-5% of the genes in genome, based on computational prediction programs. Many miRNAs have been cloned from *C.elegans*, *Arabidopsis*, *Drosophila*, mice, and humans. They are highly conserved and they were also found in fungi and in pathogenic viruses [31], [37], [38], [39].

1.3.1 MicroRNA Biogenesis and Function

MicroRNAs are usually transcribed as capped and polyadenylated full length primary transcripts transcribed by RNA polymerase III (pol III) [40], [37]. Some findings also predict that some microRNAs are transcribed by pol II [41],

[40]. These primary transcripts (pri-miRNA) undergo maturation process (see Figure 1.7) into precursor hairpins (stem-loop miRNAs or pre-miRNAs) approximately 60-80 bp with a 3' 2nt overhang by excision by RNase III enzyme Drosha. They are then transferred to cytoplasm by Exportin 5 and a second RNase III enzyme, Dicer, recognizes and cuts pre-miRNA into a ~20-22 bp RNA duplex. This duplex contains mature microRNA in one strand which is the active form designated with organism such as "hsa" for *Homo sapiens* , "miR", and a number for each microRNA (i.e., hsa-miR-xxx) [36]. One of the strands are degraded and other is associated with RISC (RNA-induced silencing complex) where it is guided to mRNA targets by the help of Argonaute proteins [42], [43], [44].

MicroRNAs are specifically and differentially expressed across different organisms, developmental stages, tissues or cell types [45], [33], [46]. For example, hsa-mir-124 is expressed exclusively in brain [33]. They have been shown in several cell functions such as development, cell proliferation, differentiation, hematopoiesis, death, stress resistance, and fat metabolism [47], [48].

Computational methods are used to predict potential microRNA targets (binding sites in 3' UTR) by using degrees of complementarity and conserved regions among related species although some algorithms such as miRanda [49] does not consider conservation as a pre-requisite [36].

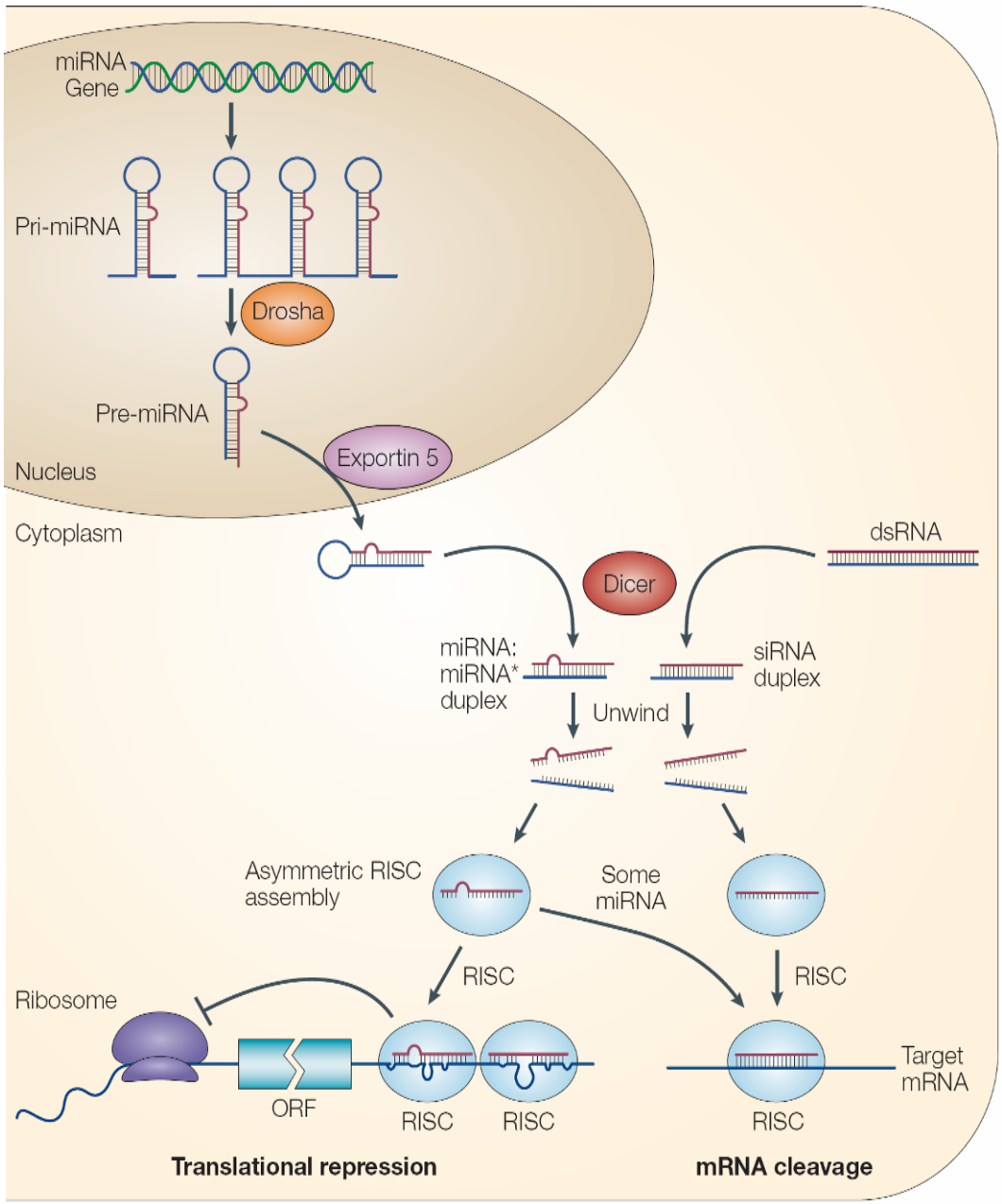

Figure 1.7: Biogenesis of microRNAs
(Figure taken from http://www.microrna.ic.cz/obr/image003.png)

1.3.2 Gene Regulation by microRNAs

MicroRNAs are predicted to regulate a large number of genes (about 30% of all human genes) [50], [51]. MicroRNAs regulate gene expression post-transcriptionally by two different mechanisms: mRNA cleavage or translational repression by binding complementary regions in 3' UTR of the target genes [41], [30], [52], [53]. In some studies, it has also been described that binding to 5' UTR regions are as efficient as binding the 3' UTR to repress the mRNAs [54]. Translational repression by partial complementarity was found to be more common in animals, whereas more perfect complementarity of miRNA:mRNA resulting in mRNA cleavage was observed in plants [31], [55], [56]. In animals, some microRNAs have been found to mediate mRNA cleavage (Figure 1.8) in addition to translational repression (Figure 1.9) [57].

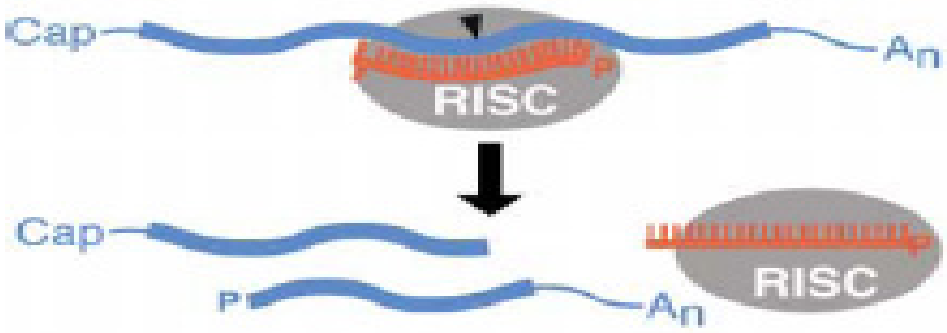

Figure 1.8: mRNA cleavage by microRNAs [41]**.**
(Figure taken from Bartel *et al*., 2004).

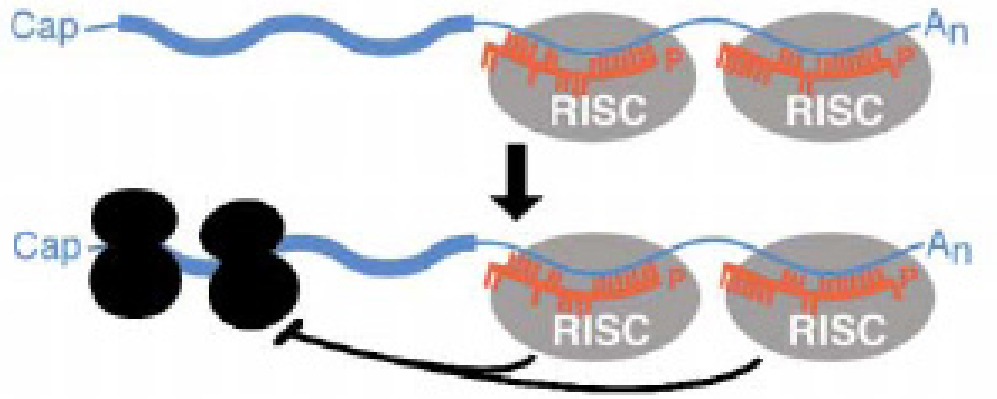

Figure 1.9: Translational repression by microRNAs [41].
(Figure taken from Bartel *et al*., 2004).

Previous reports suggest mRNA down-regulation by microRNAs is due to decreased translation [30], [58]. However, recent findings indicate that microRNAs can also decrease the amount of cellular mRNAs and destabilize them with imperfect complementation. This mechanism is through the removal of poly-A tails of mRNAs, which is not necessary in translational repression [59], [60]. Although decreasing protein levels by translational repression is known to be a common mechanism of microRNA mediated targetting [30], studies suggest that microRNAs can reduce mRNA levels [61], [59] by rapid mRNA deadenylation [60], [62] (Figure 1.10).

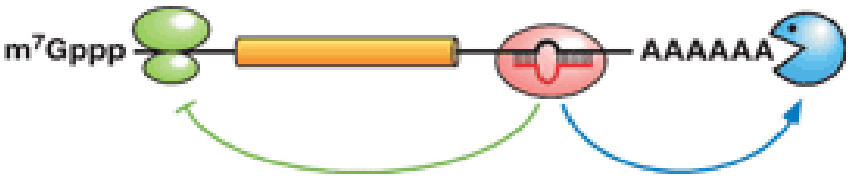

Figure 1.10: Deadenylation and translational repression by microRNAs
(Figure taken from www.ebiotrade.com)

1.3.3 MicroRNAs and Cancer

Some microRNAs have been shown to act as tumor suppressors while other microRNAs have been shown to act as oncogenes. Their mechanism of action depends on their target gene functions such as cell proliferation, apoptosis, or invasion. They were also recently shown to be important cancer biomarkers in terms of their significant expression in cancer samples compared to normal [1], [63].

MicroRNAs were previously reported to be located in chromosomal instability regions, including fragile sites. According to some estimates 50% of known microRNAs have been found to be located in cancer related regions. Alterations in microRNA genes may lead to up-regulation or down-regulation of the target genes which may lead to cancer progression depending on target gene functions (Figure 1.11) [64], [1].

Few of the over 400 known microRNAs, have been verified to be involved in cancer. Their genomic instability and differential expression have been shown to relate with tumorigenesis. For example, hsa-mir-15a and hsa-mir-16a are located on 13q14, a common deletion region of BCL in leukemia [1]. By using single nucleotide polymorphism (SNP) microarrays, Lamy *et al*, 2006 showed that microRNA copy number changes relate to expression levels in prostate and colon cancers. However, in bladder cancer they found controversial results indicating that cancer related regions and microRNA locations are that directly correlated. This might be dependent on cancer type and possibly microRNA expression is regulated by different mechanisms compared to mRNAs, such as in a target-dependent manner [64].

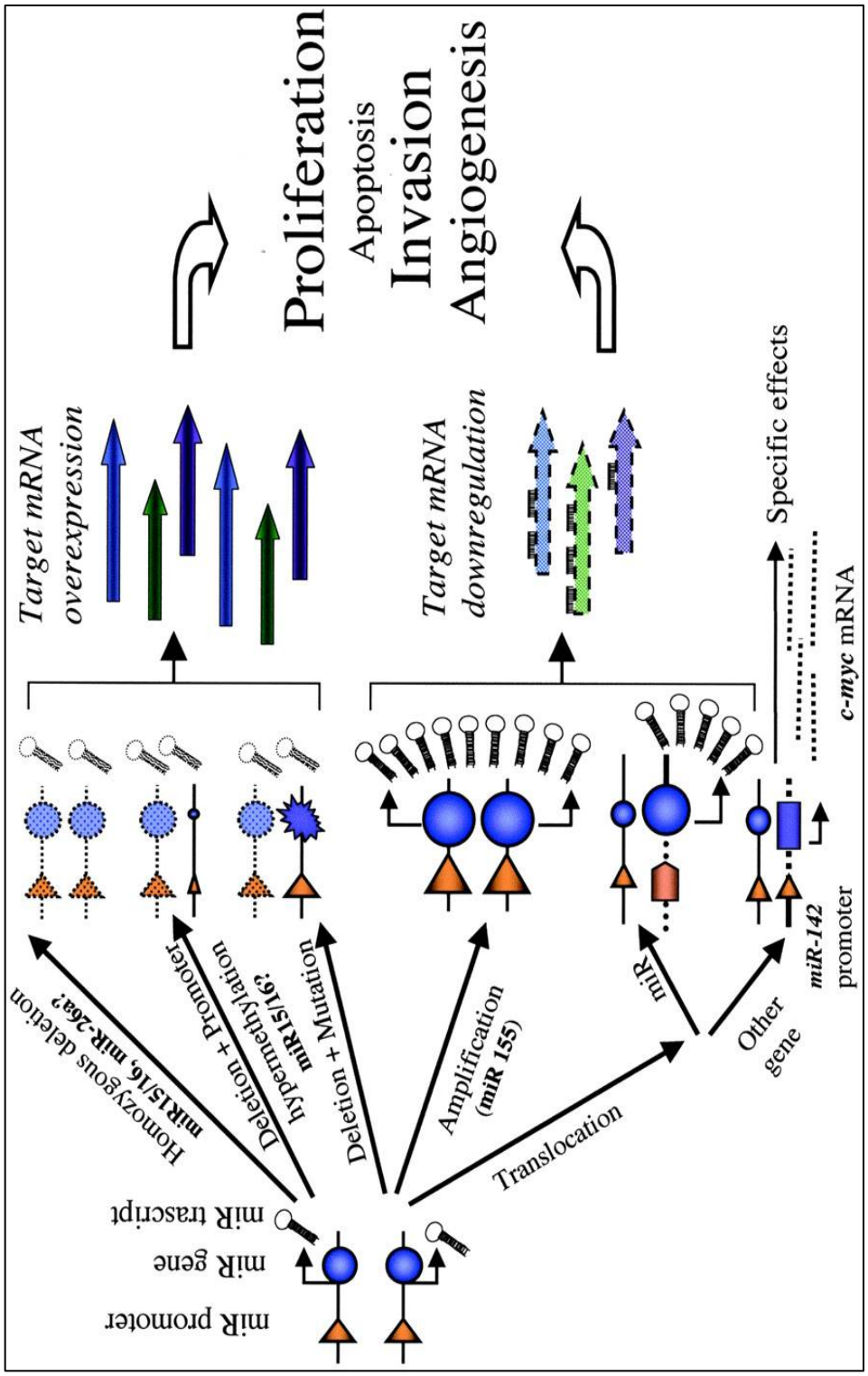

Figure 1.11:: microRNA genomic alterations and cancer relation [1].
(Figure taken from Calin *et al*, 2004)

Another microRNA, hsa-mir-142, is located on breakpoint region of a translocation t(8;17) which causes B cell leukemia. Hsa-mir-142 expression was found to be higher in B-lymohoid lineages compared to others suggesting a potential role of hsa-mir-142 in hematopoietic lineage differentiation [31], [65]. A polycistron, hsa-mir-17-92, encodes seven microRNAs, located on common amplification region 13q31.3 in B cell lymophomas and lung cancers, and is also overexpressed and this polycistron has been implicated as potential oncogene [66].

Microarray studies were conducted on poorly differentiated tumor samples by comparing mRNA profiling versus microRNA profiling. This study showed that microRNA expression profiles classified 12 of 17 tumor samples whereas mRNA expression profiles could discriminate only 1 of 17 samples despite the fact that mRNA array contains 15,000 genes but miRNA array contains 200 genes [34]. Thus, microRNAs were found to be powerful discriminators of classified human cancers as they show different expression patterns in different cancer types [67]. MicroRNAs showing abnormal expression in cancer are shown in Figure 1.12.

Cancer type	Aberrantly regulated microRNAs
CLL – chronic lymphocytic leukemia (CLL)	o *miR-15a* and *miR-16-1*, down-regulated in more than 60% of CLL cases o *miR-155*/ BIC RNA, increased levels o *miR-17-92 cluster*, only some members are abnormally expressed o *miR-2f3, miR-183, miR-190, miR-24-1*, miRNAs located exactly inside fragile sites o *miR-96, miR-182, miR-183*= 7q32 group, all members are aberrantly regulated o and many others[3] (see Calin *et al.*, 2004)
CLL – distinguish CLL samples that express unmutated IgVh gene from those that express mutated IgVh gene	*miR-186, miR-132, miR-16-1, miR-102(miR-29)* and *miR- 29c*
CLL – 13 miRNAs prognostic group, could discriminate between CLL samples that express ZAP-70 and unmutated IgVh and CLL samples that have no expression of ZAP and have a mutated IgVh	*miR-15a, miR-195, miR-223, miR-24-1, miR-29b-2, miR-29a-2, miR-16-1, miR-16-2, miR-155, miR-146, miR-22f, miR-23b* and *miR-29c*
CLL – 9 miRNAs predicting interval from diagnosis to therapy, differentiate patients with a short interval from diagnosis from patients with a longer interval	*miR-155, miR-146, miR-22f, miR-23b, miR-29c, miR-222, miR-24-2, miR-23a* and *miR-181a*
diffuse large B cell lymphoma, marginal zone lymphomas, other non-Hodgkin lymphomas and Hodgkin lymphomas	*miR-155*/ BIC RNA, increased levels
aggressive B cell leukemia	*miR-142* translocation t(8, 17) causes up-regulation of a translocated *c-MYC* gene
breast cancer	o *miR-10b, miR-125b* and *miR-145*, down-regulated o *miR-2f* and *miR-155*, up-regulated
lung cancer	o *let-7*, reduced expression o *miR-155*, over-expression o *miR-17-92 cluster*, over-expression
glioblastoma	o *miR-22f , miR-2f*, strongly over-expressed o *miR-128, miR-181a, miR-181b and miR-181c*, down-regulated
colorectal tumors	*miR-143* and *miR-145*, down-regulated
for chromosomal location of microRNAs see: *http://microrna.sanger.ac.uk*	miR-17-92 cluster: *miR-17-5p, miR-17-3p, miR-18, miR-19a, miR-20, miR-19b1, miR-92-1*

Figure 1.12: Abberantly regulated microRNAs and cancer types [31].
(Figure taken from Kusenda *et al*, 2006)

To date, microRNA involvement in tumorigenesis has been implicated in targeting genes with significant functions in cancer pathways such as angiogenesis or cell signaling [63], [31]. Involvement of microRNAs and their deregulation in cancer have been attributed to its target gene functions. Potential targets of some microRNAs are listed in Figure 1.13.

Target (gene)	*Potential microRNA*	*Supporting observations*
Cell adhesion		
E-cadherin (CDH1)	mir-9	mir-9 increased in breast cancers (Iorio *et al.*, 2005), but downregulated in lung cancers (Yanaihara *et al.*, 2006)
β-Catenin (CTNNB1)	mir-139, mir-200*	
Integrin α 4 ITGA4	none	
Integrin α V (ITGAV)	mir-25/32/92/367 mir-142-3p	mir-32 downregulated in lung cancer (Yanaihara *et al.*, 2006); mir-92 downregulated in six solid cancer types by PAM (Volinia *et al.*, 2006)
Integrin β 1 (ITGB1)	mir-124, mir-183, mir-223, mir-29	mir-124a-3 downregulated in lung cancer (Yanaihara *et al.*, 2006); ITGB1 validated as mir-124 downregulated gene (Lim *et al.*, 2005)
Integrin β 3 (ITGB3)	let-7/mir98, mir-30, mir-125, 1/206	let-7a-2 downregulated in lung cancer (Yanaihara *et al.*, 2006; Johnson *et al.*, 2005); let-7a-2, 7a-3, 7d, 7f-2 downregulated in breast cancer (Iorio *et al.*, 2005); let-7a-1 downregulated in six solid cancer types by PAM and SAM (Volinia *et al.*, 2006); mir-30a-5p downregulated in lung cancer (Yanaihara *et al.*, 2006); mir-30d downregulated in six solid cancer types by SAM (Volinia *et al.*, 2006); mir-125a, b1, b2 downregulated in breast cancer (Iorio *et al.*, 2005; ITGB3 also identified as putative target gene in this study)
Integrin α 5 (ITGA5)	mir-30, mir-25/32/92/367, mir-128, mir-26, mir-148/152	See ITGAV (mir-32/92), ITGB3 (mir-30); mir-26a-1-prec downregulated in lung cancer, deleted in epithelial cancers (Yanaihara *et al.*, 2006)
Fibronectin (FN1)	mir-1/206, mir-199a*, mir-200b, mir-217	
Syndecan-1 (SDC1)	mir-19, mir-9, mir-10, mir-93/302/372/373	See E-cadherin (mir-9); mir-10b downregulated in breast cancer (Iorio *et al.*, 2005); mir-372/373 shown to be oncogenes cooperating with Ras (Voorhoeve *et al.*, 2006)
Paxillin (PXN)	mir-137, mir-218, mir-145	mir-145 downregulated in breast cancer (Iorio *et al.*, 2005) and lung cancer and deleted in prostate cancer (Yanaihara *et al.*, 2006); mir-218-2 downregulated in lung cancer (Yanaihara *et al.*, 2006)
FAK (PTK2)	mir-138, mir-135, mir-25/32/92/367, mir-7, mir-199	See ITGAV (mir-32/92); FN1 (mir-199)
CD44	mir-27	
LOX	mir-145	See Paxillin (PXN)
Angiogenesis		
VEGF-A	mir-125	See ITGB3
VEGF-B	mir-128	
VEGF-C	None	
FIGF (VEGF-D)	None	
VEGFR2 (KDR)	None	
VEGFR1 (FLT1)	mir-17/20/106, mir-181, mir-10, mir-24	See HIF-1α (mir-17/20/106); mir-181c-prec downregulated in lung cancer (Yanaihara *et al.*, 2006); see syndecan-1 (mir-10)
HIF-1α (HIF-1A)	mir-17/20/106, mir-138, mir-199, mir-135, mir-19, mir-18, mir-203, mir-155	Elevated mir-17/20/106 seen as part of a 'solid cancer signature' (Volinia *et al.*, 2006); see FN1 (mir-199). High mir-155 associated with poor prognosis in lung cancer (Yanaihara *et al.*, 2006).
ARNT	mir-221/222, mir-9, mir-135, mir-153, mir-10, mir-103/107, mir-29	See E-cadherin (mir-9), syndecan-1 (mir-10)
Angiopoietin 1 (ANGPT1)	mir-124, 204/211	Downregulated mir-124a1 in lung cancer (Yanaihara *et al.*, 2006); see ITGB1 (mir-124)
Angiopoietin 2 (ANGPT2)	mir-145	See Paxillin (PXN)
FLT4	None	
Proteolysis and cell signalling		
MMP1	None	
MMP2	mir-29	
MMP7	None	
MMP8	None	
MMP9	None	
MMP14	mir-26, mir-24, mir-181	See VEGFR1/FLT1 (mir-181); ITGA5 (mir-26)
ADAM-17	mir-145	See Paxillin (PXN)
TIMP-1	None	
TIMP-2	mir-30	See ITGB3 (mir-30)
TIMP-3	mir-181, mir-1/206, mir-30, mir-199a*, mir-21, mir-221/222, mir-17/20/106	Upregulated mir-221/222 in papillary thyroid cancer (He *et al.*, 2005); mir-21 upregulated in glioblastoma and associated with antiapoptosis (Chen *et al.*), and

Figure 1.13: MicroRNAs and predicted target genes that have significant functions in tumorigenesis.(Figure taken from Dalmay *et al*, 2006) [63]

Among thousands of target genes predicted, few have been experimentally confirmed. For instance, hsa-miR-21 has been shown to regulate tumor growth and apoptosis through regulating genes directly or indirectly that are involved in

cancer pathways (i.e. *PTEN, BCL-2, PDCD4, TPM1*) [68], [69], [70], [71]. It has also been shown that hsa-let-7 regulates RAS, hsa-miR-17-5p regulates E2F1 expression, and hsa-miR-15 and hsa-miR-16 downregulate BCL-2 and induce apoptosis [72], [73], [74]. Moreover, hsa-miR-142 has been found to target *c-myc* (myelocytomatosis viral oncogene), hsa-miR-20a targets *E2FI*, and hsa-mir-19a targets *PTEN*. [75], [76].

On the other hand, in a study by Bommer et al, 2007, hsa-mir-34 was reported to be targeted by p53 tumor suppressor gene in human and mouse cells. It has been attributed as "significant downstream effecter of p53 function" and it is suggested that the inactivation of hsa-mir-34 might contribute to certain cancer types [77].

In recent studies on microRNAs and breast cancer, few microRNAs have been shown to be deregulated in genomic level and expression level. For example, a CGH study on 283 microRNAs in ovarian cancer, breast cancer, and melanoma found common microRNAs deregulated in all three cancer types as well as some microRNAs unique to a certain cancer type. They showed copy number changes of microRNAs in 72.8 % of breast cancer samples [78] (Figure 1.14).

In addition, hsa-miR-21 which is thought to be correlated with breast cancer has also been found to be amplified and overexpressed and involved in many cancer types indicating an oncogenic role [71], [68], [69], [70]. The target of hsa-miR-21, the tumor suppressor gene tropomyosin 1 (*TPM1*), has been identified and verified using MCF7 cells [70]. This was verified by the suppression of tumor growth after treatment of cells with anti-miR-21 to knock down hsa-miR-21 [70], [69].

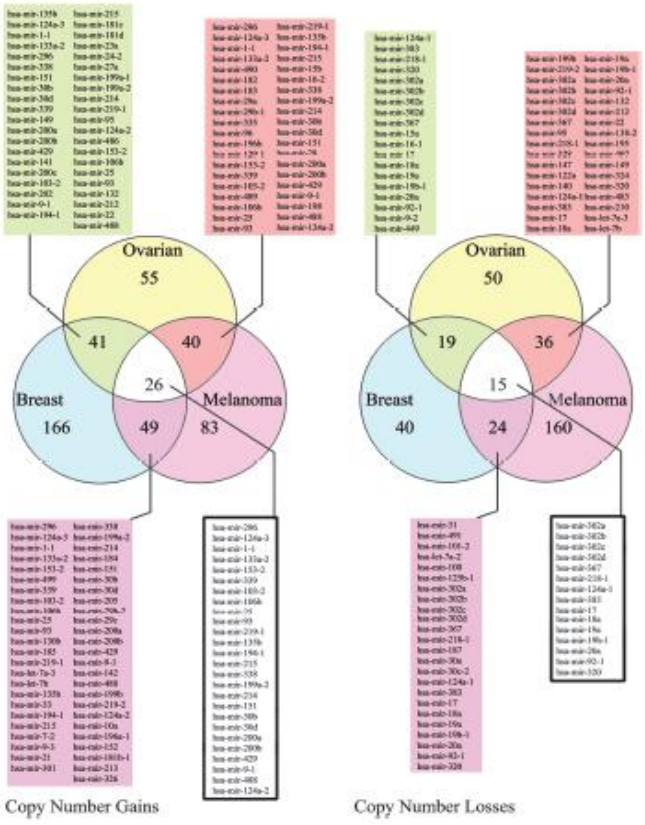

Figure 1.14: Copy number changes of 283 microRNAs in breast, ovarian and melanoma cancer samples by CGH.

In terms of comparison of miRNA expressions in breast cancer cell lines and tumors, Mattie et al, 2006, analyzed many microRNAs in 10 breast tumors (ErbB2 +) and SKBR3 cell line (ErbB2 +). This study suggested that unique sets of microRNAs are associated with phenotypic status of breast cancer samples. Similar expression patterns of 56 microRNAs in ErbB2 + tumor samples and in ErbB2 + cell line SKBR3 are shown in Figure 1.15.

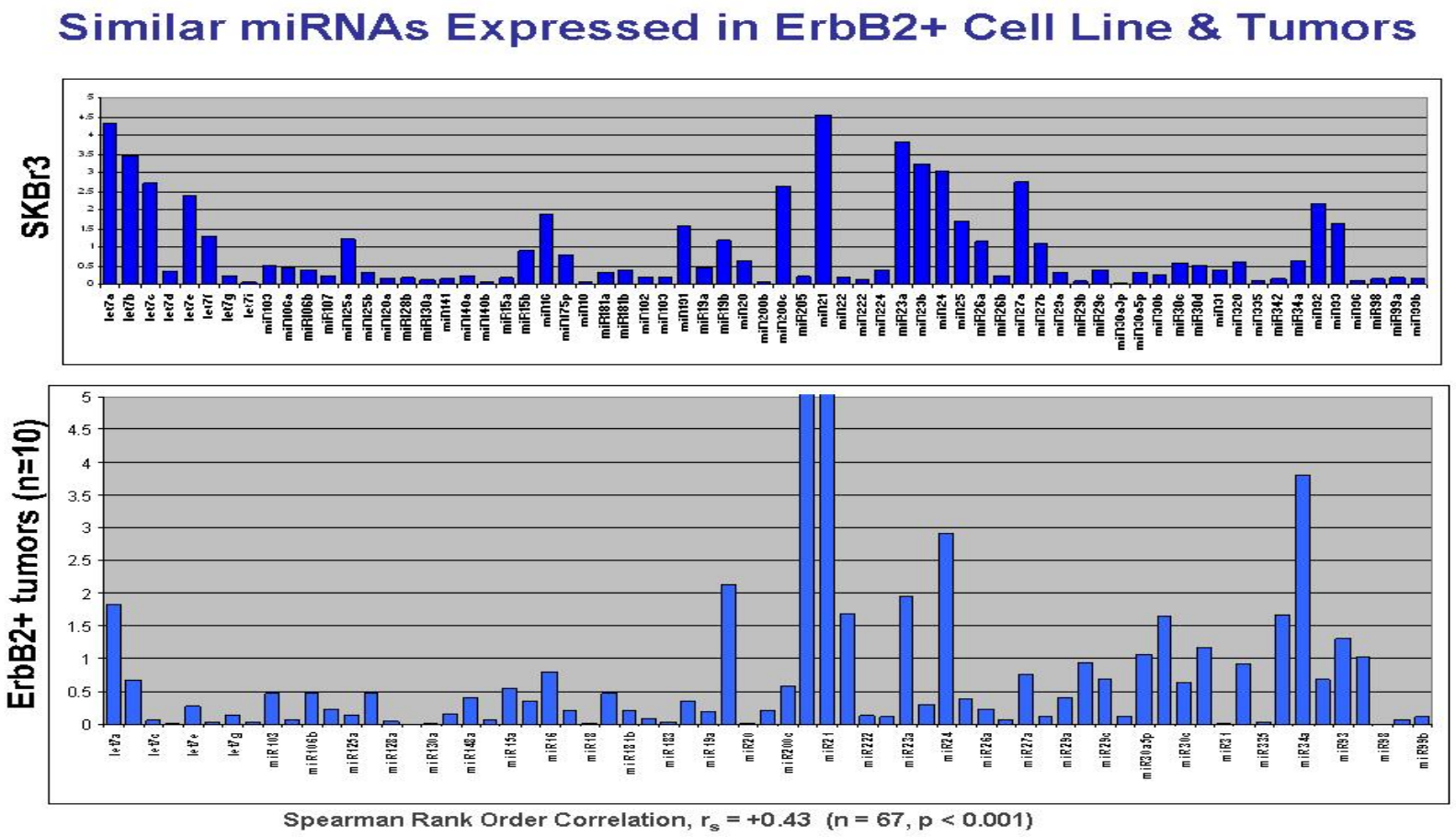

Figure 1.15: Expression levels of 56 microRNAs in SKBR3 and breast tumors
Figure taken from Mattie et al, 2006

MicroRNA microarray study by Iorio et al, 2005, analyzed breast cancer tumors and cell lines and showed that compared to normal breast tissue, hsa-mi125b, hsa-miR-145, hsa-miR-21, and hsa-miR-155 were significantly deregulated in breast cancer. MicroRNA expression profiling was clustered and breast cancer samples were clearly differentiated from normal samples also according to biopathological features. They found that let-7, miR-125b, and miR-145 were down-regulated, whereas miR-155 and miR-21 were up-regulated [79].

1.4 Aim of the Study

Genomic instability is commonly seen in breast cancer cells. Loss or gain of particular chromosomal segments may harbor potential tumor suppressor genes or oncogenes that may contribute to tumorigenesis when lost or gained, respectively [11], [13], [14].

microRNAs have already shown to be involved in cancer related pathways/mechanisms. Our aim was to investigate microRNAs mapping to breast cancer genomic instability regions, and to confirm their fold changes (loss or gain) in 20 breast cancer cell lines, 2 immortalized mammary cell lines and 2 normal DNAs compared to a housekeeping gene, *GAPDH*.

CHAPTER 2

MATERIALS AND METHODS

2.1 Materials:

2.1.1 Cancer Cell Lines

Twenty breast cancer cell line DNAs (BT20, BT474, BT549, CAL51, DU4475, Hs578T, MCF7, MDA-MB157, MDA-MB231, MDA-MB361, MDA-MB435, MDA-MB468, SUM-52, SUM-102, SUM-149, SUM-159, SUM-185, SUM-229, SK-BR3, and T-47D) and 2 immortalized mammary cell line DNAs (HPV4-12 and MCF10) were kindly provided by E.M. Petty from the University of Michigan, Ann Arbor, U.S.A. and were used in semi-quantitative duplex PCR experiments. Two normal DNA controls were isolated from blood and used for comparison to cancer cell lines.

Cancer cell lines MCF7, MDA-MB-231, SUM-159, Hs578T, HeLa and SHSY-5Y and rat brain tissue were kindly provided by Biochemistry department of University College Cork, Ireland and were used in real-time RT-PCR expression analysis of hsa-miR-21 and hsa-miR-383.

2.1.1.1 Mammalian Cell Culture Conditions

MCF7, HS578T, HeLa, and SYSY-5Y cell lines were grown as monolayers in tissue culture plates (Sarstedt) in Dulbecco's Minimum Essential Medium (DMEM) (Sigma, D6429). Composition of the media is presented in Appendix A. The MCF10 cell was grown in Ham's F-12 nutrient mixture (Sigma-Aldrich, N6760) with supplements given in Table A.1. The MDA-MB-231 cell line was grown in Leibovitz's L15 media (Sigma-Aldrich, L4386). All media included 1 % L-Glutamine (Biowhittaker, BE17-605E), 10 % Fetal Bovine Serum (Biosera, S1900/500), and 1 % Penicillin / Streptomycin (10 000 IU/ 10 000 µg/ml), (Biowhittaker, DE17-602E) filtered through 0, 45 µm filters. All cell lines were incubated in 37^{o}C incubators with 95% air and 5% CO_2. Details of culture medium are given in Table A.1.

1X PBS (phosphate buffered saline) was used in cell culture wash 2-3 times a week to remove metabolic wastes and fresh media was added to cells.

1X Trypsin-EDTA (Sigma, T4174) was used to detach the cells from the flask when the cells were confluent. Subculturing of the cells was done according to doubling time of each cell line with 1:2, 1:3, or 1:4 ratios. Centrifugation at 1400 rpm for 4 min was used to pellet the cells before subculturing and freezing.

Cells were frozen in liquid nitrogen when they reached 90% confluency. Five percent (5%) DMSO (dimethyl sulfoxide) (Sigma, 154938) was used in the corresponding media for each cell line for long term storage of frozen cells. Cells were frozen and kept at -80^{o}C for 1-2 days and transferred to liquid nitrogen. Cells were thawed in a 37^{o}C water bath. Counting of the dead cells was done by staining cells with tryphan blue to discriminate them from living cells in hemocytometer under light microscope.

2.2 Methods

2.2.1 Literature Research on Common Genomic Instability Regions in Breast Cancer

Literature search was performed by using NCBI PubMed database for published studies about genomic instability regions (homozygous deletion, loss of heterozygosity and amplification) in breast cancer cells. The chromosomal regions found to be frequently altered were selected and listed. Positions of instability regions were defined by single nucleotide polymorphism (SNP) markers available for some regions.

2.2.2 Mapping microRNAs to Common Loss and Gain Regions

After defining common regions of alterations, microRNAs in these regions were located by using two approaches. First, by using Human Genome Browser (http://genome.ucsc.edu/cgi-bin/hgGateway) and Sanger Institute miRBase database (http://microrna.sanger.ac.uk/sequences/), microRNAs were mapped to these regions. Second, combined DNA sequences of microRNAs in FASTA format were blasted against genomic instability region sequences using NCBI BLAST program (http://www.ncbi.nlm.nih.gov/blast/Blast.cgi).

2.2.3 Investigation of microRNA Gene Fold Changes in Breast Cancer Cell Line Genomes

Fold changes of 39 microRNAs were investigated in 20 breast cancer cell lines, 2 immortalized mammary cell lines, and 2 normal DNAs by semi-quantitative duplex PCR.

2.2.3.1 Primer Designs

Primers for DNA regions of the 39 pre-miRNAs and for housekeeping gene, *GAPDH*, were designed by using Primer3 program (http://frodo.wi.mit.edu/). Specificity of primers was tested by using UCSC *in-silico* PCR program (http://genome.brc.mcw.edu/cgi-bin/hgPcr). MicroRNA PCR products ranged from 190bp to 350bp and for *GAPDH*, 2 primer sets to generate 472 bp and 644 bp were designed (Table B.1).

For pre-miRNA expression analysis, sequences were obtained from miRBase database and cDNA primers were designed manually, example of hsa-mir-21 pre-miRNA primers design is shown in Figure 2.1. PCR product sizes were approximately 70bp-80bp and *GAPDH* primers were designed to yield a PCR product of 115 bp. Specificity of designed primers were checked by using UCSC *in-silico* PCR program (http://genome.brc.mcw.edu/cgi-bin/hgPcr). All primers were resuspended in RNase-free water to a final concentration of 100µM.

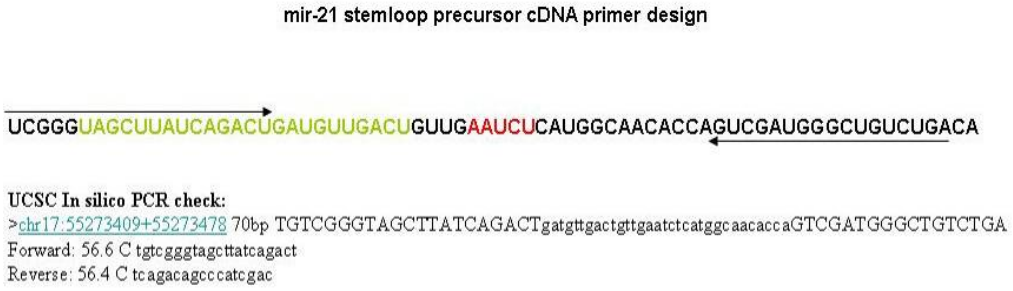

Figure 2.1: cDNA primer design for hsa-mir-21 pre-miRNA.
Green; mature microRNA sequence, arrows; forward (21 nt) and reverse (17 nt) primers, red; stem-loop region. UCSC In-Silico PCR primer specificity program shows 70 bp PCR product specific for the hsa-mir-21 pre-miRNA cDNA on 17q23.

2.2.3.2 Semi-quantitative Duplex PCR

DNAs from 2 normal samples isolated from blood were used in optimization of duplex PCRs such as adjusting *GAPDH* and microRNA primer concentrations. A total of 30 µL PCR master mixture included: 3µL 10X complete Taq Pol buffer, 3 µL dNTP mix (2nM each), and 3µL microRNA forward primer (5 µM) and 3µL microRNA reverse primer (5 µM), 16.25 µL dH_2O, 0.25 µL Taq Polymerase (Applichem, A5186), and 2 µL DNA (50ng/µL).

PCR was performed in a thermal cycler using ~3-4ºC lower Tm of each primer pair in PCR program: 1 cycle denaturation step at 94ºC for 2 min, 35 cycles of amplification at 94ºC for 30 sec (Tm-3) ºC for 30 sec, extension step at 72ºC for 30 sec) and final extension step at 72ºC for 10 min was performed. For nonspecific bands, relatively higher temperatures were used for amplification step ((Tm-1)ºC). For some of the microRNA PCRs, the following touchdown program was used: 1 cycle denaturation step at 94ºC for 2 min., 3 cycles of amplification at 94ºC 30 sec., annealing at (Tm-1)ºC 30 sec and extension step at 72ºC for 30 sec), 3 cycles of (94ºC 30 sec., (Tm-3)ºC 30 sec., 72ºC 30 sec), 29 cycles (94ºC 30 sec., (Tm-5)ºC 30 sec., 72ºC 30 sec), and 72ºC 10 min.

Semi-quantitative duplex PCR master mixture included 3µL 10X complete Taq Pol Buffer, 3 µL dNTP mix (2mM each), 3 µL *GAPDH* forward primer (5µM) and 3 µL *GAPDH* reverse primer (5µM), 3 µL microRNA forward primer (5µM) and 3 µL microRNA reverse primer (5µM), 9.75 µL dH2O and 0.25 µL Taq Polymerase, finally 2 ul of 50ng/µL DNA template (total 100 ng) was added for a final 30 µL reaction mix. PCR conditions such as Tm, primer:primer amounts and amplification cycles were first optimized in normal DNA samples (See Figure 2.2 for an example of cycle optimization) and later cancer cell line DNAs were used in previously optimized PCR conditions listed in Table B.2.

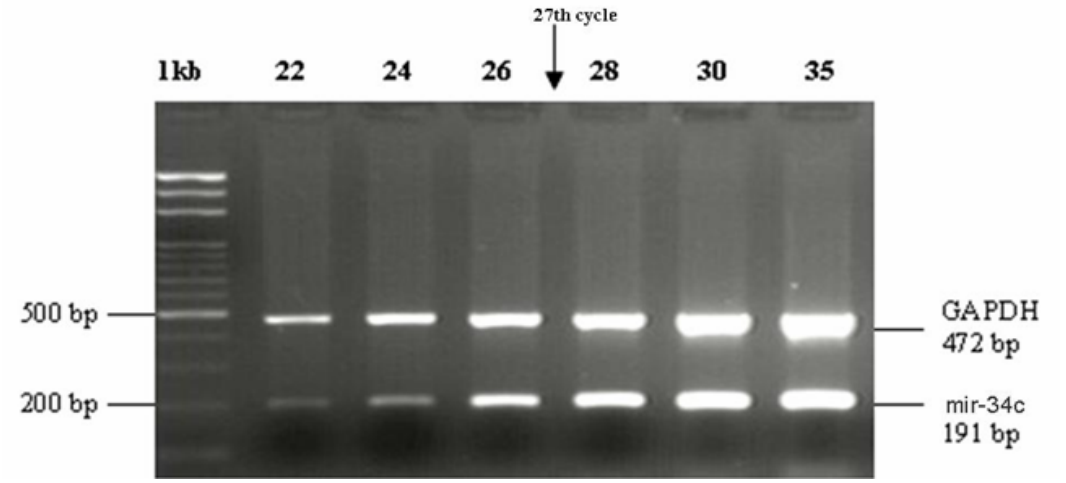

Figure 2.2: An example of PCR optimization by cycle selection
In this case, hsa-mir-34c was optimized at cycle 27 before saturation of the bands.

2.2.3.3 Densitometry Analysis and Fold Change Calculation

Semi-quantitative duplex PCR gel images were analyzed using Scion Image program (National Institute of Health). Fold changes calculated for normal DNAs for *GAPDH* and microRNA band intensities were used in normalization of cancer cell line DNA fold changes. The formula used in calculation of fold change of microRNAs in cancer cell lines normalized to normal DNAs is shown in Figure 2.3.

$$\text{Fold change} = \frac{\text{C (mir} / \textit{GAPDH})}{\text{AVG (N1 (mir} / \textit{GAPDH}) \text{ , N2 (mir} / \textit{GAPDH})}$$

Figure 2.3: Formula used in normalization and calculation of fold changes of microRNAs.
Ratios of peak values generated by Densitometry analysis program were used. (C): Cancer cell line; (N1) and (N2): Normal DNAs

2.2.4 Expression Analysis of microRNAs

Expression analysis of selected microRNAs was performed in two stages. First, pre-miRNAs (precursor) expression was investigated by using RT-PCR. Second, expression of mature miRNAs (active form) was investigated by using real-time RT-PCR method.

2.2.4.1 RNA Isolation and DNase Treatment

All the solutions were prepared with DEPC-treated water and micropipettes were UV cross linked. RNase free tubes and filtered tips (Biosphere) were used. The bench was cleaned with RNase AWAY solution (Molecular BioProducts, 7000) and DNA AWAY (Molecular BioProducts, 7010) to remove any contaminating RNases or DNases. Two different isolation methods were used: (a) Trizol Reagent (Invitrogen, 15596-026) and (b) *mir*Vana microRNA Isolation Kit (Ambion, AM1560). RNAs were DNase treated following isolation by TURBO DNA-free kit (Ambion, AM1907) to remove any contaminating DNA template.

2.2.4.1.1 RNA Isolation by Trizol Reagent

RNA was isolated from MCF7, MDA-MB-231, HS578T, SUM-159, MCF10A, SHSY-5Y, and HeLa (cervical carcinoma) cell lines for RT-PCR analysis of pre-microRNAs and mature microRNAs by using Trizol Reagent. Additionally, normal breast RNA (Ambion, 7952) was used as a control in pre-miRNA RT-PCR.

For RNA isolation by Trizol Reagent, cells were grown in T75 cell culture flasks to 70% confluency. Trizol reagent (1 ml) was used to lyse the cells, passing

them through the pipette several times and transferred to an eppendorf tube. 0.2 ml of isopropanol (Sigma, I9516) per 1 ml Trizol reagent was added to cells, and the tube was shaken for 15 sec. the tube was centrifuged at 12,000 x g for 15 min at 2-8^{o}C. Following centrifugation, mixture separates into 3 levels; phenol chloroform phase, interphase and aqueous phase from bottom to top. Aqueous phase containing RNA was transferred to a new tube. 0.5 ml isopropyl alcohol was added and mixture was incubated at 15-30^{o}C for 10 min. Then, it was centrifuged at 12,000 x g for 10 min at 2-8^{o}C. RNA precipitated, supernatant was removed and RNA pellet was washed once with 1 ml of 75% ethanol. Sample was mixed by vortexing and centrifuged at 7,500 x g for 5 min. at 2-8 ^{o}C. The RNA pellet was air-dried for 5-10 min. RNA was dissolved in 30-50µL RNase-free water and stored at -80^{o}C. RNA concentrations were measured in Nanodrop Spectrophotometer (ND-1000).

50 µl RNA (~200ng/ul) was treated with 1 µl DNase I supplied in TURBO DNA-free Kit, and incubated at 37^{o}C for 30 min. 5 µl of DNase inactivating reagent was added and incubated at room temperature for 2 min. After centrifugation at 10,000 x g for 1.5 min, supernatant containing RNA was transferred to a fresh tube. DNase treated RNAs were stored at -80^{o}C.

2.2.4.1.2 RNA Isolation by mirVana microRNA Isolation Kit

Optimization of expression analysis experiments included comparison of two RNA isolation methods; by *mir*Vana miRNA isolation kit and by Trizol Reagent.

Total RNA was isolated from MCF7 by using *mir*Vana miRNA isolation kit. Seventy percent (70%) confluent cells were washed with 5ml 1X PBS. 3ml of 1X Trypsin was added to detach the cells and cells were incubated at 37^{o}C, 5% CO_2 incubator for 10-15 min. Supernatant was removed by centrifuging the cells

at 1400 rpm for 4 min in 5-6 ml culture medium. The media was removed and cells were washed once with 1x PBS and kept on ice. Lysis buffer (600 µL) was added to cells and vortexed. MiRNA homogenate additive (60 µl) was added to the cell lysate, mixed, and incubated on ice for 10 min. Then, 600 µl acid:phenol:chloroform was added to cells and vortexed for 1 min. Cells were centrifuged at 10,000 x g for 5 min at room temperature to separate organic and aqueous phases. For isolation of total RNA, 1.25 volumes of 100% ethanol was added to aqueous phase and mixed. The lysate was filtered through cartridge and centrifuged at 10,000 x g for 15 sec. The flow through was discarded. MiRNA wash solution (700 µL) was added to the filter cartridge, and the filter cartridge was centrifuged for 5-10 sec and the flow through was discarded. The filter cartridge was transferred to a new microcentrifuge tube and RNA was eluted by applying 100 µl RNase-free water to filter and centrifuging at 10,000 x g for 20-30 sec. RNA was stored at -80^{o}C.

2.2.4.2 Expression Analysis of pre-microRNAs by RT-PCR

Overview of expression analysis for pre-miRNAs is as follows:

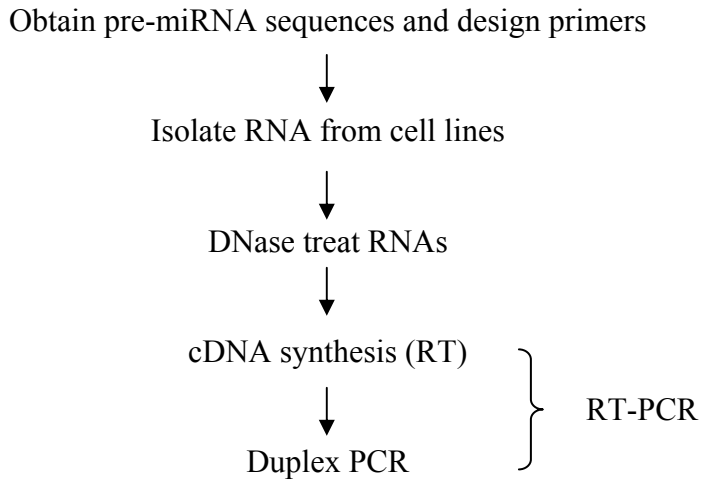

Expression analysis of 7 candidate pre-miRNAs (hsa-mir-633, hsa-mir-145, hsamir-21, hsa-mir-361, hsa-mir-486, and hsa-mir-301) was done by RT-PCR. MCF7, MDA-MB-231, HeLa, and normal breast RNAs were used in cDNA synthesis. Duplex PCR was performed by coamplifying *GAPDH,* as a housekeeping control after setting optimized PCR conditions in DNA templates.

Three different cDNA synthesis kits were used and compared; RevertAid First Strand cDNA synthesis kit (Fermentas, K1632), Superscript II RT (Invitrogen, 11904-018), and Omniscript RT kit (Qiagen, 205110). Both oligodT and random hexamer primers were used. Table 2.1, Table 2.2 and Table 2.3 show master mix preparation and protocol for the kits used.

Table 2-1: cDNA synthesis (RT) protocol and reaction mixture by RevertAid First strand cDNA synthesis Kit

RNA	1 µg (1-2 µL)
Primer (oligodT or random hexamer)	1 µL
dNTP mix	2 µL
DEPC- treated water	variable
TOTAL	12 µL
Briefly centrifuged, incubated at 70C for 5 min., chilled on ice and briefly centrifuged.	
5X reaction buffer	4 µL
Ribolock RNase inhibitor	1 µL
Briefly centrifuged and incubated at 37^{o}C for 5 min (25^{o}C for random hexamer primers)	
Revertaid RT enzyme	1 µL
TOTAL	20 µL
Mixed and incubated at 42^{o}C for 60 min (25^{o}C for 10 min,, 42^{o}C for 60 min for random hexamer primers), reaction was stopped by heating to 70^{o}C for 10 min. and chilling on ice.	

Table 2-2: cDNA synthesis (RT) protocol and reaction mixture by Superscript II cDNA synthesis Kit

RNA	1 µg (1-2 µL)
heated to 70°C for 10 min. to avoid secondary structure, briefly centrifuged and put on ice.	
Primer (oligodT or random hexamer)	1 µL
dNTP mix	1 µL
DEPC- treated water	variable
TOTAL	12 µL
Mixed and heated to 70oC for 5 min., put on ice	
5X 1st strand reaction buffer	4 µL
0.1 M DTT	2 µL
Ribolock RNase inhibitor	1 µL
Mixed and incubated at 42°C for 2 min (25°C for random hexamer primers)	
Superscript II	1 ul
Mixed and incubated at 42°C for 50 min (25°C for 10 min, 42°C for 50 min for random hexamer primers) and 70°C for 15 min.	

Table 2-3: cDNA synthesis (RT) protocol and reaction mixture by Omniscript cDNA synthesis Kit

RNA	1 µg (1-2 µL)
heated to 65oC for 5 min to avoid secondary structure, briefly centrifuged and put on ice.	
10X reaction buffer	2 µL l
Primer (oligodT or random hexamer)	2 µL
dNTP mix	2 µL
DEPC- treated water	variable
Ribonuclease inhibitor, 10U/ul (Fermentas, cat#)	1 µL
Omniscript RT enzyme	1 µL
TOTAL	20 µL
Mixed and heated to 37°C for 60 min	

First, PCR conditions such as Tm for primers and PCR program for hsa-mir-21, mir-633, mir-145, mir-383 and mir-361 were optimized by using normal DNAs. PCR reaction mixture and PCR program used are shown in Table 2.4 and Table 2.5.

Table 2-4: PCR reaction mixture to amplify pre-miRNA

1X master mix	
10 X buffer with $MgCl_2$	3 µL
dNTP mix	3 µL
microRNA forward primer	3 µL
microRNA reverse primer	3 µL
DMSO (to prevent secondary structures)	3 µL
DEPC-treated water	13.75 µL
Taq Polymerase	0.25 µL
DNA(100ng /ul)	1 µL
TOTAL	30 µL

Table 2-5:.PCR cycling conditions for pre-miRNA

95°C	3:00 min	
95°C	0:30 min	35 cycles
48-60°C	0:30 min	
72°C	0:30 min	
72°C	10:00 min	

Thirteen tubes were prepared for optimization and each tube was placed in a well in the thermocycler and 13 different annealing temperatures ranging from 48°C to 60°C were used in a gradient PCR program.

Hsa-miR-383 and *GAPDH* were co-amplified in the duplex PCR reaction and program (Table 2.6 and Table 2.7) in cancer cell line cDNAs and normal breast cDNA

Table 2-6: Duplex PCR reaction mixture to amplify pre- miRNA and *GAPDH.*

1X master mix	
10 X buffer with $MgCl_2$	3 µL
dNTP mix (2mM each)	3 µL
microRNA forward primer (100%)	3 µL
microRNA reverse primer (100%)	3 µL
GAPDH forward primer (12.5 %)	4 µL
GAPDH reverse primer (12.5 %)	4 µL
DMSO	3 µL
DEPC-treated water	5.75 µL
Taq Polymerase	0.25 µL
cDNA	1 µL
TOTAL	30 µL

Table 2-7: Duplex PCR cycling conditions for pre-miRNA.
(Annealing temperature differs for all microRNAs)

95°C	3:00 min	
95°C	0:30 min	35 cycles
55°C	0:30 min	
72°C	0:15 min	
72°C	10:00 min	

2.2.4.3 Expression Analysis of Mature microRNAs by Real-Time RT-PCR

For expression analysis of mature microRNAs (hsa-miR-21 and hsa-miR-383), Taqman microRNA Reverse Transcription Kit (ABI, 4366596) and commercially available Taqman microRNA Assays (ABI, 4373381), and Taqman Universal Master Mix (ABI, 4304437). An ABI Prism 7900 HT Sequence Detection System was utilized for detection. Data analysis was conducted using SDS 2.0 software. U6 was used as internal control but not used in normalization.

In our study where a suitable endogenous gene was not present, absolute quantification was used. Absolute quantification detects the quantity of a single

nucleic acid in an unknown sample. A sample with known quantity (calculated by spectrophotometer and molecular weight) is used to construct a standard curve to determine the quantities of other samples according to Ct detected and quantity matches that Ct value in the constructed curve. The Ct value is defined as threshold cycle, the fractional cycle number that fluorescence from the products passes a certain threshold. One Ct value difference between samples equals to 2 fold difference. An efficient PCR reaction (100% efficiency) gives slope of -3.3 on standard curve.

Three biological replicates of 6 cell lines were grown in tissue culture and RNA was isolated separately. Each replicate was loaded into 3 wells of a 384-well plate as 3 technical replicates for statistical significance. For rat brain tissue, whole brain RNA was used in the experiments.

Taqman microRNA assay protocol by real time qRT-PCR includes two steps as represented in Figure 2.3. The first step was cDNA synthesis (by reverse transcriptase, RT) of mature microRNAs by microRNA RT kit; extension by looped primers specific to particular microRNA from 10 ng total RNA of starting material, shown in Table 2.8. The second step was synthesis of second strand of cDNA and PCR amplification of microRNA by using specific primers, Taqman Universal master mix. Amplitaq Gold DNA Polymerase provided in Assay kit was also used. After the RNA was added to master mix, the mixture was centrifuged briefly and tubes were placed into the ABI 2720 thermal cycler for the RT reaction with the program shown in Table 2.9.

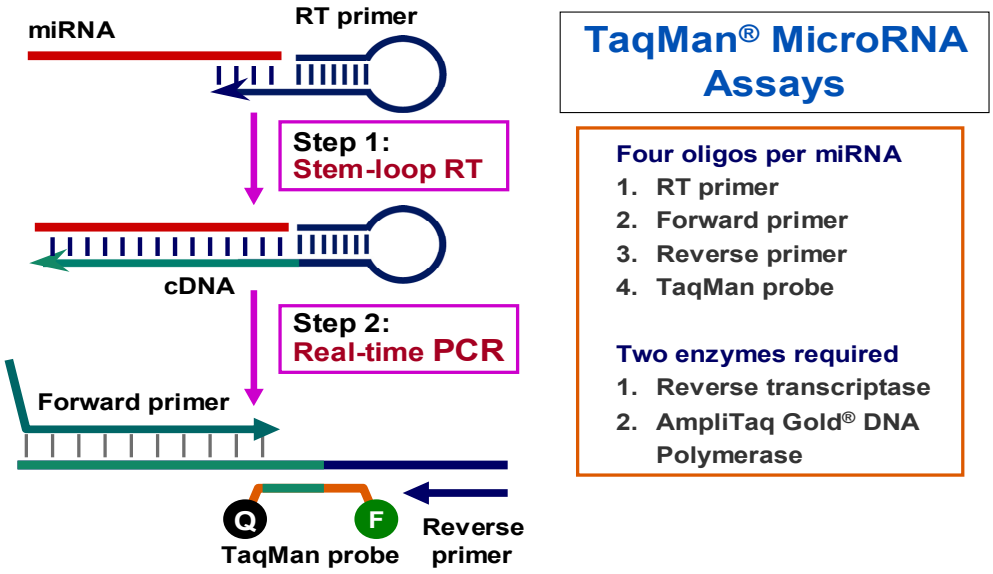

Figure 2.4: Taqman microRNA real-time RT-PCR Assay
(Figure taken from www.appliedbiosystems.com)

Table 2-8: cDNA synthesis (RT) mixture by Taqman microRNA RT Kit

Component	**Volume ul / 15 µL reaction**
dNTP mix (100mM total)	0.15 µL
Multiscribe RT enzyme (50U/µL)	1 µL
10X RT Buffer	1.5 µL
RNase inhibitor (20U/µL)	0.19 µLl
Nuclease-free water	8.16 µL
Specific primer mix	3 µL
RNA (10ng/µL)	1 µL
Total	15 µL

Table 2-9: Taqman miRNA cDNA synthesis reaction program.

16°C	30:00 min
42°C	30:00 min
85°C	5:00 min
4°C	Hold

MCF10 was used as standard sample in U6 and hsa-mir-21 analyses. Brain tissue was used in hsa-mir-383 analysis. Standard samples were diluted in certain ratios and quantities were set. For example, 4 serials dilutions were done for MCF10 cDNA as follows; no dilution (neat), 1:2, 1:4, 1:8 and quantities of 1, 0.5, 0.25, and 0.125 were attributed to each dilution, respectively and set to program before run. Constructed curves were used by the program to calculate quantities of other samples.

After cDNA products are prepared, master mixture was prepared for PCR amplification of RT products (Table 2.10) loaded on 384-well clear optical plates (ABI, 4309849) and covered with optical adhesive covers (ABI, 4313663). The PCR program is shown in Table 2.11 and was performed using the ABI Prism 7900 HT Fast Real-Time PCR System. FAM reporter dye linked to 5' of the probe was used to label the products with fluorescence.

Table 2-10: . Taqman miRNA cDNA PCR reaction mixture

Component	**Volume µL / 10µLreaction**
Taqman microRNA Assay (20X)	0.5 µL
Product from RT reaction (cDNA)	0.7 µL
Taqman 2X Universal Master mix	5 µL
Nuclease-free water	3.8 µL
Total	10 µL

Table 2-11: Taqman miRNA PCR reaction conditions for real-time RT-PCR

95°C	10:00 min	
95°C	0:10 min	40 cycles
60°C	1:00 min	

2.2.5 Target Search for hsa-miR-21 and hsa-miR-383

Four microRNA target prediction programs available online MiRanda (www.microrna.org) (For web interface, see Figure 2.5) [49], miRBase (http://microrna.sanger.ac.uk/sequences/) (For web interface, see Figure 2.6) [36], TargetScan, version 3.0 (http://www.targetscan.org/) (For web interface, see Figure 2.7) [76] and PicTar (http://pictar.bio.nyu.edu/) (For web interface, see Figure 2.8) [80] were used to find predicted target genes of hsa-miR-21 and hsa-miR-383. All programs were screened and listed for high scored genes from top to bottom.

About 40 high scored genes were selected from each prediction program. Common genes predicted by at least 2 of the programs were selected. Also, functions of the predicted genes were obtained from NCBI web site and the genes with potential function in tumorigenesis were included in candidate list.

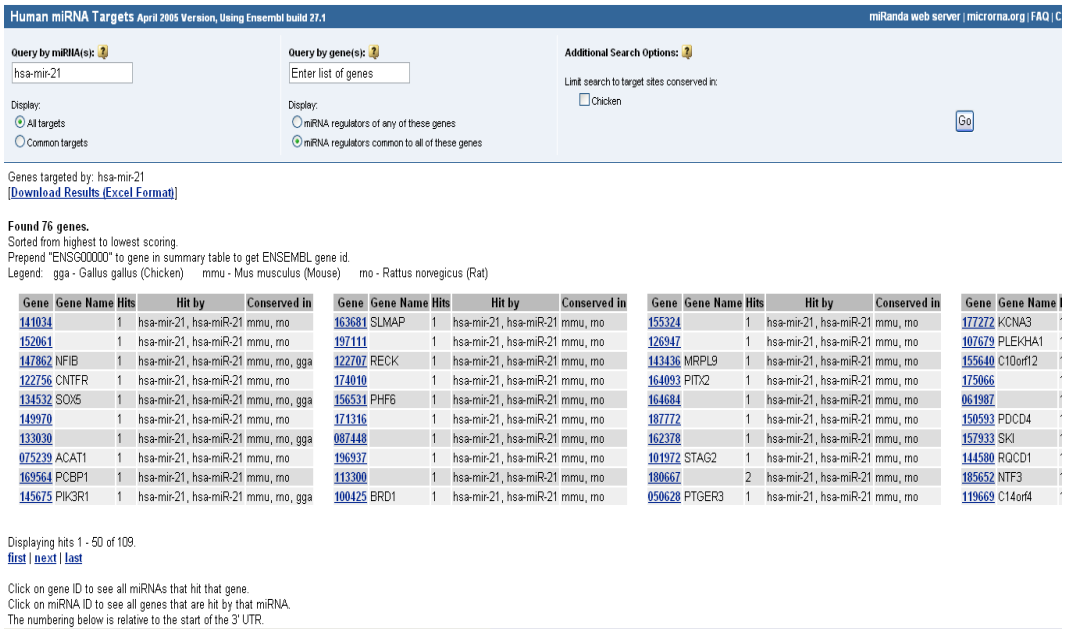

Figure 2.5: miRanda web interface, microRNA targets search page

Figure 2.6: miRBase web interface, microRNA targets search page
(Accessible from MiRanda link in http://microrna.sanger.ac.uk/sequences/)

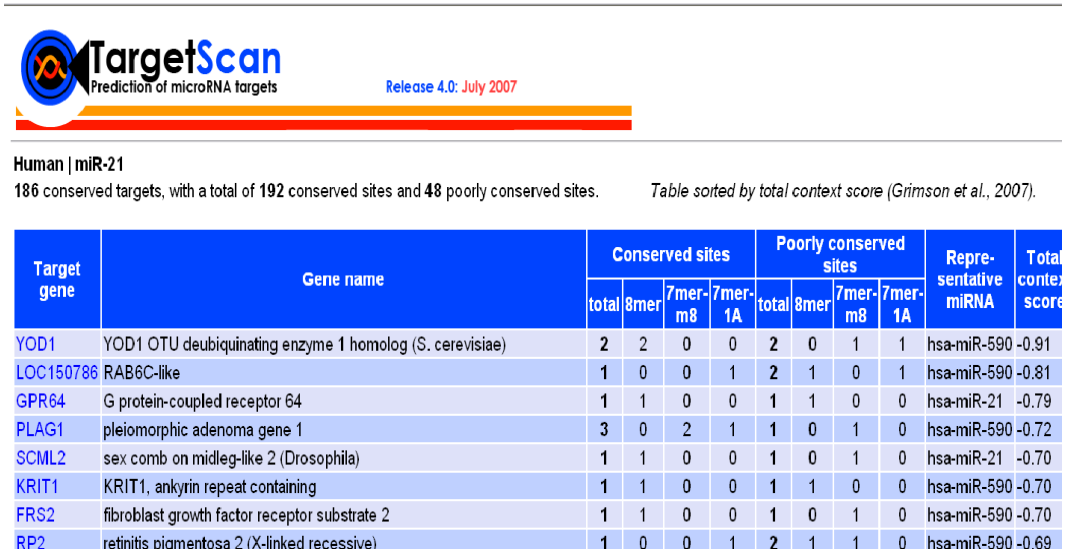

Figure 2.7: TargetScan web interface, microRNA targets search page

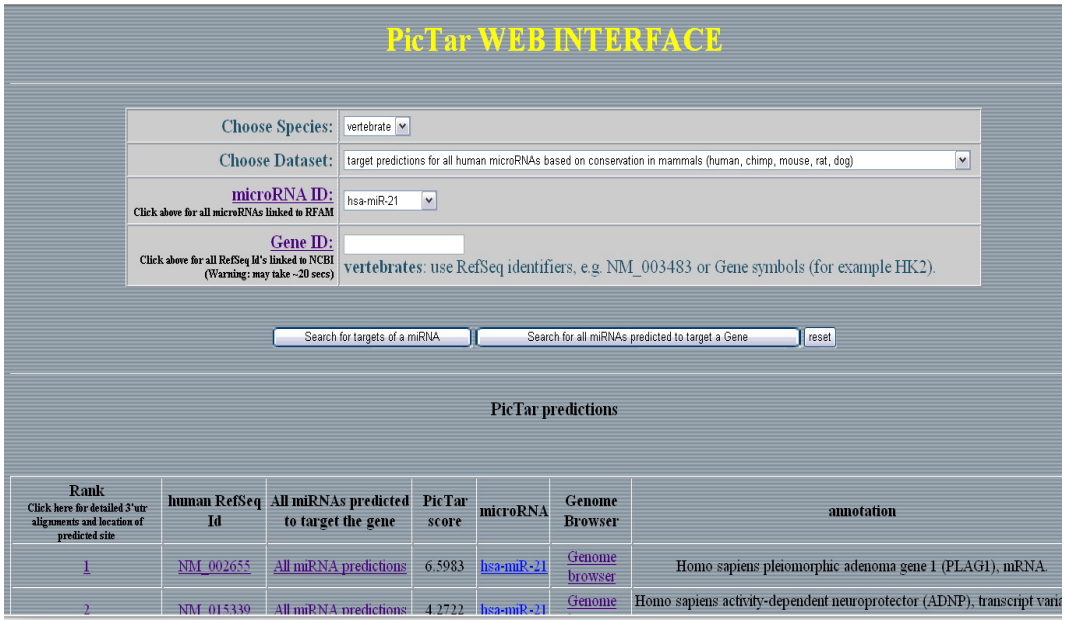

Figure 2.8: PicTar web interface, microRNA targets search page

CHAPTER 3

RESULTS AND DISCUSSION

3.1 MicroRNAs Mapping to Reported Common Genomic Instability Regions in Breast Cancer

Literature research on more than 40 publications on common genomic instabilities in breast resulted in several regions. Among these, 18 regions were selected for finding microRNAs mapping these regions.

These genomic instabilities were reported as loss (homozygous deletion or loss of heterozygosity-LOH), gain (amplifications), and genomic imbalances (reported as loss or gain) by using different methods such as CGH (Comparative Genomic Hybridization) or microarray analysis. Selected regions include losses in: **2q** [26], **3p** [81], **3p21** [14], [82], [83], **3q13.3** [29], **5q32** [14], [84], [85], **8p11-21** [86], **8p21** [81], [86], **8p21-8p23** [14], [81], [87], [88], **11q23-24** [89], [90], [91], **13q14** [92], [81], [29], [93], **17q21** [81], [94], [95], [96], [97], **19p13** [29], [98], [99], **21q21** [100], and **Xq21** [29]. Gains were found in: **2q31-32** [101], **3q** [102], [103], **8p11-12** [104], [105], [106], **8p23** [14], **11q23-24** [91], **13q31** [29], [107], **17q22-24** [108], [109], [110], **17q23** [95], [109], [21], [110], [108], [109], [111], [110], [112], and **20p** [21], [113], [112].

Boundaries of lost or gained regions were defined by SNP markers when available in reports. UCSC Genome Browser (According to Human May 2004 Assembly) and miRBase databases (Version 7.1) were used to find microRNAs

mapping between these boundaries. Thirty-nine microRNAs were found to be mapping these 18 regions. For example, hsa-mir-143 and hsa-mir-145 were located on common loss region 5q33, as shown in Figure 3.1.

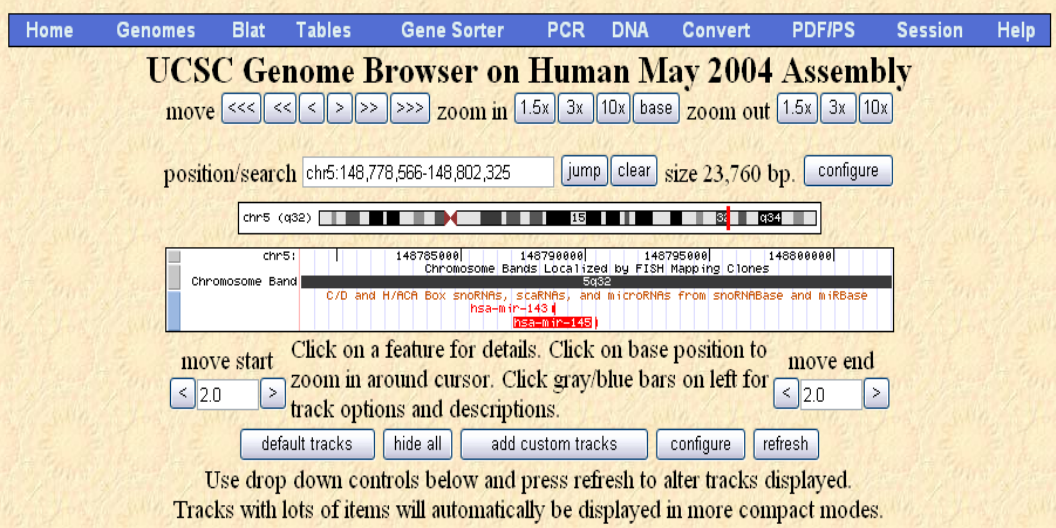

Figure 3.1: Example of finding microRNAs mapping to common loss region by using UCSC Genome Browser. Hsa-mir-143 and hsa-mir-145 were found to be mapping to 5q33 region.

Among 39 microRNAs selected, 16 of them were mapping to common loss regions, 13 of them were in common gain regions and 10 of them were mapping to regions reported as loss or gain. Literature research on common genomic instability regions in breast cancer and microRNAs mapping to these regions are summarized in Table 3.1.

Table 3-1: Selected common genomic instability regions in breast cancer and microRNAs mapping to these regions

	Genomic Loci	Gain / Loss	Samples	References	microRNA genes mapping
1	2q31-32	gain	MDA-MB-231	[101]	hsa-mir-10b
	2q	loss	breast tumors	[26]	
2	3p21	loss	breast cancer cell lines and breast tumors	[14],[82], [83]	hsa-mir-135a-1, let7g, hsa-mir-191, hsa-mir-138-1, hsa-mir-425
	3p	loss	breast tumors	[81]	
3	3q	gain	breast tumors	[102], [103]	hsa-mir-15b, hsa-mir-16-2
4	3q13.3	loss	MCF7	[29]	hsa-mir-198
5	5q32	loss	breast tumors	[14], [84], [85]	hsa-mir-143, hsa-mir-145
6	8p11-12	gain	breast cancer cell lines and breast tumors	[104], [105], [106]	hsa-mir-486
	8p11-21	loss	breast tumors	[86]	
7	8p21	loss	breast tumors	[81], [86]	hsa-mir-320
8	8p21-8p23	loss	breast cancer cell lines and breast tumors	[14], [81], [87], [88]	hsa-mir-383, hsa-mir-124a-1
		gain	breast tumors	[14]	
9	11q23-24	gain	breast tumors	[91]	hsa-mir-34c, hsa-mir-34b, hsa-mir-100, hsa-let7a-2, hsa-mir-125b-1
		loss	breast tumors	[89], [90], [91]	
10	13q14	loss	breast cancer cell lines and breast tumors	[92], [81], [29], [93]	hsa-mir-15a, hsa-mir-16-1
11	13q31	gain	breast cancer cell lines	[29], [107]	hsa-mir-17, hsa-mir-18a, hsa-mir-20a, hsa-mir-19a, hsa-mir-19b-1, hsa-mir-92-1
12	17q21	loss	breast tumors	[81], [94], [95], [96], [97]	hsa-mir-152
13	17q22-24	gain	breast cancer cell lines and breast tumors	[109], [21], [110]	hsa-mir-301, hsa-mir-142
14	17q23	gain	breast cancer cell lines and breast tumors	[95], [109], [21], [110], [108], [114], [111], [110], [112]	hsa-mir-21, hsa-mir-633
15	19p13	loss	breast tumors and cancer cell lines	[29], [98], [99]	hsa-mir-7-3
16	20p	gain	breast cancer cell lines and breast tumors	[21], [113], [112]	hsa-mir-103-2
17	21q21	loss	breast tumors	[100]	hsa-mir-125b-2
18	Xq21	loss	breast cancer cell lines	[29]	hsa-mir-384, hsa-mir-325, hsa-mir-361

3.2 Semi-quantitative Duplex PCR Results and Fold Changes of microRNAs

First, primers were specifically designed for each of the microRNA genes and *GAPDH,* a housekeeping gene. Primers were used in duplex PCR with 2 normal DNAs. In PCR optimizations, microRNA and *GAPDH* bands were set to equal or near equal intensities by adjusting PCR conditions such as primer: primer concentrations, Tm and cycle number were optimized for each microRNA. The assumption behind this approach was that normal genomes are considered to have equal amounts (2 copies) of each gene (microRNA and *GAPDH*). On the other hand, cancer genomes may show imbalances in other genes but are considered to have 2 copies of *GAPDH* gene as it is a housekeeping gene, despite the fact that some cancer cell lines showed imbalanced *GAPDH* gene as well (i.e., CAL51). Then, using optimized conditions, 36 pre-microRNA DNA regions were successfully co-amplified with *GAPDH* gene by using semi-quantitative duplex PCR in 20 breast cancer cell lines, 2 immortalized mammary cell lines and 2 normal DNAs.

PCR results were further analyzed for fold changes of microRNAs by using Scion Image densitometry analysis program that detects band intensities from agarose gel images and creates peaks. Area of each peak is attributed to a value. Values of mir/gapdh for each cell lines were compared to mir/gapdh ratios of normal DNAs resulted in a normalized fold change all microRNAs in each cell line.

Fold changes calculated for each microRNA in cancer cells versus controls were classified with the following cut off values and represented as 0- 0.5 fold (loss, ▨), 0.5-1.5 folds (no significant change, □), 1.5-2.5 folds (low gain, ▩), 2.5-4 folds (moderate gain, ■) and > 4 folds (significant gain, ■). Semi-quantitative duplex PCR results, fold changes calculates and fold graphs for 36

microRNAs are shown in Figure 3.3-38. Analyses results showed that in 61% (22/36) of selected microRNAs exhibited genomic instabilities (loss or moderate to significant gain) in at least 3 cell lines of 22 analyzed.

3.2.1 Fold Change Results for microRNAs mapping to common gain regions

MicroRNAs mapping to common gain regions showed both gains and losses in some cell lines. For instance, mir-17-92 polycistron, located on 13q31 reported as gain region, encodes hsa-mir-17, hsa-mir-18a, hsa-mir-19a, hsa-mir-19b-1, hsa-mir-20a, and hsa-mir-92-1 (Figure 3.2). These clustered microRNAs were previously found to be amplified in B cell lymphomas and lung cancers [66].

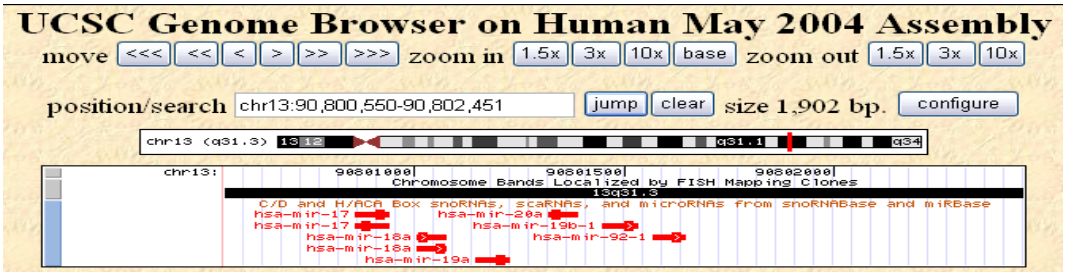

Figure 3.2: mir-17-92 polycistron mapping to common loss region 13q31
(Figure taken from UCSC Genome Browser)

Fold change calculations on these clustered microRNAs showed that there were low gains in some cell lines but no consistent gain along all breast cancer cell lines was detected. Hsa-mir-92-1 showed significant gain (more than 4 fold) in BT-549 (see Figure 3.3). Interestingly, hsa-mir-19a showed loss in 15 cell lines (see Figure 3 4), 7 of them were consistent with hsa-mir-19b-loss (MDA-MB-435,

MDA-MB-361, BT-549, SKBR3, BT20, HS578T, and MDA-MB-468) as well as immortalized cell lines MCF10 and HPV4-12 (Figure 3.5).

Moreover, hsa-mir-301, located on 17q22, showed moderate gains in 27% (6/22) of the cell lines (Figure 3.6), hsa-mir-21, located on 17q23, showed moderate gains in 22% (5/22) of the cell lines and significant gain in MDA-MB-231 (Figure 3.7). Another microRNA located on 17q23, hsa-mir-633, showed moderate gains in 18% (4/22) of the cell lines (Figure 3.8), whereas hsa-mir-103-2 showed significant gain in MDA-MB-231 (Figure 3.9)

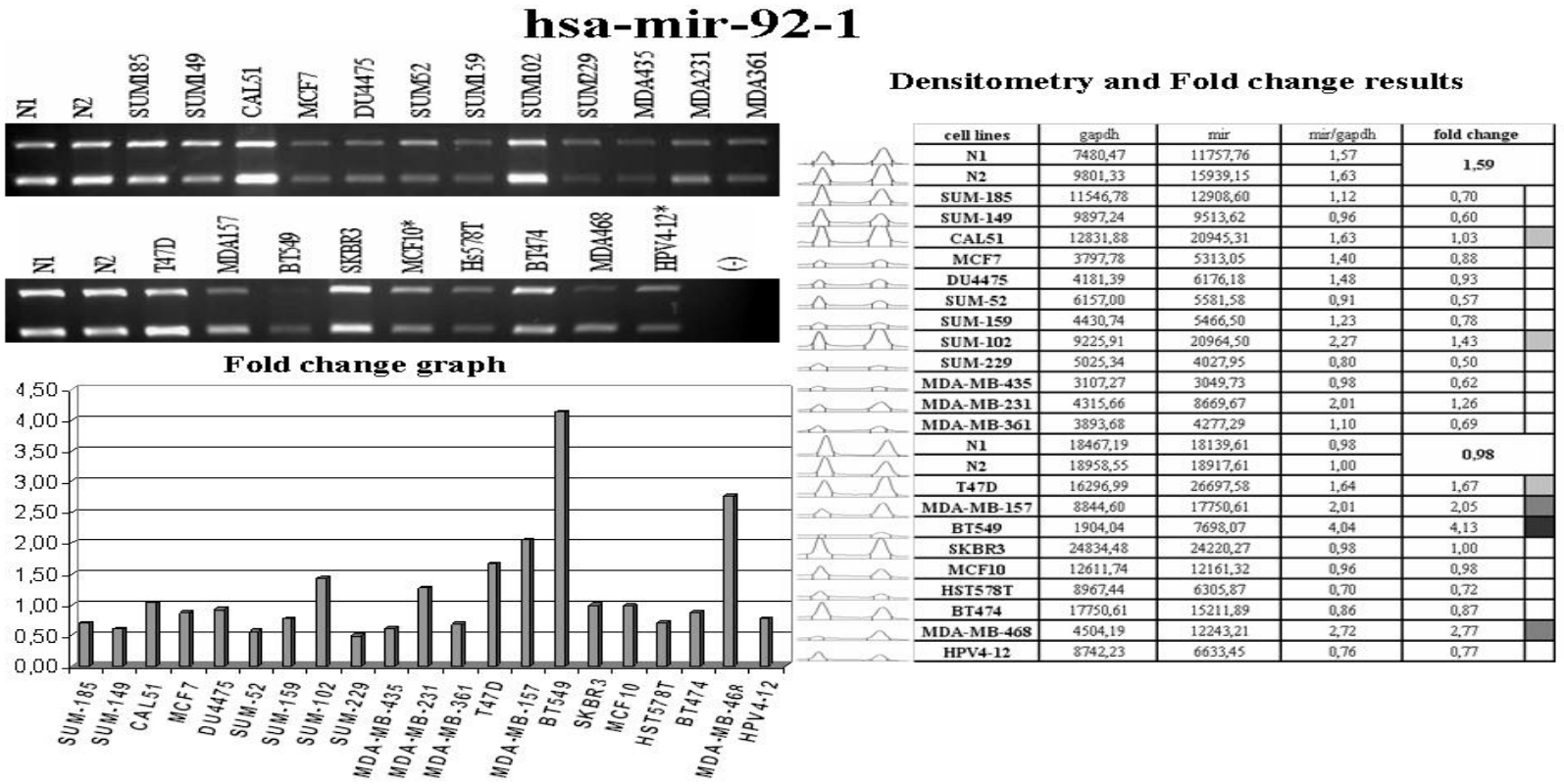

cell lines	gapdh	mir	mir/gapdh	fold change
N1	7480,47	11757,76	1,57	1,59
N2	9801,33	15939,15	1,63	
SUM-185	11546,78	12908,60	1,12	0,70
SUM-149	9897,24	9513,62	0,96	0,60
CAL51	12831,88	20945,31	1,63	1,03
MCF7	3797,78	5313,05	1,40	0,88
DU4475	4181,39	6176,18	1,48	0,93
SUM-52	6157,00	5581,58	0,91	0,57
SUM-159	4430,74	5466,50	1,23	0,78
SUM-102	9225,91	20964,50	2,27	1,43
SUM-229	5025,34	4027,95	0,80	0,50
MDA-MB-435	3107,27	3049,73	0,98	0,62
MDA-MB-231	4315,66	8669,67	2,01	1,26
MDA-MB-361	3893,68	4277,29	1,10	0,69
N1	18467,19	18139,61	0,98	0,98
N2	18958,55	18917,61	1,00	
T47D	16296,99	26697,58	1,64	1,67
MDA-MB-157	8844,60	17750,61	2,01	2,05
BT549	1904,04	7698,07	4,04	4,13
SKBR3	24834,48	24220,27	0,98	1,00
MCF10	12611,74	12161,32	0,96	0,98
HST578T	8967,44	6305,87	0,70	0,72
BT474	17750,61	15211,89	0,86	0,87
MDA-MB-468	4504,19	12243,21	2,72	2,77
HPV4-12	8742,23	6633,45	0,76	0,77

Figure 3.3: hsa-mir-92-1 semi-quantitative duplex PCR results .
Upper bands are GAPDH and lower bands are microRNA genes. in gel images. Fold changes are represented as colored boxes from grey to black scale with increasing fold change respectively and dashed boxes represent fold changes of loss.

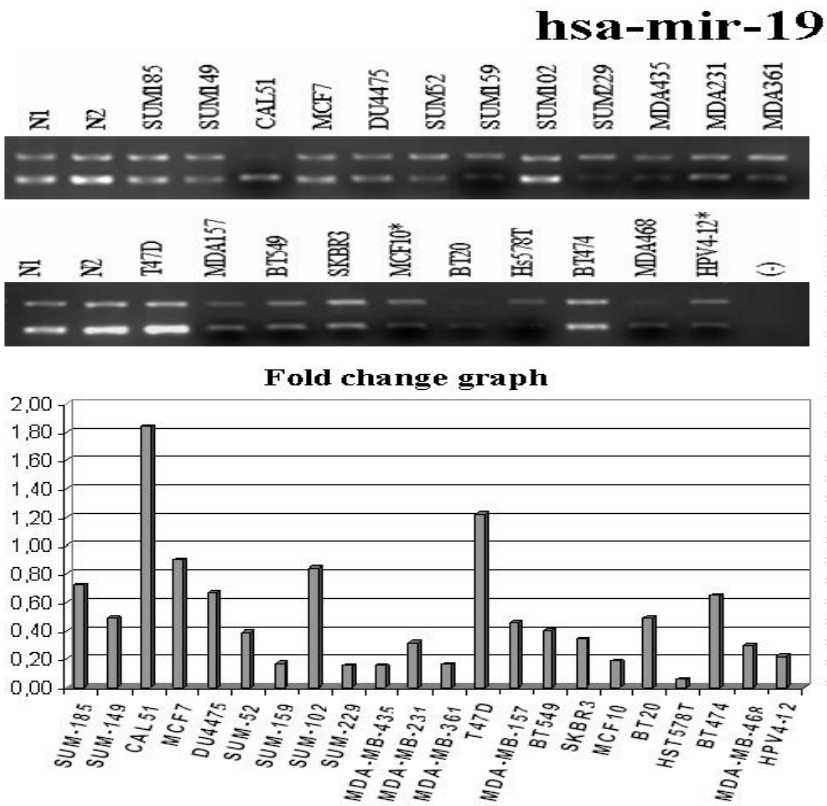

Densitometry and Fold change results

cell lines	gapdh	mir	mir/gapdh	fold change
N1	5333,76	8176,16	1,53	1,68
N2	6715,32	12275,57	1,83	
SUM-185	5775,40	6975,78	1,21	0,72
SUM-149	5311,11	4359,86	0,82	0,49
CAL51	1200,38	3703,05	3,08	1,84
MCF7	4110,73	6217,05	1,51	0,90
DU4475	3748,35	4212,65	1,12	0,67
SUM-52	4450,46	2921,68	0,66	0,39
SUM-159	4325,89	1223,03	0,28	0,17
SUM-102	5095,95	7224,92	1,42	0,84
SUM-229	4393,84	1121,11	0,26	0,15
MDA-MB-435	3080,22	792,70	0,26	0,15
MDA-MB-231	4642,97	2480,03	0,53	0,32
MDA-MB-361	6364,27	1766,59	0,28	0,17
N1	7827,02	15603,94	1,99	2,06
N2	10957,82	23355,82	2,13	
T47D	11095,58	27901,75	2,51	1,22
MDA-MB-157	5397,51	5109,48	0,95	0,46
BT549	6775,07	5572,84	0,82	0,40
SKBR3	10669,79	7538,98	0,71	0,34
MCF10	6800,11	2579,78	0,38	0,18
BT20	1953,62	1978,67	1,01	0,49
HST578T	5284,80	626,16	0,12	0,06
BT474	10143,81	13550,13	1,34	0,65
MDA-MB-468	4257,90	2604,83	0,61	0,30
HPV4-12	6173,95	2855,30	0,46	0,22

Figure 3.4: hsa-mir-19a semi-quantitative duplex PCR results
Upper bands are GAPDH and lower bands are microRNA genes. in gel images. Fold changes are represented as colored boxes from grey to black scale with increasing fold change respectively and dashed boxes represent losses.

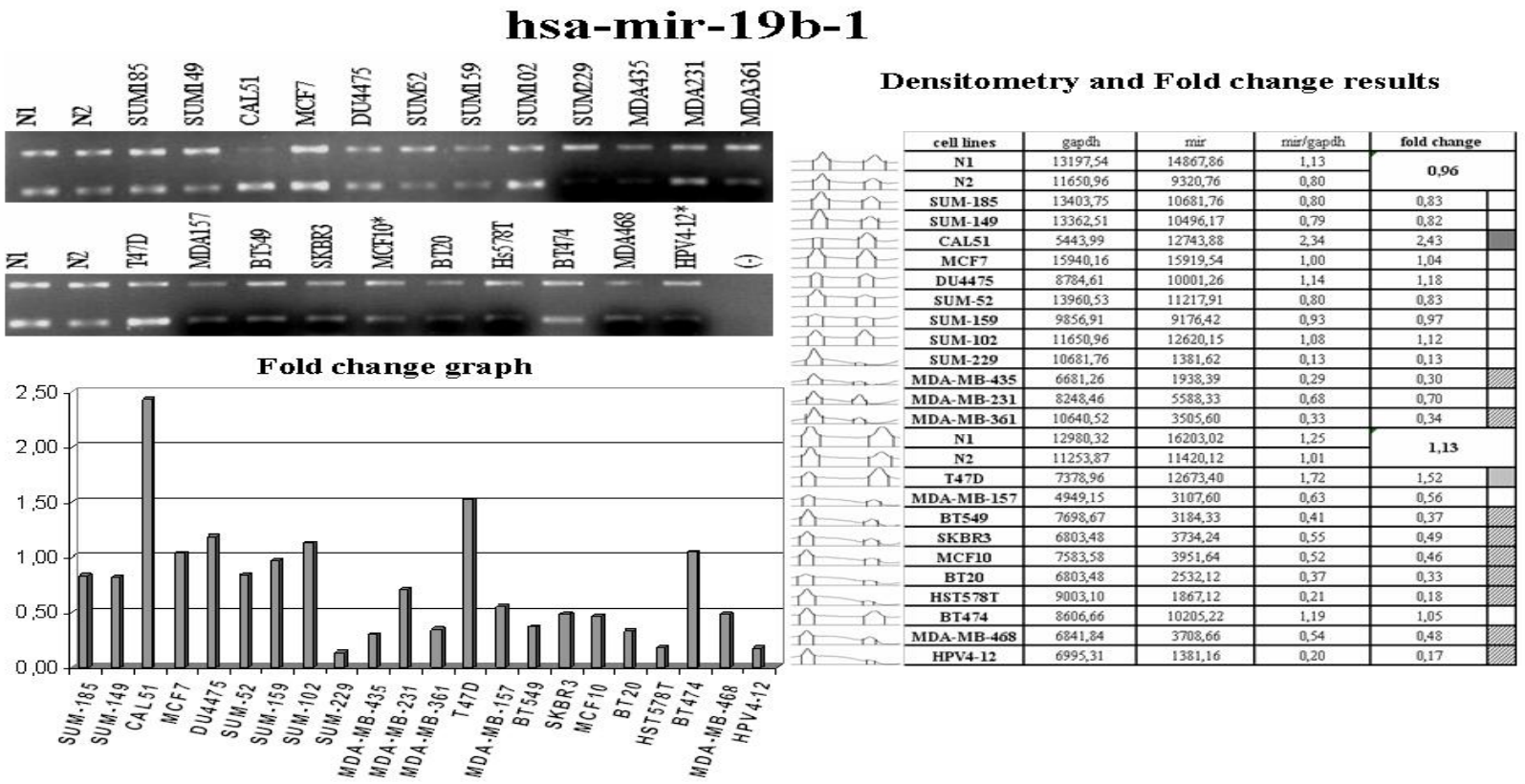

cell lines	gapdh	mir	mir/gapdh	fold change
N1	13197,54	14867,86	1,13	0,96
N2	11650,96	9320,76	0,80	
SUM-185	13403,75	10681,76	0,80	0,83
SUM-149	13362,51	10496,17	0,79	0,82
CAL51	5443,99	12743,88	2,34	2,43
MCF7	15940,16	15919,54	1,00	1,04
DU4475	8784,61	10001,26	1,14	1,18
SUM-52	13960,53	11217,91	0,80	0,83
SUM-159	9856,91	9176,42	0,93	0,97
SUM-102	11650,96	12620,15	1,08	1,12
SUM-229	10681,76	1381,62	0,13	0,13
MDA-MB-435	6681,26	1938,39	0,29	0,30
MDA-MB-231	8248,46	5588,33	0,68	0,70
MDA-MB-361	10640,52	3505,60	0,33	0,34
N1	12980,32	16203,02	1,25	1,13
N2	11253,87	11420,12	1,01	
T47D	7378,96	12673,40	1,72	1,52
MDA-MB-157	4949,15	3107,60	0,63	0,56
BT549	7698,67	3184,33	0,41	0,37
SKBR3	6803,48	3734,24	0,55	0,49
MCF10	7583,58	3951,64	0,52	0,46
BT20	6803,48	2532,12	0,37	0,33
HST578T	9003,10	1867,12	0,21	0,18
BT474	8606,66	10205,22	1,19	1,05
MDA-MB-468	6841,84	3708,66	0,54	0,48
HPV4-12	6995,31	1381,16	0,20	0,17

Figure 3.5: hsa-mir-19b-1 semi-quantitative duplex PCR result**s.**
Upper bands are GAPDH and lower bands are microRNA genes. in gel images. Fold changes are represented as colored boxes from grey to black scale with increasing fold change respectively and dashed boxes represent fold changes of loss.

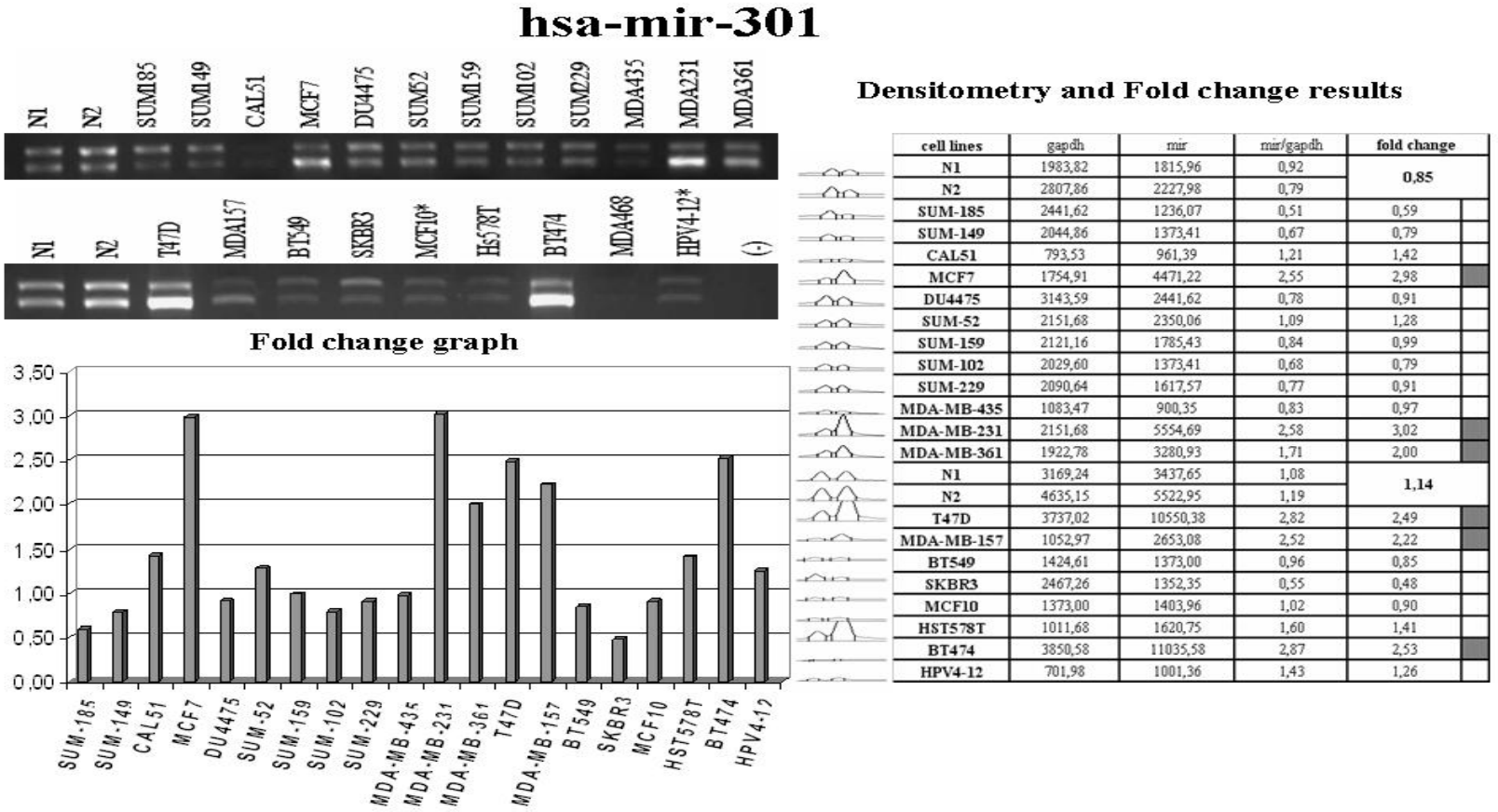

Densitometry and Fold change results

cell lines	gapdh	mir	mir/gapdh	fold change
N1	1983,82	1815,96	0,92	0,85
N2	2807,86	2227,98	0,79	
SUM-185	2441,62	1236,07	0,51	0,59
SUM-149	2044,86	1373,41	0,67	0,79
CAL51	793,53	961,39	1,21	1,42
MCF7	1754,91	4471,22	2,55	2,98
DU4475	3143,59	2441,62	0,78	0,91
SUM-52	2151,68	2350,06	1,09	1,28
SUM-159	2121,16	1785,43	0,84	0,99
SUM-102	2029,60	1373,41	0,68	0,79
SUM-229	2090,64	1617,57	0,77	0,91
MDA-MB-435	1083,47	900,35	0,83	0,97
MDA-MB-231	2151,68	5554,69	2,58	3,02
MDA-MB-361	1922,78	3280,93	1,71	2,00
N1	3169,24	3437,65	1,08	1,14
N2	4635,15	5522,95	1,19	
T47D	3737,02	10550,38	2,82	2,49
MDA-MB-157	1052,97	2653,08	2,52	2,22
BT549	1424,61	1373,00	0,96	0,85
SKBR3	2467,26	1352,35	0,55	0,48
MCF10	1373,00	1403,96	1,02	0,90
HST578T	1011,68	1620,75	1,60	1,41
BT474	3850,58	11035,58	2,87	2,53
HPV4-12	701,98	1001,36	1,43	1,26

Figure 3.6: hsa-mir-301 semi-quantitative duplex PCR results.
Upper bands are GAPDH and lower bands are microRNA genes. in gel images. Fold changes are represented as colored boxes from grey to black scale with increasing fold change respectively and dashed boxes represent fold changes of loss.

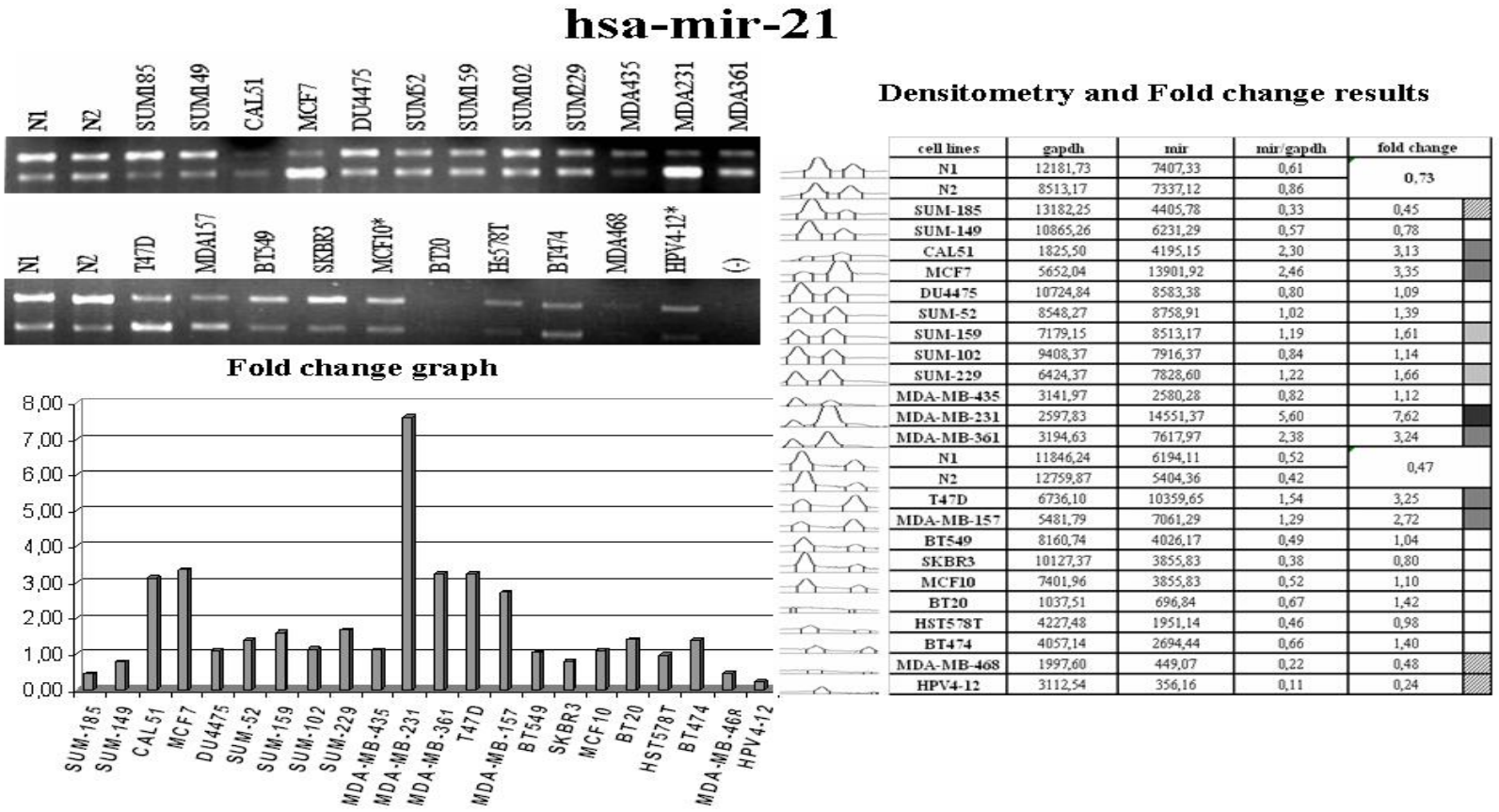

Densitometry and Fold change results

cell lines	gapdh	mir	mir/gapdh	fold change
N1	12181,73	7407,33	0,61	0,73
N2	8513,17	7337,12	0,86	
SUM-185	13182,25	4405,78	0,33	0,45
SUM-149	10865,26	6231,29	0,57	0,78
CAL51	1825,50	4195,15	2,30	3,13
MCF7	5652,04	13901,92	2,46	3,35
DU4475	10724,84	8583,38	0,80	1,09
SUM-52	8548,27	8758,91	1,02	1,39
SUM-159	7179,15	8513,17	1,19	1,61
SUM-102	9408,37	7916,37	0,84	1,14
SUM-229	6424,37	7828,60	1,22	1,66
MDA-MB-435	3141,97	2580,28	0,82	1,12
MDA-MB-231	2597,83	14551,37	5,60	7,62
MDA-MB-361	3194,63	7617,97	2,38	3,24
N1	11846,24	6194,11	0,52	0,47
N2	12759,87	5404,36	0,42	
T47D	6736,10	10359,65	1,54	3,25
MDA-MB-157	5481,79	7061,29	1,29	2,72
BT549	8160,74	4026,17	0,49	1,04
SKBR3	10127,37	3855,83	0,38	0,80
MCF10	7401,96	3855,83	0,52	1,10
BT20	1037,51	696,84	0,67	1,42
HST578T	4227,48	1951,14	0,46	0,98
BT474	4057,14	2694,44	0,66	1,40
MDA-MB-468	1997,60	449,07	0,22	0,48
HPV4-12	3112,54	356,16	0,11	0,24

Figure 3.7: hsa-mir-21 semi-quantitative duplex PCR results **.**
Upper bands are GAPDH and lower bands are microRNA genes. in gel images. Fold changes are represented as colored boxes from grey to black scale with increasing fold change respectively and dashed boxes represent fold changes of loss.

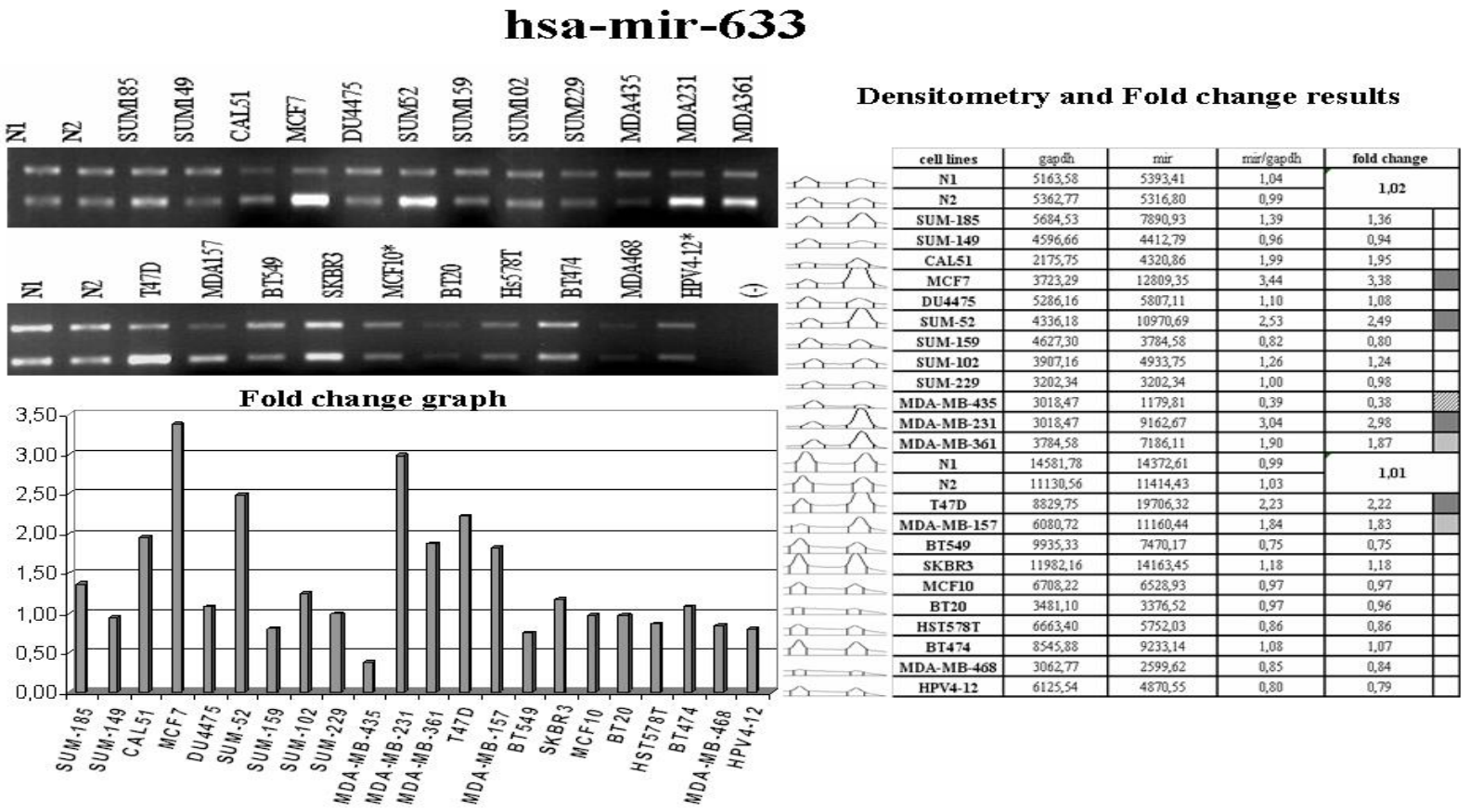

cell lines	gapdh	mir	mir/gapdh	fold change
N1	5163,58	5393,41	1,04	1,02
N2	5362,77	5316,80	0,99	
SUM-185	5684,53	7890,93	1,39	1,36
SUM-149	4596,66	4412,79	0,96	0,94
CAL51	2175,75	4320,86	1,99	1,95
MCF7	3723,29	12809,35	3,44	3,38
DU4475	5286,16	5807,11	1,10	1,08
SUM-52	4336,18	10970,69	2,53	2,49
SUM-159	4627,30	3784,58	0,82	0,80
SUM-102	3907,16	4933,75	1,26	1,24
SUM-229	3202,34	3202,34	1,00	0,98
MDA-MB-435	3018,47	1179,81	0,39	0,38
MDA-MB-231	3018,47	9162,67	3,04	2,98
MDA-MB-361	3784,58	7186,11	1,90	1,87
N1	14581,78	14372,61	0,99	1,01
N2	11130,56	11414,43	1,03	
T47D	8829,75	19706,32	2,23	2,22
MDA-MB-157	6080,72	11160,44	1,84	1,83
BT549	9935,33	7470,17	0,75	0,75
SKBR3	11982,16	14163,45	1,18	1,18
MCF10	6708,22	6528,93	0,97	0,97
BT20	3481,10	3376,52	0,97	0,96
HST578T	6663,40	5752,03	0,86	0,86
BT474	8545,88	9233,14	1,08	1,07
MDA-MB-468	3062,77	2599,62	0,85	0,84
HPV4-12	6125,54	4870,55	0,80	0,79

Figure 3.8: hsa-mir-633 semi-quantitative duplex PCR results**.**
Upper bands are GAPDH and lower bands are microRNA genes. in gel images. Fold changes are represented as colored boxes from grey to black scale with increasing fold change respectively and dashed boxes represent fold changes of loss.

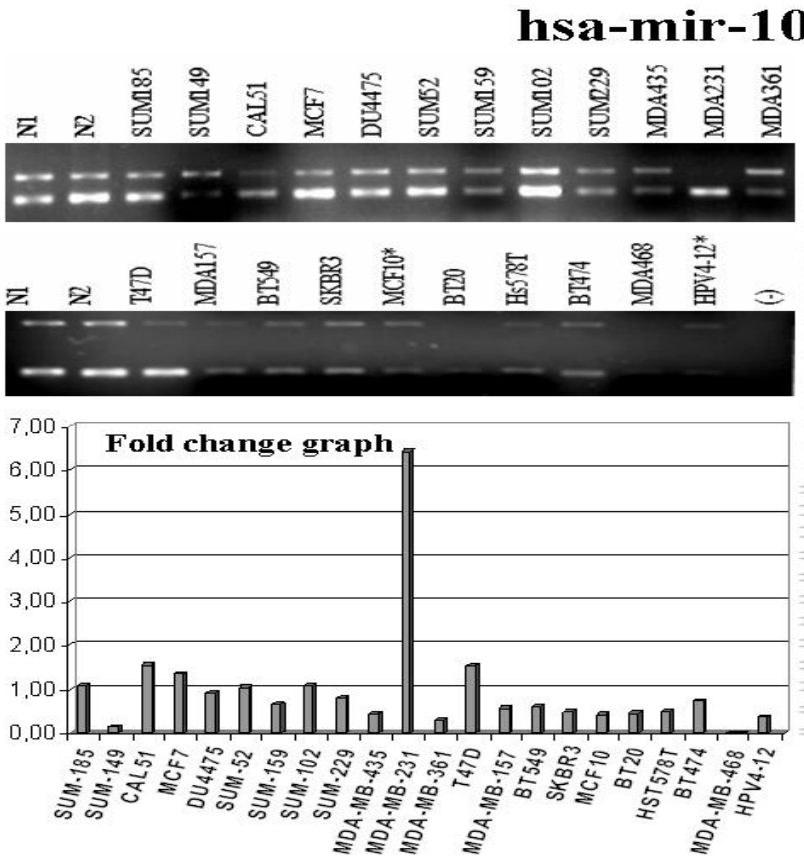

Densitometry and Fold change results

cell lines	gapdh	mir	mir/gapdh	fold change	
N1	9362,10	11363,87	1,21	1,52	
N2	8022,46	14659,08	1,83		
SUM-185	7036,97	11564,04	1,64	1,08	
SUM-149	4342,29	908,49	0,21	0,14	
CAL51	2109,55	4973,62	2,36	1,55	
MCF7	7760,69	15875,54	2,05	1,35	
DU4475	8746,17	11979,79	1,37	0,90	
SUM-52	7914,67	12580,32	1,59	1,05	
SUM-159	4203,71	4142,11	0,99	0,65	
SUM-102	9285,11	15228,81	1,64	1,08	
SUM-229	4758,04	5820,52	1,22	0,80	
MDA-MB-435	3541,58	2340,53	0,66	0,43	
MDA-MB-231	785,31	7683,70	9,78	6,44	
MDA-MB-361	5558,75	2371,32	0,43	0,28	
N1	10291,58	20766,61	2,02	1,97	
N2	14602,67	28086,30	1,92		
T47D	9777,92	29700,66	3,04	1,55	
MDA-MB-157	6934,43	7723,27	1,11	0,57	
BT549	8713,91	10236,55	1,17	0,60	
SKBR3	11924,29	11502,36	0,96	0,49	
MCF10	8420,39	6971,12	0,83	0,42	
BT20	4861,44	4384,47	0,90	0,46	
HST578T	7264,65	7062,85	0,97	0,49	
BT474	7796,65	11025,38	1,41	0,72	
MDA-MB-468	5118,27	5301,72	1,04	0,53	n/a
HPV4-12	5925,46	4292,75	0,72	0,37	

Figure 3.9: hsa-mir-103-2 semi-quantitative duplex PCR results **.**
Upper bands are GAPDH and lower bands are microRNA genes. in gel images. Fold changes are represented as colored boxes from grey to black scale with increasing fold change respectively and dashed boxes represent fold changes of loss.

3.2.2 Fold Change Results for microRNAs mapping to common loss regions

MicroRNAs mapping to common loss regions show consistent losses in hsa-mir-135a-1 (Figure 3.10) and hsa-mir-125b-2 (Figure 3.11). Hsa-mir-135a-1, located on 3p21, showed losses (less than 0.5 fold) in 31% (7/22) of the cell lines whereas hsa-mir-125b-2 showed losses in 54% (12/22) of the cell lines. Also, some microRNAs were observed to show low gains (1.5-2.5 folds) or losses in some cell lines. Besides these, hsa-mir-145 (Figure 3.12) showed low gains in 31% (7/22), and moderate gains (more than 2.5 folds) in 59 % (13/22) of the cell lines, unlike the previous reports on common loss region 5q32 [14], [85], [84].

Hsa-mir-138-1 in the MDA-MB-231 cell line (Figure 3.13) and hsa-mir-191 in the CAL51 and MCF10 cell lines (Figure 3.14) showed significant gains (more than 4 fold) are both are located on 3p21. Also, hsa-mir-361, located on Xq21, showed significant gain in MDA-MB-231 (Figure 3.15).

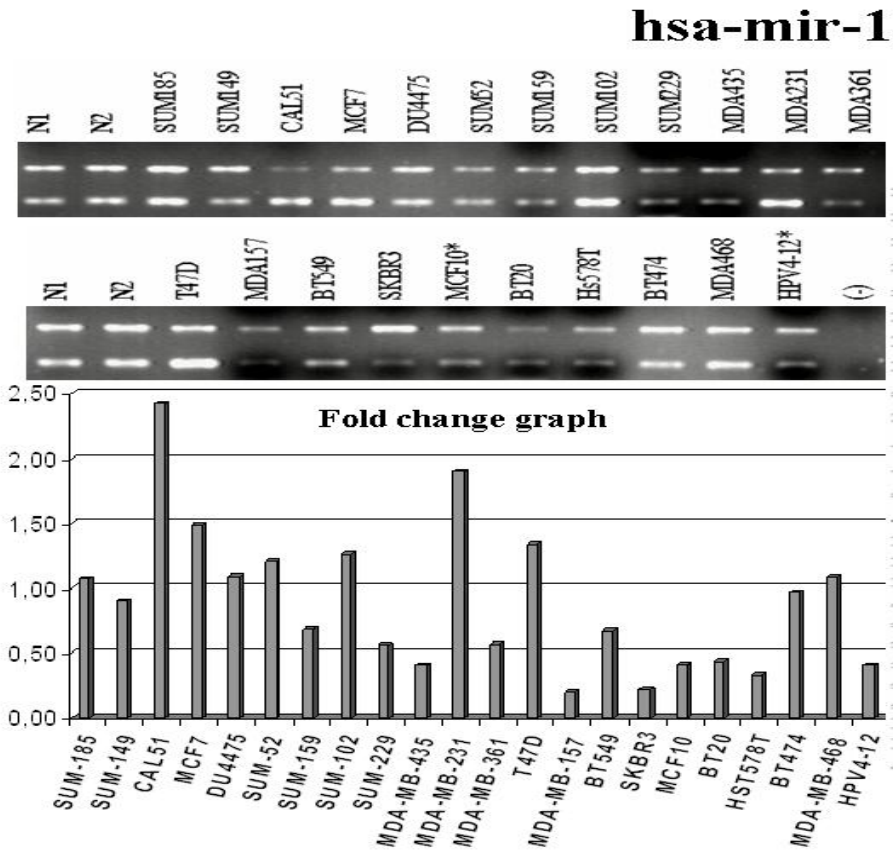

Densitometry and Fold change results

cell lines	gapdh	mir	mir/gapdh	fold change
N1	10839,49	10955,42	1,01	1,01
N2	11670,33	11863,54	1,02	
SUM-185	13950,29	15167,56	1,09	1,07
SUM-149	12810,31	11747,61	0,92	0,91
CAL51	5757,88	14143,51	2,46	2,42
MCF7	10163,23	15283,49	1,50	1,48
DU4475	12887,60	14259,44	1,11	1,09
SUM-52	9699,51	11882,87	1,23	1,21
SUM-159	10858,81	7554,80	0,70	0,69
SUM-102	12848,95	16462,12	1,28	1,26
SUM-229	6144,31	3497,23	0,57	0,56
MDA-MB-435	6105,67	2511,83	0,41	0,41
MDA-MB-231	7535,48	14529,94	1,93	1,90
MDA-MB-361	5854,49	3381,30	0,58	0,57
T47D	11193,08	15216,40	1,36	1,34
MDA-MB-157	5132,31	1031,62	0,20	0,20
BT549	7621,09	5183,89	0,68	0,67
SKBR3	11747,58	2579,05	0,22	0,22
MCF10	9516,70	3958,84	0,42	0,41
BT20	5016,25	2230,88	0,44	0,44
HST578T	7608,20	2553,26	0,34	0,33
BT474	11683,10	11463,88	0,98	0,97
MDA-MB-468	11708,89	12843,67	1,10	1,08
HPV4-12	9581,17	3920,16	0,41	0,40

Figure 3.10: hsa-mir-135a-1 semi-quantitative duplex PCR results
Upper bands are GAPDH and lower bands are microRNA genes. in gel images. Fold changes are represented as colored boxes from grey to black scale with increasing fold change respectively and dashed boxes represent fold changes of loss.

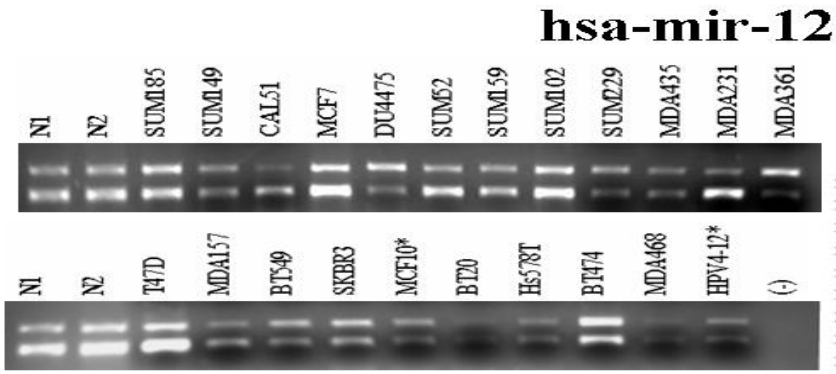

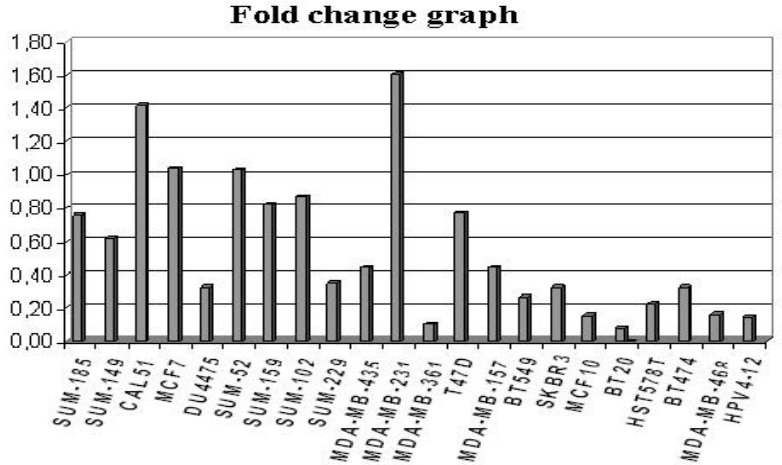

Densitometry and Fold change results

cell lines	gapdh	mir	mir/gapdh	fold change	
N1	11876,55	15847,22	1,33	1,335	
N2	14872,28	20030,61	1,35		
SUM-185	16538,54	16698,08	1,01	0,76	
SUM-149	9111,27	7515,91	0,82	0,62	
CAL51	4786,07	9075,81	1,90	1,42	
MCF7	16857,62	23380,86	1,39	1,04	
DU4475	14907,73	6470,06	0,43	0,33	
SUM-52	11202,96	15368,62	1,37	1,03	
SUM-159	11096,60	12160,17	1,10	0,82	
SUM-102	16254,93	18754,32	1,15	0,86	
SUM-229	10210,29	4786,07	0,47	0,35	
MDA-MB-435	6558,69	3846,59	0,59	0,44	
MDA-MB-231	6097,81	13064,21	2,14	1,60	
MDA-MB-361	13436,46	1772,62	0,13	0,10	
N1	5458,30	10740,84	1,97	1,76	
N2	7997,04	12430,08	1,55		
T47D	7840,81	10652,96	1,36	0,77	
MDA-MB-157	3329,66	2577,80	0,77	0,44	
BT549	5350,89	2519,21	0,47	0,27	
SKBR3	6464,03	3700,71	0,57	0,33	
MCF10	4481,86	1201,02	0,27	0,15	
BT20	3144,14	419,87	0,13	0,08	n/a
HST578T	4003,40	1591,60	0,40	0,23	
BT474	9168,77	5204,42	0,57	0,32	
MDA-MB-468	2323,93	673,74	0,29	0,16	
HPV4-12	2958,61	742,09	0,25	0,14	

Figure 3.11: hsa-mir-125b-2 semi-quantitative duplex PCR results
Upper bands are GAPDH and lower bands are microRNA genes. in gel images. Fold changes are represented as colored boxes from grey to black scale with increasing fold change respectively and dashed boxes represent fold changes of loss.

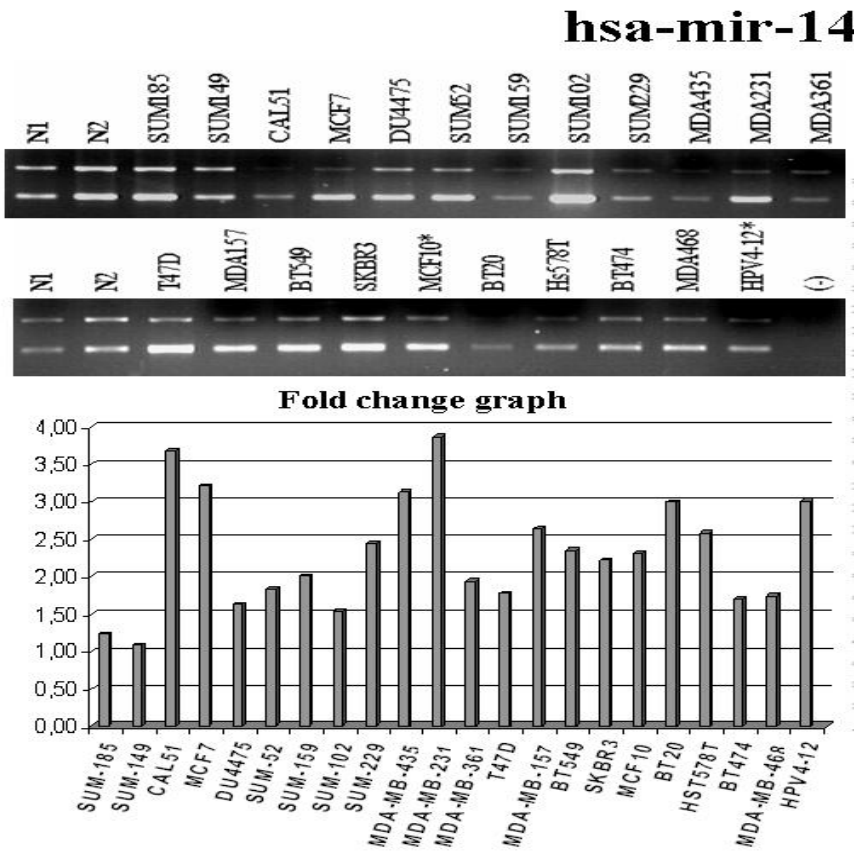

Densitometry and Fold change results

cell lines	gapdh	mir	mir/gapdh	fold change
N1	4515.94	6263.32	1,386	1,41
N2	5934.27	8464.55	1,426	
SUM-185	5457.71	9519.79	1,744	1,24
SUM-149	3767.07	5741.37	1,524	1,08
CAL51	726.18	3767.07	5,187	3,68
MCF7	1815.45	8214.93	4,525	3,21
DU4475	3596.87	8260.32	2,296	1,63
SUM-52	3608.21	9338.24	2,588	1,84
SUM-159	1872.19	5321.55	2,842	2,02
SUM-102	6127.16	13252.81	2,162	1,53
SUM-229	1713.33	5900.23	3,443	2,44
MDA-MB-435	680.80	3006.85	4,416	3,13
MDA-MB-231	1531.79	8362.44	5,459	3,87
MDA-MB-361	1168.70	3188.39	2,728	1,93
N1	4596.89	6616.34	1,439	1,50
N2	6177.91	9672.08	1,565	
T47D	6217.77	16580.71	2,666	1,78
MDA-MB-157	3374.60	13392.11	3,968	2,65
BT549	4158.46	14680.83	3,53	2,35
SKBR3	4716.47	15730.41	3,335	2,22
MCF10	3932.60	13644.54	3,469	2,31
BT20	1395.01	6270.91	4,495	3,00
HST578T	2271.88	8835.07	3,888	2,59
BT474	4211.61	10801.37	2,564	1,71
MDA-MB-468	4078.75	10668.52	2,615	1,74
HPV4-12	1913.16	8649.07	4,52	3,01

Figure 3.12: hsa-mir-145 semi-quantitative duplex PCR results
Upper bands are GAPDH and lower bands are microRNA genes. in gel images. Fold changes are represented as colored boxes from grey to black scale with increasing fold change respectively and dashed boxes represent fold changes of loss.

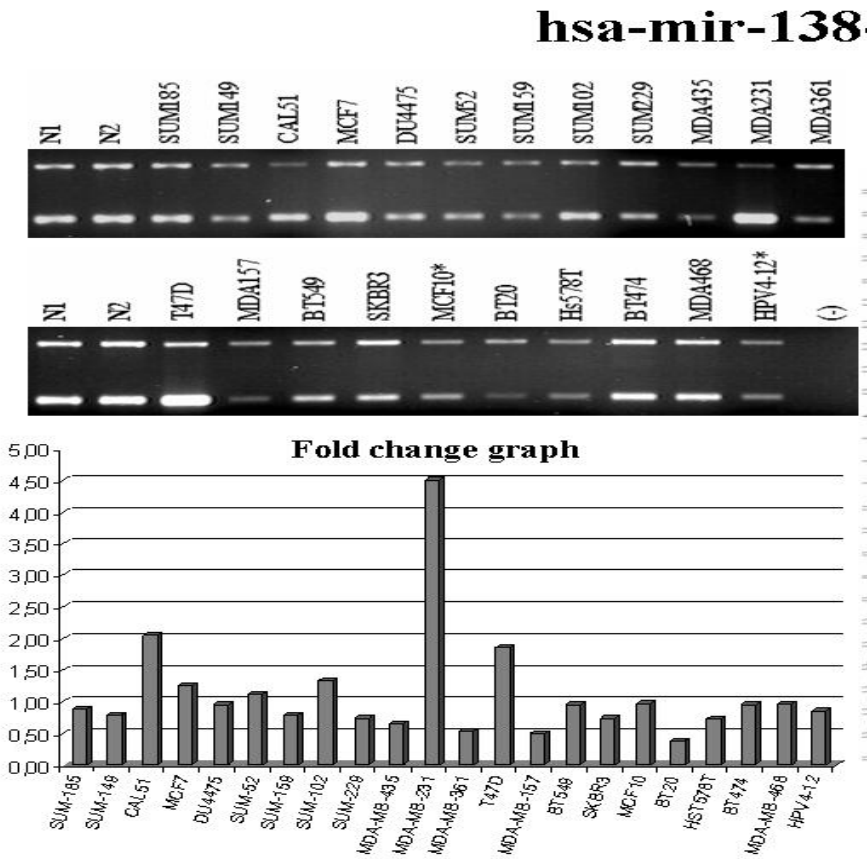

Densitometry and Fold change results

cell lines	gapdh	mir	mir/gapdh	fold change
N1	9730,65	17717,78	1,82	1,80
N2	10649,52	18895,83	1,77	
SUM-185	10720,20	16963,84	1,58	0,88
SUM-149	7186,07	10272,55	1,43	0,80
CAL51	5159,83	19037,19	3,69	2,05
MCF7	11686,20	26505,99	2,27	1,26
DU4475	8316,99	14277,90	1,72	0,96
SUM-52	6738,41	13618,19	2,02	1,12
SUM-159	6809,10	9683,52	1,42	0,79
SUM-102	8246,31	19838,26	2,41	1,34
SUM-229	9118,06	12110,29	1,33	0,74
MDA-MB-435	4217,40	4924,22	1,17	0,65
MDA-MB-231	3180,72	25799,17	8,11	4,51
MDA-MB-361	6974,02	6738,41	0,97	0,54
N1	12541,07	19334,94	1,54	1,51
N2	14120,59	20933,49	1,48	
T47D	10714,14	30163,26	2,82	1,86
MDA-MB-157	5937,50	4434,09	0,75	0,49
BT549	8792,07	12712,34	1,45	0,96
SKBR3	12883,61	14367,99	1,12	0,74
MCF10	7364,78	10828,33	1,47	0,97
BT20	8658,85	4966,95	0,57	0,38
HST578T	7498,00	8335,34	1,11	0,74
BT474	13092,95	18840,14	1,44	0,95
MDA-MB-468	11227,96	16347,15	1,46	0,96
HPV4-12	6222,96	8068,91	1,30	0,86

Figure 3.13:.hsa-mir-138-1 semi-quantitative duplex PCR results
Upper bands are GAPDH and lower bands are microRNA genes. in gel images. Fold changes are represented as colored boxes from grey to black scale with increasing fold change respectively and dashed boxes represent fold changes of loss.

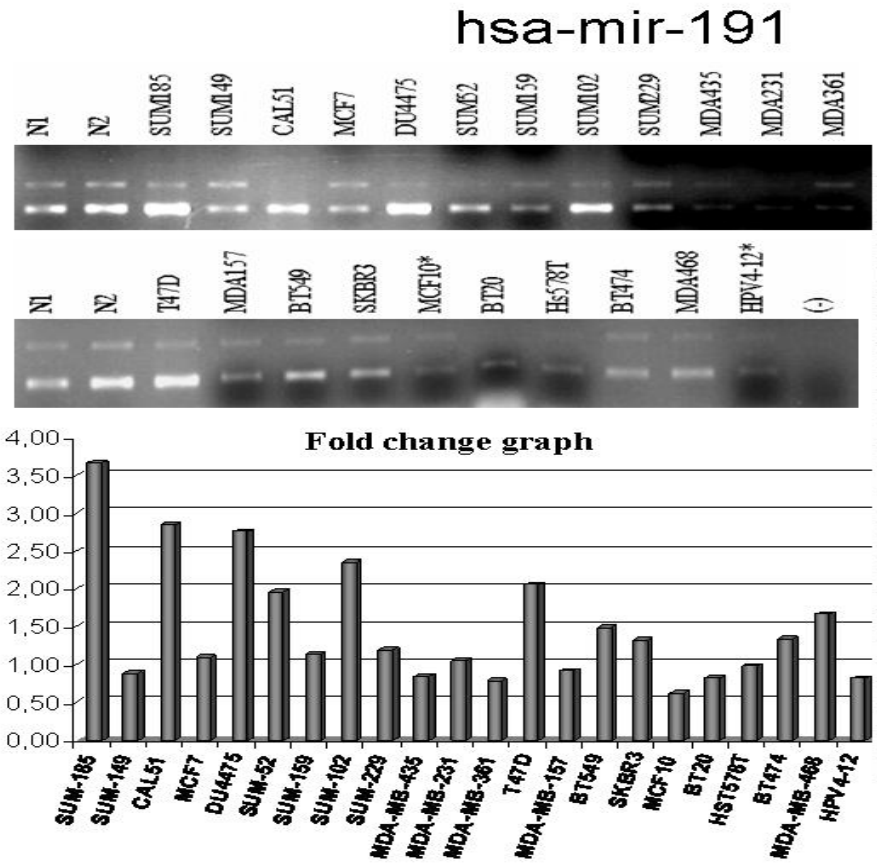

Densitometry and Fold change results

cell lines	gapdh	mir	mir/gapdh	fold change
N1	7719,67	10397,92	1,35	1,57
N2	7334,56	13093,68	1,79	
SUM-185	5233,97	19167,89	3,66	2,34
SUM-149	11448,22	10205,37	0,89	0,57
CAL51	5023,91	14284,02	2,84	1,82
MCF7	8910,01	9645,21	1,08	0,69
DU4475	7387,08	20340,72	2,75	1,76
SUM-52	4498,77	8839,99	1,96	1,25
SUM-159	5549,06	6301,77	1,14	0,73
SUM-102	5496,55	12901,13	2,35	1,50
SUM-229	3606,01	4306,21	1,19	0,76
MDA-MB-435	2573,22	2188,12	0,85	0,54
MDA-MB-231	1890,53	1978,06	1,05	0,67
MDA-MB-361	2240,63	1732,99	0,77	0,49
N1	9042,92	11334,03	1,25	1,65
N2	7810,58	15933,59	2,04	
T47D	7862,65	16124,52	2,05	1,25
MDA-MB-157	5415,34	4964,06	0,92	0,56
BT549	5050,84	7515,52	1,49	0,90
SKBR3	4703,71	6196,40	1,32	0,80
MCF10	4113,57	2551,46	0,62	0,38
BT20	1857,18	1527,40	0,82	0,50
HST578T	2898,59	2829,17	0,98	0,59
BT474	7012,17	9390,06	1,34	0,81
MDA-MB-468	5085,56	8435,43	1,66	1,01
HPV4-12	2395,25	1943,97	0,81	0,49

Figure 3.14: hsa-mir-191 semi-quantitative duplex PCR results
Upper bands are GAPDH and lower bands are microRNA genes. in gel images. Fold changes are represented as colored boxes from grey to black scale with increasing fold change respectively and dashed boxes represent fold changes of loss.

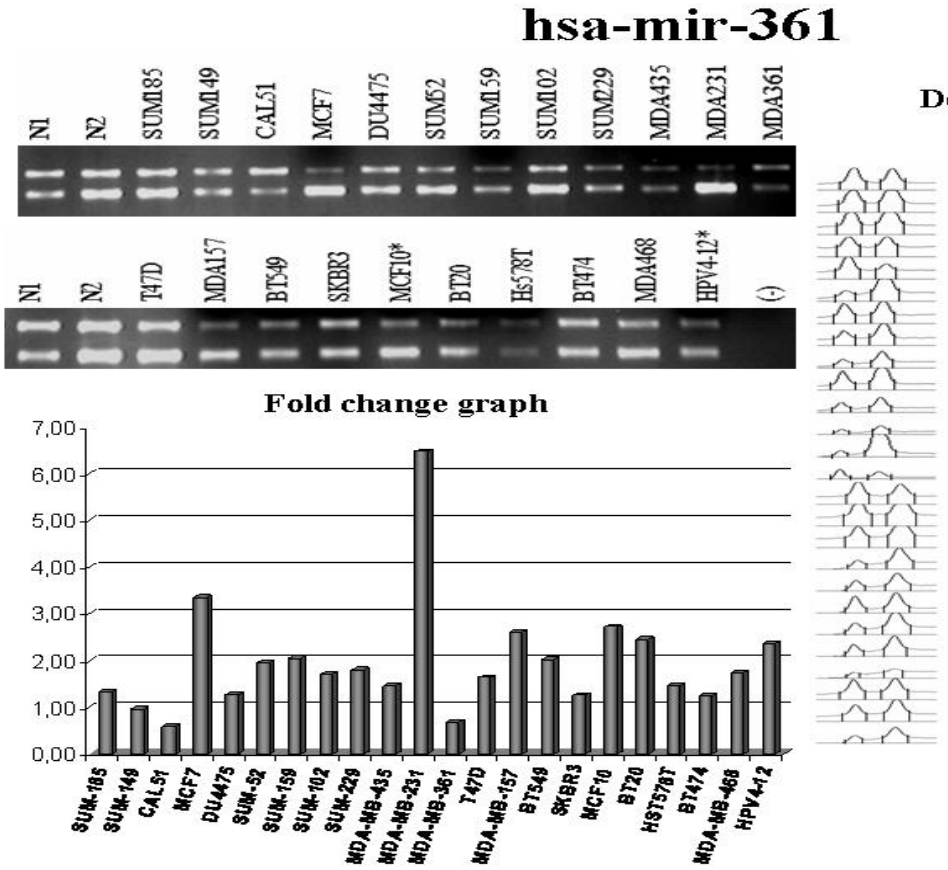

Densitometry and Fold change results

cell lines	gapdh	mir	mir/gapdh	fold change
N1	9989,29	8552,23	0,86	1,06
N2	9586,21	12162,39	1,27	
SUM-185	10322,26	14528,28	1,41	1,33
SUM-149	10304,74	10479,99	1,02	0,96
CAL51	9954,24	6081,20	0,61	0,58
MCF7	3890,56	13827,27	3,55	3,35
DU4475	6764,67	9148,08	1,35	1,27
SUM-52	4836,92	9989,29	2,07	1,94
SUM-159	2944,21	6396,65	2,17	2,05
SUM-102	6344,07	11478,92	1,81	1,70
SUM-229	2839,06	5397,72	1,90	1,79
MDA-MB-435	1542,21	2383,41	1,55	1,46
MDA-MB-231	2103,01	14440,65	6,87	6,47
MDA-MB-361	2471,03	1787,56	0,72	0,68
N1	9510,73	8106,77	0,85	0,99
N2	11412,88	12805,52	1,12	
T47D	8854,04	14175,52	1,60	1,62
MDA-MB-157	3645,78	9363,54	2,57	2,60
BT549	3226,85	6408,42	1,99	2,01
SKBR3	5276,19	6499,00	1,23	1,25
MCF10	3543,88	9465,44	2,67	2,71
BT20	3068,34	7382,14	2,41	2,44
HST578T	1845,53	2638,10	1,43	1,45
BT474	7178,34	8763,46	1,22	1,24
MDA-MB-468	5717,76	9714,53	1,70	1,72
HPV4-12	2434,29	5615,86	2,31	2,34

Figure 3.15: hsa-mir-361 semi-quantitative duplex PCR results
Upper bands are GAPDH and lower bands are microRNA genes. in gel images. Fold changes are represented as colored boxes from grey to black scale with increasing fold change respectively and dashed boxes represent fold changes of loss.

3.2.3 Fold Change Results for microRNAs mapping to common loss or gain regions

MicroRNAs mapping to genomic imbalance regions were found to be hsa-mir-10b, hsa-mir-198, hsa-mir-486, hsa-mir-383, hsa-mir-34, hsa-mir-125b-1, hsa-let-7a-2, and hsa-mir-100.

Among these 8 microRNAs reported in imbalanced regions (loss or gain), 4 microRNAs showed fold changes in at least 3 cell lines. Hsa-mir-383 exhibited moderate gain (more than 2.5 folds) in 13% (3/22) of the cell lines (MCF7, MDA-MB-231, and T47D) (Figure 3.16). Hsa-mir-125b-1 showed loss in 18% (4/22) of the cell lines (Figure 3.17). Hsa-let-7a-2 showed loss in 27% (6/22) of the cell lines whereas it showed moderate gain in 13% (3/22) of the cell lines (Figure 3.18). For significant gains, more than 4 fold, hsa-mir-100 exhibited gains in 2 cell lines (Figure 3.19) and hsa-mir-198 exhibited gain in MDA-MB-231 (Figure 3.20).

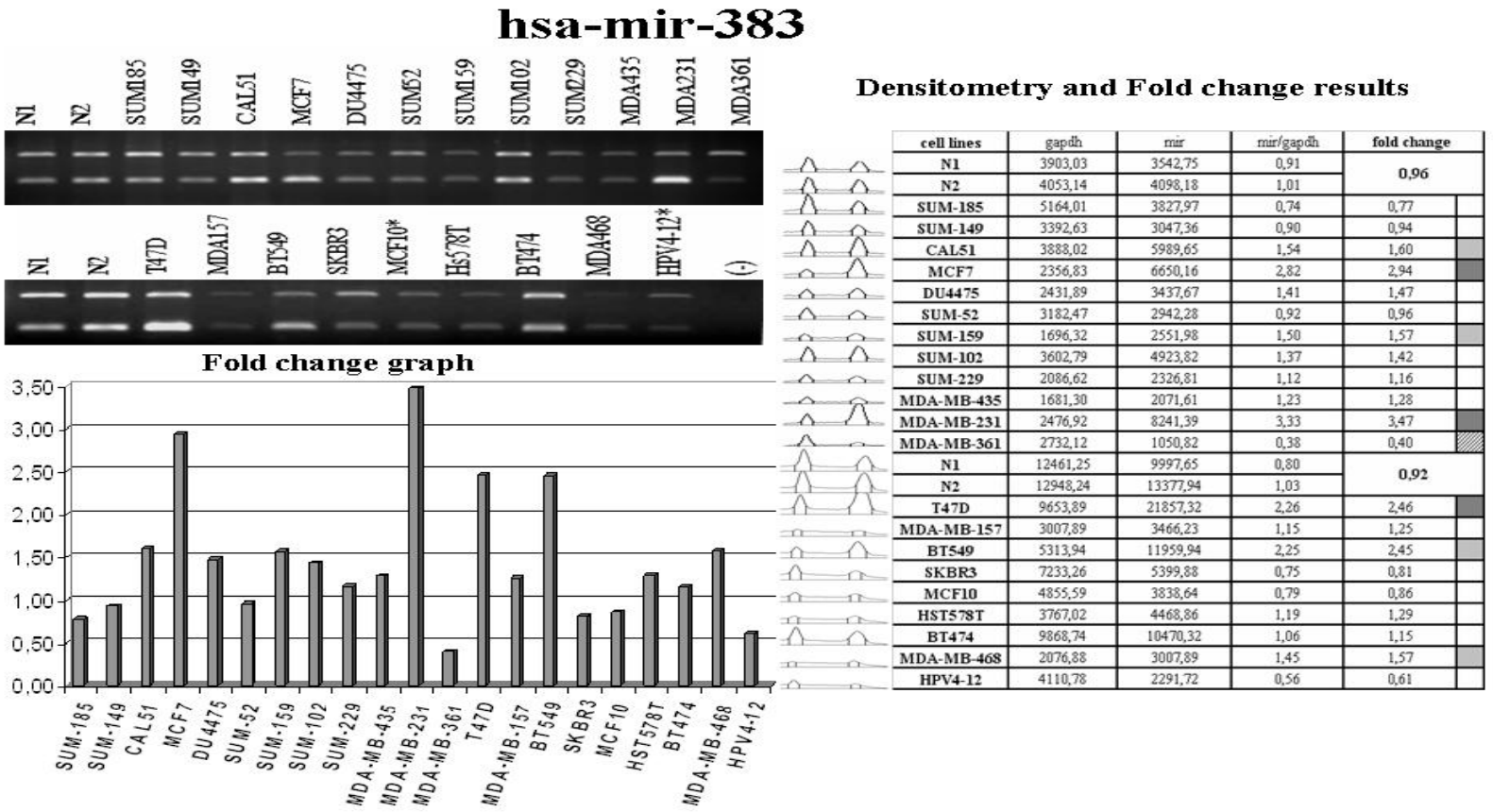

Densitometry and Fold change results

cell lines	gapdh	mir	mir/gapdh	fold change
N1	3903,03	3542,75	0,91	0,96
N2	4053,14	4098,18	1,01	
SUM-185	5164,01	3827,97	0,74	0,77
SUM-149	3392,63	3047,36	0,90	0,94
CAL51	3888,02	5989,65	1,54	1,60
MCF7	2356,83	6650,16	2,82	2,94
DU4475	2431,89	3437,67	1,41	1,47
SUM-52	3182,47	2942,28	0,92	0,96
SUM-159	1696,32	2551,98	1,50	1,57
SUM-102	3602,79	4923,82	1,37	1,42
SUM-229	2086,62	2326,81	1,12	1,16
MDA-MB-435	1681,30	2071,61	1,23	1,28
MDA-MB-231	2476,92	8241,39	3,33	3,47
MDA-MB-361	2732,12	1050,82	0,38	0,40
N1	12461,25	9997,65	0,80	0,92
N2	12948,24	13377,94	1,03	
T47D	9653,89	21857,32	2,26	2,46
MDA-MB-157	3007,89	3466,23	1,15	1,25
BT549	5313,94	11959,94	2,25	2,45
SKBR3	7233,26	5399,88	0,75	0,81
MCF10	4855,59	3838,64	0,79	0,86
HST578T	3767,02	4468,86	1,19	1,29
BT474	9868,74	10470,32	1,06	1,15
MDA-MB-468	2076,88	3007,89	1,45	1,57
HPV4-12	4110,78	2291,72	0,56	0,61

Figure 3.16: hsa-mir-383 semi-quantitative duplex PCR results
Upper bands are GAPDH and lower bands are microRNA genes. in gel images. Fold changes are represented as colored boxes from grey to black scale with increasing fold change respectively and dashed boxes represent fold changes of loss.

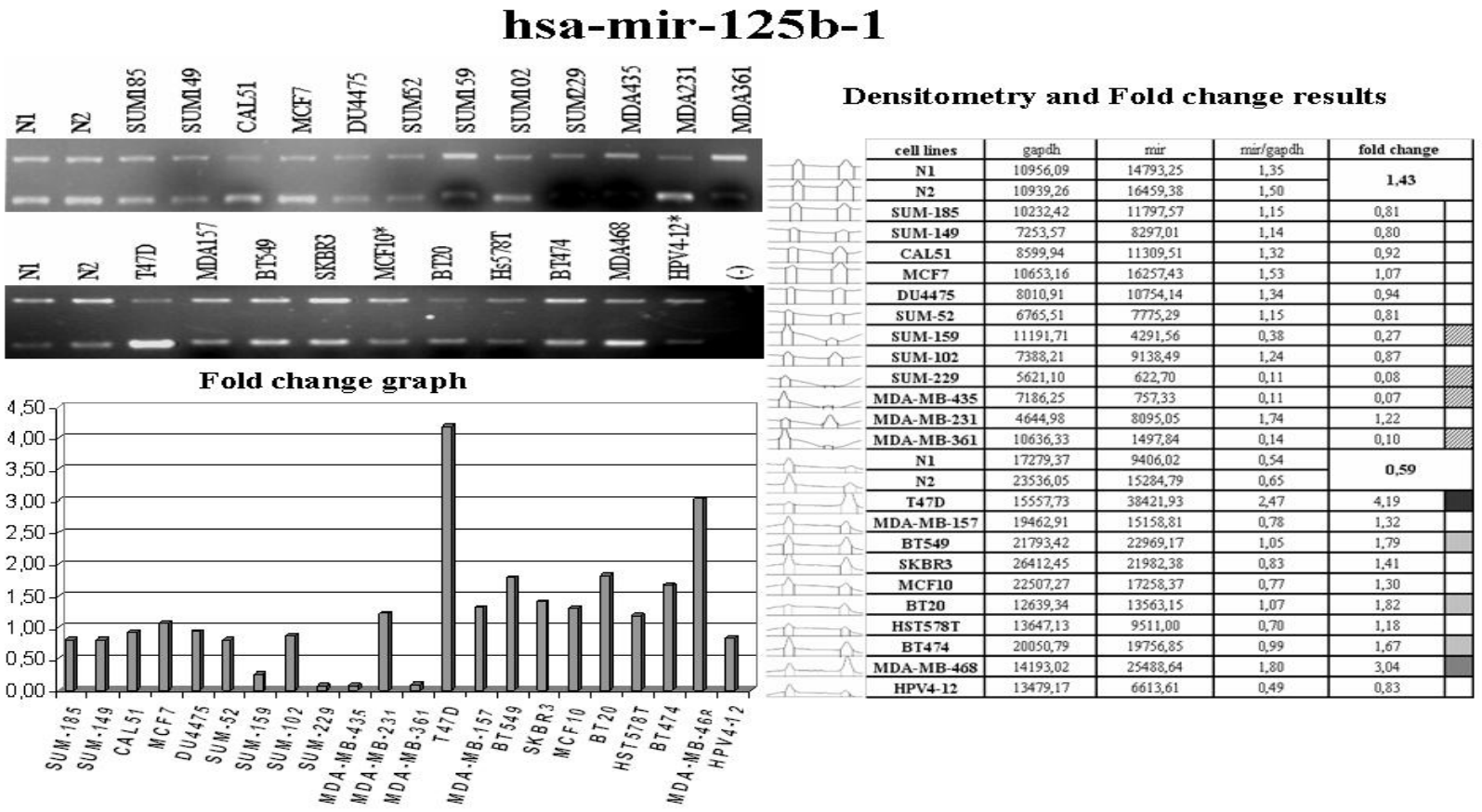

Densitometry and Fold change results

cell lines	gapdh	mir	mir/gapdh	fold change
N1	10956,09	14793,25	1,35	1,43
N2	10939,26	16459,38	1,50	
SUM-185	10232,42	11797,57	1,15	0,81
SUM-149	7253,57	8297,01	1,14	0,80
CAL51	8599,94	11309,51	1,32	0,92
MCF7	10653,16	16257,43	1,53	1,07
DU4475	8010,91	10754,14	1,34	0,94
SUM-52	6765,51	7775,29	1,15	0,81
SUM-159	11191,71	4291,56	0,38	0,27
SUM-102	7388,21	9138,49	1,24	0,87
SUM-229	5621,10	622,70	0,11	0,08
MDA-MB-435	7186,25	757,33	0,11	0,07
MDA-MB-231	4644,98	8095,05	1,74	1,22
MDA-MB-361	10636,33	1497,84	0,14	0,10
N1	17279,37	9406,02	0,54	0,59
N2	23536,05	15284,79	0,65	
T47D	15557,73	38421,93	2,47	4,19
MDA-MB-157	19462,91	15158,81	0,78	1,32
BT549	21793,42	22969,17	1,05	1,79
SKBR3	26412,45	21982,38	0,83	1,41
MCF10	22507,27	17258,37	0,77	1,30
BT20	12639,34	13563,15	1,07	1,82
HST578T	13647,13	9511,00	0,70	1,18
BT474	20050,79	19756,85	0,99	1,67
MDA-MB-468	14193,02	25488,64	1,80	3,04
HPV4-12	13479,17	6613,61	0,49	0,83

Figure 3.17: hsa-mir-125b-1 semi-quantitative duplex PCR results
Upper bands are GAPDH and lower bands are microRNA genes. in gel images. Fold changes are represented as colored boxes from grey to black scale with increasing fold change respectively and dashed boxes represent fold changes of loss.

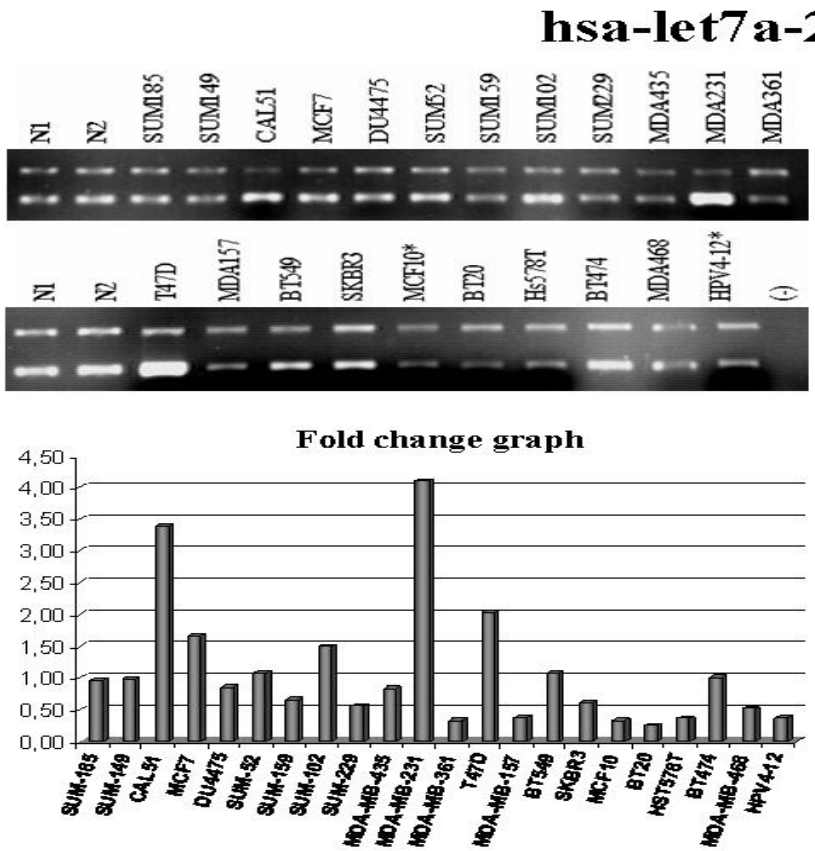

Densitometry and Fold change results

cell lines	gapdh	mir	mir/gapdh	fold change
N1	4667,85	8584,92	1,84	1,72
N2	7001,77	11196,3	1,60	
SUM-185	6479,49	10576,1	1,63	0,95
SUM-149	4814,74	8111,61	1,68	0,98
CAL51	2284,96	13334,37	5,84	3,39
MCF7	4537,28	12958,99	2,86	1,66
DU4475	6659,03	9727,4	1,46	0,85
SUM-52	6006,18	11033,09	1,84	1,07
SUM-159	5859,29	6610,06	1,13	0,66
SUM-102	6430,53	16517	2,57	1,49
SUM-229	7230,27	6887,52	0,95	0,55
MDA-MB-435	3525,37	5026,91	1,43	0,83
MDA-MB-231	2774,59	19552,73	7,05	4,10
MDA-MB-361	6593,74	3704,9	0,56	0,33
N1	9931,4	14890,01	1,50	1,51
N2	11759	17879,35	1,52	
T47D	8939,67	27484,89	3,07	2,04
MDA-MB-157	7310,41	4136,9	0,57	0,37
BT549	6162,85	9888,89	1,60	1,06
SKBR3	10554,76	9733,05	0,92	0,61
MCF10	6318,69	3131,01	0,50	0,33
BT20	9109,68	3357,69	0,37	0,24
HST578T	10073,07	5426,14	0,54	0,36
BT474	13402,43	20358,65	1,52	1,01
MDA-MB-468	10044,74	7735,44	0,77	0,51
HPV4-12	11263,14	6092,01	0,54	0,36

Figure 3.18: hsa-let-7a-2 semi-quantitative duplex PCR results
Upper bands are GAPDH and lower bands are microRNA genes. in gel images. Fold changes are represented as colored boxes from grey to black scale with increasing fold change respectively and dashed boxes represent fold changes of loss.

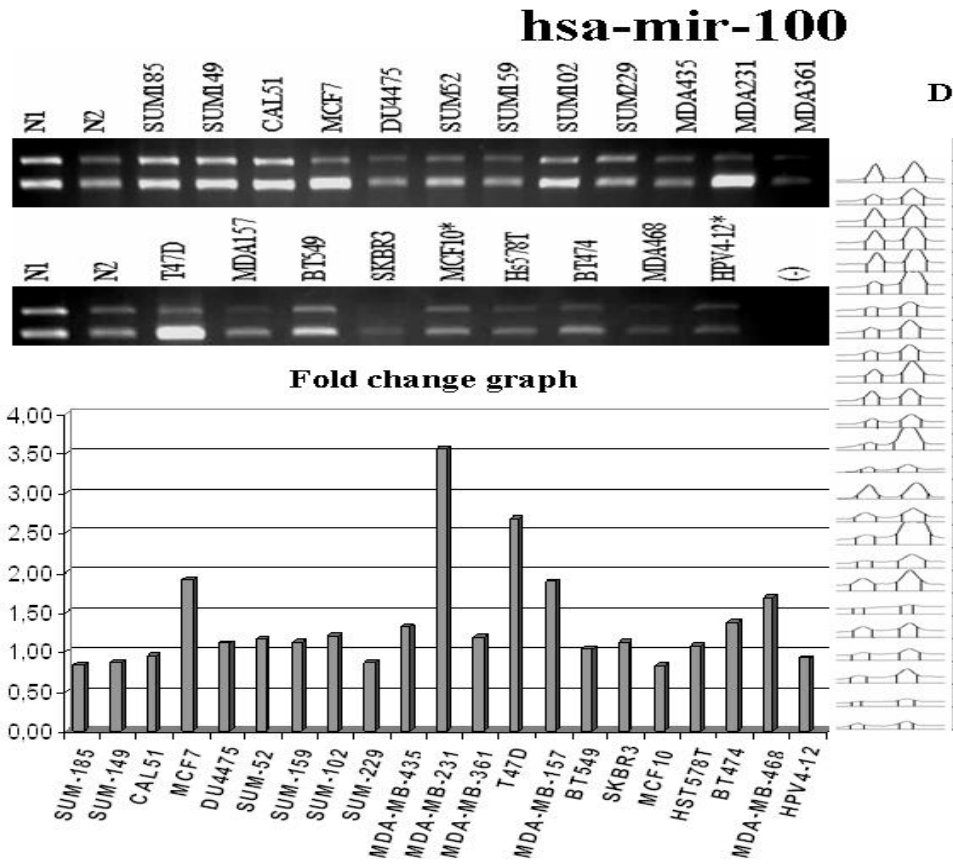

Densitometry and Fold change results

cell lines	gapdh	mir	mir/gapdh	fold change
N1	6563,34	9803,05	1,49	1,73
N2	4414,73	8728,74	1,98	
SUM-185	8023,73	11615,94	1,45	0,84
SUM-149	8376,24	12488,82	1,49	0,86
CAL51	7771,94	12774,18	1,64	0,95
MCF7	4817,59	15896,38	3,30	1,91
DU4475	3407,57	6512,99	1,91	1,10
SUM-52	4481,87	8997,32	2,01	1,16
SUM-159	3961,51	7637,65	1,93	1,11
SUM-102	5623,32	11649,51	2,07	1,20
SUM-229	5472,25	8158,02	1,49	0,86
MDA-MB-435	3055,06	6966,21	2,28	1,32
MDA-MB-231	2685,77	16500,68	6,14	3,55
MDA-MB-361	1812,89	3709,72	2,05	1,18
N1	4997,06	7271,37	1,46	1,51
N2	4004,06	6299,72	1,57	
T47D	4206,93	16987,88	4,04	2,67
MDA-MB-157	2519,89	7185,95	2,85	1,89
BT549	6086,17	9513,64	1,56	1,04
SKBR3	1590,95	2680,05	1,68	1,12
MCF10	4217,61	5253,32	1,25	0,82
HST578T	3064,44	4965,03	1,62	1,07
BT474	2797,50	5797,87	2,07	1,37
MDA-MB-468	1078,43	2744,11	2,54	1,69
HPV4-12	1751,11	2413,11	1,38	0,91

Figure 3.19: hsa-mir-100 semi-quantitative duplex PCR results
Upper bands are GAPDH and lower bands are microRNA genes. in gel images. Fold changes are represented as colored boxes from grey to black scale with increasing fold change respectively and dashed boxes represent fold changes of loss.

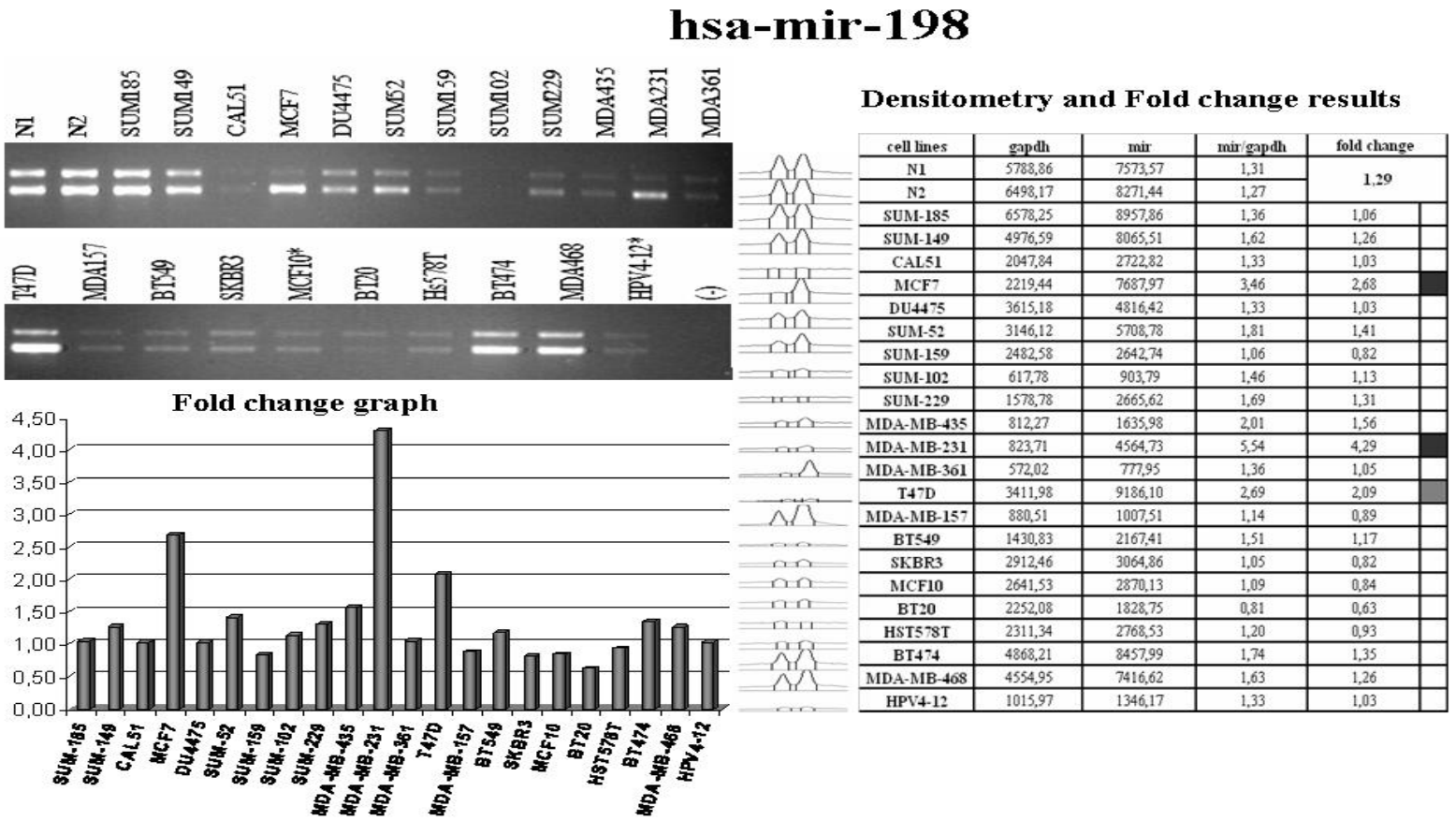

Densitometry and Fold change results

cell lines	gapdh	mir	mir/gapdh	fold change
N1	5788,86	7573,57	1,31	1,29
N2	6498,17	8271,44	1,27	
SUM-185	6578,25	8957,86	1,36	1,06
SUM-149	4976,59	8065,51	1,62	1,26
CAL51	2047,84	2722,82	1,33	1,03
MCF7	2219,44	7687,97	3,46	2,68
DU4475	3615,18	4816,42	1,33	1,03
SUM-52	3146,12	5708,78	1,81	1,41
SUM-159	2482,58	2642,74	1,06	0,82
SUM-102	617,78	903,79	1,46	1,13
SUM-229	1578,78	2665,62	1,69	1,31
MDA-MB-435	812,27	1635,98	2,01	1,56
MDA-MB-231	823,71	4564,73	5,54	4,29
MDA-MB-361	572,02	777,95	1,36	1,05
T47D	3411,98	9186,10	2,69	2,09
MDA-MB-157	880,51	1007,51	1,14	0,89
BT549	1430,83	2167,41	1,51	1,17
SKBR3	2912,46	3064,86	1,05	0,82
MCF10	2641,53	2870,13	1,09	0,84
BT20	2252,08	1828,75	0,81	0,63
HST578T	2311,34	2768,53	1,20	0,93
BT474	4868,21	8457,99	1,74	1,35
MDA-MB-468	4554,95	7416,62	1,63	1,26
HPV4-12	1015,97	1346,17	1,33	1,03

Figure 3.20: hsa-mir-198 semi-quantitative duplex PCR results
Upper bands are GAPDH and lower bands are microRNA genes. in gel images. Fold changes are represented as colored boxes from grey to black scale with increasing fold change respectively and dashed boxes represent fold changes of loss.

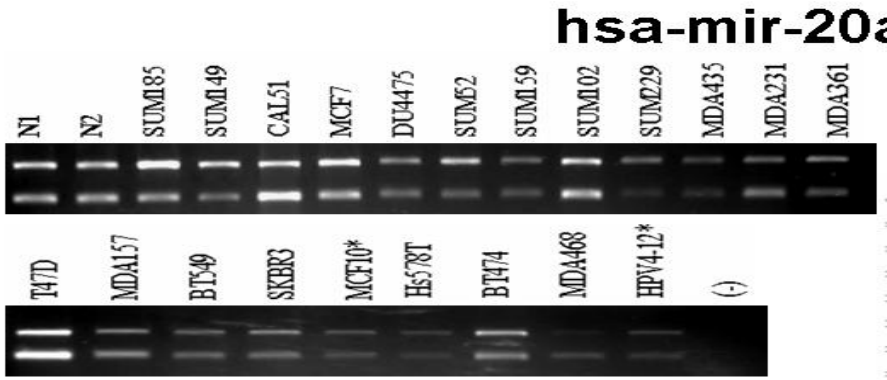

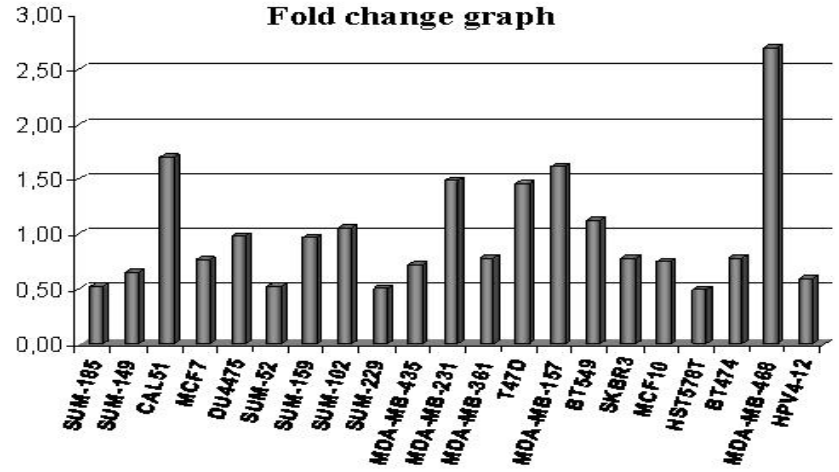

Densitometry and Fold change results

cell lines	gapdh	mir	mir/gapdh	fold change
N1	16935,97	16245,07	0,96	1,02
N2	18087,47	19451,56	1,08	
SUM-185	28947,04	15447,87	0,53	0,52
SUM-149	17839,46	11851,63	0,66	0,65
CAL51	17874,89	30860,31	1,73	1,70
MCF7	24482,75	19026,39	0,78	0,76
DU4475	11550,47	11497,33	1,00	0,98
SUM-52	17095,41	9070,31	0,53	0,52
SUM-159	9105,74	8981,73	0,99	0,97
SUM-102	17432,00	18796,09	1,08	1,06
SUM-229	8910,87	4623,73	0,52	0,51
MDA-MB-435	5987,82	4358,00	0,73	0,72
MDA-MB-231	7706,22	11674,48	1,51	1,49
MDA-MB-361	9371,47	7440,49	0,79	0,78
T47D	32260,38	47891,31	1,48	1,46
MDA-MB-157	12376,54	20278,30	1,64	1,61
BT549	9516,63	10847,97	1,14	1,12
SKBR3	14965,26	11821,82	0,79	0,78
MCF10	8308,56	6360,85	0,77	0,75
HST578T	5029,51	2490,10	0,50	0,49
BT474	18848,34	14940,61	0,79	0,78
MDA-MB-468	1701,16	4672,02	2,75	2,70
HPV4-12	4277,55	2588,72	0,61	0,59

Figure 3.21: hsa-mir-20a semi-quantitative duplex PCR results
Upper bands are GAPDH and lower bands are microRNA genes. in gel images. Fold changes are represented as colored boxes from grey to black scale with increasing fold change respectively and dashed boxes represent fold changes of loss.

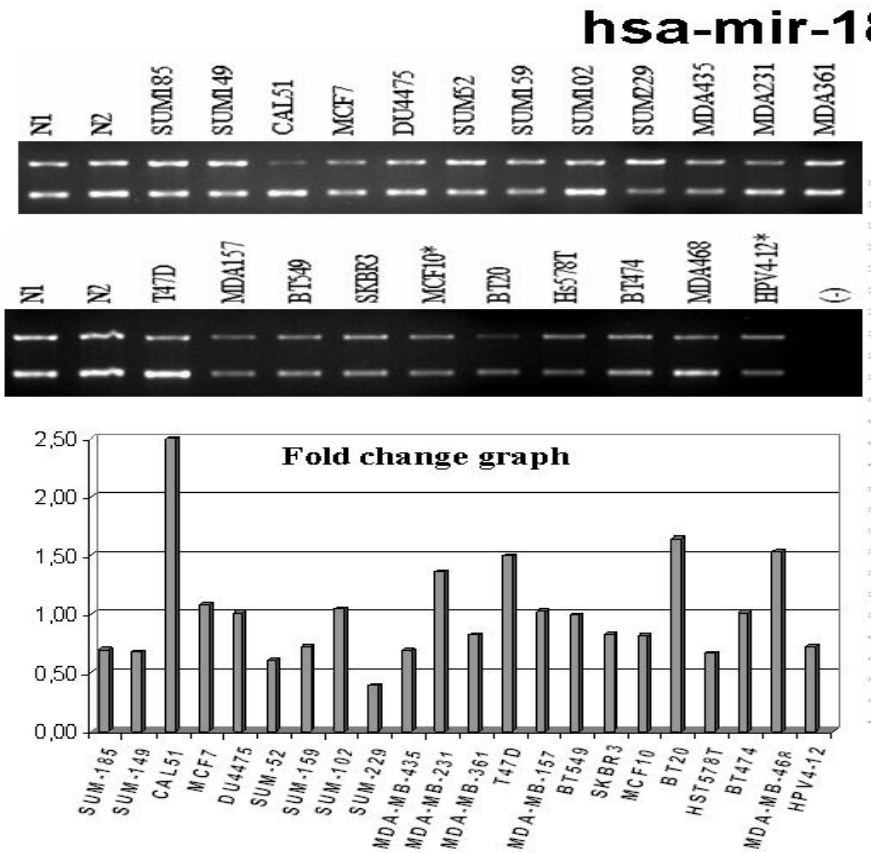

Densitometry and Fold change results

cell lines	gapdh	mir	mir/gapdh	fold change
N1	8439,01	11875,40	1,41	1,48
N2	10052,01	15685,81	1,56	
SUM-185	12179,30	12670,21	1,04	0,70
SUM-149	12085,79	12109,17	1,00	0,68
CAL51	4418,21	16316,98	3,69	2,49
MCF7	6755,89	10800,07	1,60	1,08
DU4475	10075,39	15124,77	1,50	1,01
SUM-52	11781,89	10542,92	0,89	0,60
SUM-159	8836,42	9467,59	1,07	0,72
SUM-102	10075,39	15639,06	1,55	1,05
SUM-229	11174,10	6451,99	0,58	0,39
MDA-MB-435	7270,17	7457,19	1,03	0,69
MDA-MB-231	5516,92	11150,72	2,02	1,36
MDA-MB-361	9420,84	11501,37	1,22	0,82
N1	9294,60	12512,62	1,35	1,44
N2	9636,94	14720,72	1,53	
T47D	7274,78	15627,93	2,15	1,50
MDA-MB-157	3971,17	5854,06	1,47	1,03
BT549	5049,55	7206,31	1,43	0,99
SKBR3	6418,92	7634,24	1,19	0,83
MCF10	5049,55	5922,52	1,17	0,82
BT20	2105,41	4981,08	2,37	1,65
HST578T	4655,86	4467,57	0,96	0,67
BT474	4861,26	7086,49	1,46	1,01
MDA-MB-468	4844,15	10663,97	2,20	1,53
HPV4-12	4313,51	4501,80	1,04	0,73

Figure 3.22: hsa-mir-18a semi-quantitative duplex PCR results
Upper bands are GAPDH and lower bands are microRNA genes. in gel images. Fold changes are represented as colored boxes from grey to black scale with increasing fold change respectively and dashed boxes represent fold changes of loss.

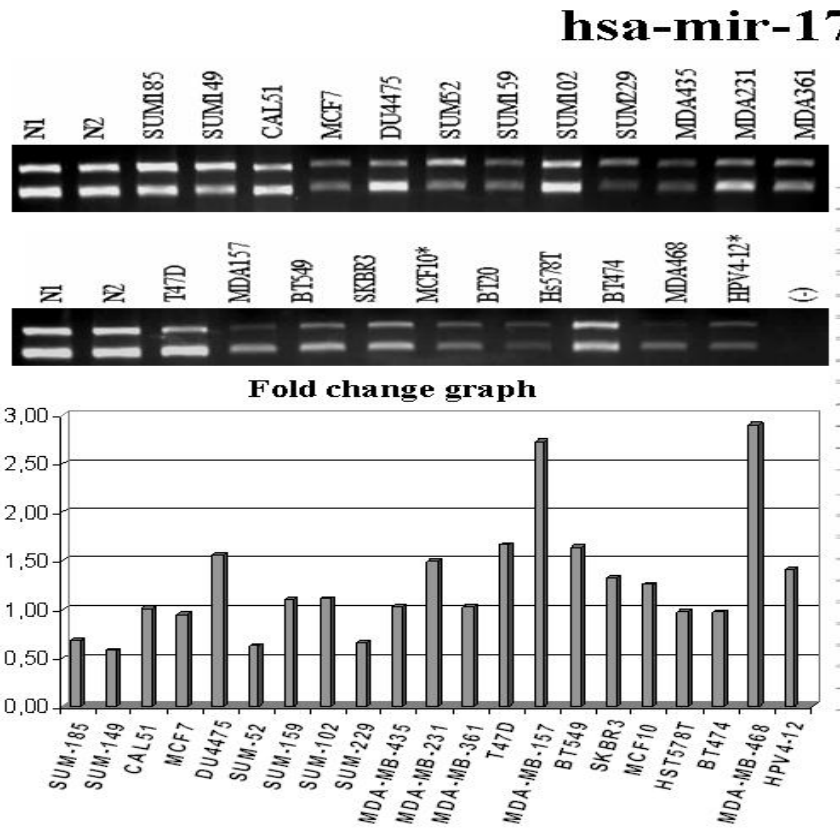

Densitometry and Fold change results

cell lines	gapdh	mir	mir/gapdh	fold change
N1	9859,89	14516,56	1,47	1,39
N2	10953,01	14385,39	1,31	
SUM-185	12876,89	12221,02	0,95	0,68
SUM-149	11980,54	9597,55	0,80	0,58
CAL51	8395,12	11761,91	1,40	1,01
MCF7	5706,06	7498,77	1,31	0,95
DU4475	6383,79	13860,69	2,17	1,56
SUM-52	9182,16	7936,01	0,86	0,62
SUM-159	4765,98	7323,87	1,54	1,11
SUM-102	9400,79	14538,42	1,55	1,11
SUM-229	5793,51	5268,81	0,91	0,65
MDA-MB-435	3869,63	5509,30	1,42	1,02
MDA-MB-231	5793,51	12067,99	2,08	1,50
MDA-MB-361	5837,23	8329,53	1,43	1,03
N1	7130,28	9048,14	1,27	1,25
N2	6826,46	8468,99	1,24	
T47D	4376,91	9114,60	2,08	1,67
MDA-MB-157	1471,63	5022,53	3,41	2,73
BT549	3009,72	6190,34	2,06	1,65
SKBR3	4082,58	6760,00	1,66	1,32
MCF10	2563,48	4035,11	1,57	1,26
HST578T	1832,42	2250,17	1,23	0,98
BT474	5497,25	6665,05	1,21	0,97
MDA-MB-468	1091,85	3959,16	3,63	2,90
HPV4-12	1718,48	3038,20	1,77	1,41

Figure 3.23: hsa-mir-17 semi-quantitative duplex PCR results
Upper bands are GAPDH and lower bands are microRNA genes. in gel images. Fold changes are represented as colored boxes from grey to black scale with increasing fold change respectively and dashed boxes represent fold changes of loss.

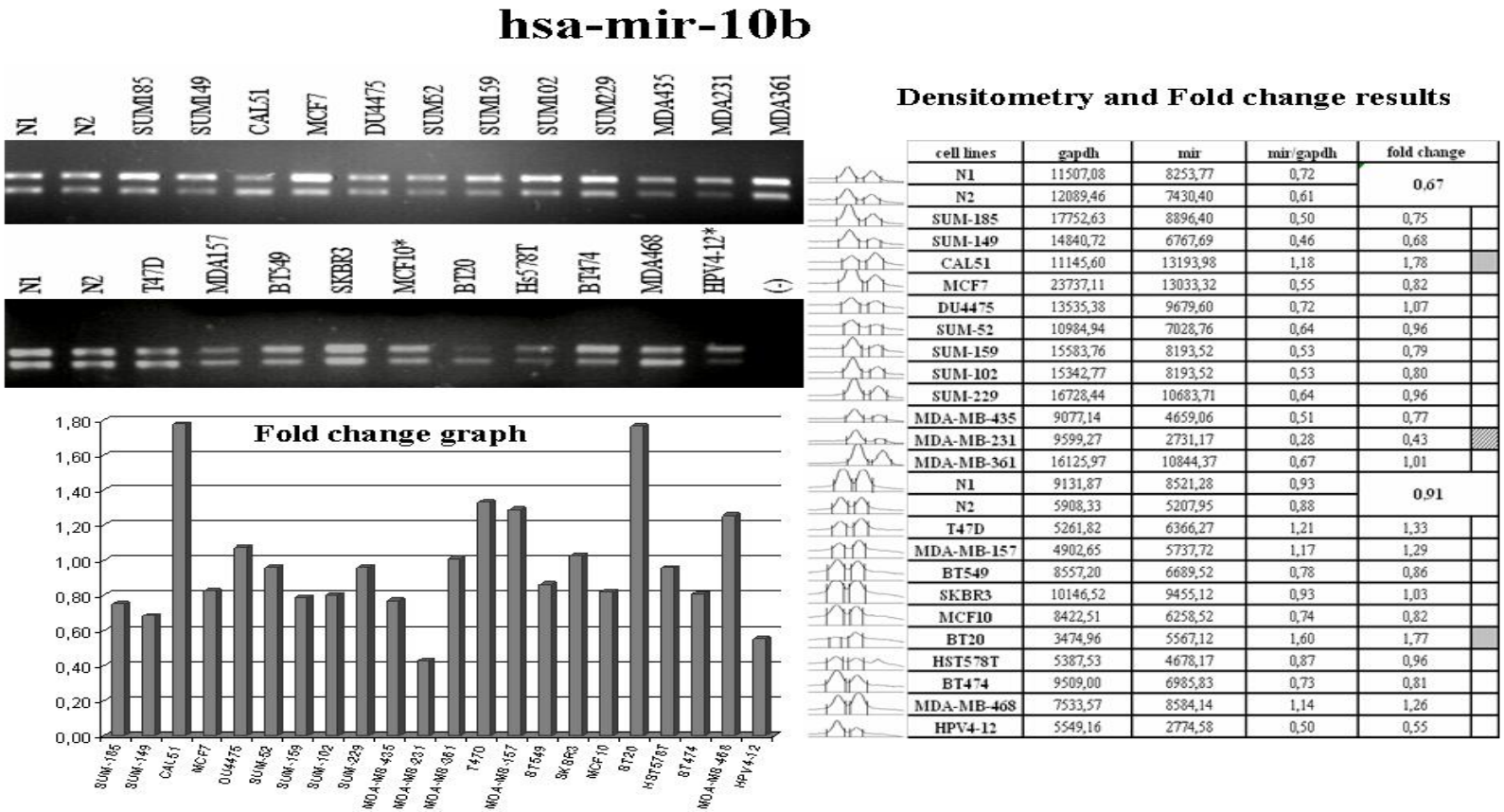

cell lines	gapdh	mir	mir/gapdh	fold change
N1	11507,08	8253,77	0,72	0,67
N2	12089,46	7430,40	0,61	
SUM-185	17752,63	8896,40	0,50	0,75
SUM-149	14840,72	6767,69	0,46	0,68
CAL51	11145,60	13193,98	1,18	1,78
MCF7	23737,11	13033,32	0,55	0,82
DU4475	13535,38	9679,60	0,72	1,07
SUM-52	10984,94	7028,76	0,64	0,96
SUM-159	15583,76	8193,52	0,53	0,79
SUM-102	15342,77	8193,52	0,53	0,80
SUM-229	16728,44	10683,71	0,64	0,96
MDA-MB-435	9077,14	4659,06	0,51	0,77
MDA-MB-231	9599,27	2731,17	0,28	0,43
MDA-MB-361	16125,97	10844,37	0,67	1,01
N1	9131,87	8521,28	0,93	0,91
N2	5908,33	5207,95	0,88	
T47D	5261,82	6366,27	1,21	1,33
MDA-MB-157	4902,65	5737,72	1,17	1,29
BT549	8557,20	6689,52	0,78	0,86
SKBR3	10146,52	9455,12	0,93	1,03
MCF10	8422,51	6258,52	0,74	0,82
BT20	3474,96	5567,12	1,60	1,77
HST578T	5387,53	4678,17	0,87	0,96
BT474	9509,00	6985,83	0,73	0,81
MDA-MB-468	7533,57	8584,14	1,14	1,26
HPV4-12	5549,16	2774,58	0,50	0,55

Figure 3.24: hsa-mir-10b semi-quantitative duplex PCR results
Upper bands are GAPDH and lower bands are microRNA genes. in gel images. Fold changes are represented as colored boxes from grey to black scale with increasing fold change respectively and dashed boxes represent fold changes of loss.

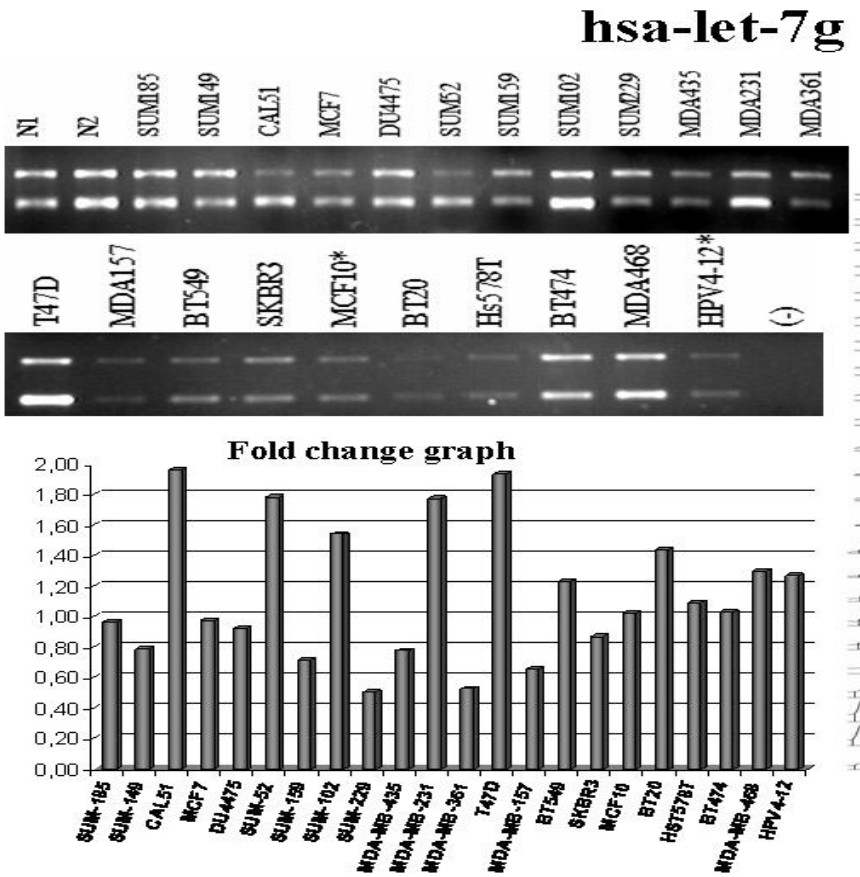

Densitometry and Fold change results

cell lines	gapdh	mir	mir/gapdh	fold change
N1	8659,05	8365,26	0,97	1,12
N2	10545,49	13406,07	1,27	
SUM-185	8133,32	8782,75	1,08	0,97
SUM-149	9153,85	8025,08	0,88	0,78
CAL51	5458,29	11937,12	2,19	1,96
MCF7	6695,30	7282,88	1,09	0,97
DU4475	10019,76	10313,55	1,03	0,92
SUM-52	5303,67	10576,41	1,99	1,78
SUM-159	8411,65	6757,15	0,80	0,72
SUM-102	8937,38	15369,82	1,72	1,54
SUM-229	8643,59	4886,18	0,57	0,51
MDA-MB-435	4700,63	4066,66	0,87	0,77
MDA-MB-231	6958,17	13777,17	1,98	1,77
MDA-MB-361	5025,34	2953,35	0,59	0,53
T47D	8706,77	18846,13	2,16	1,94
MDA-MB-157	2865,17	2100,20	0,73	0,66
BT549	3880,49	5326,99	1,37	1,23
SKBR3	6829,11	6592,67	0,97	0,86
MCF10	5118,36	5841,60	1,14	1,02
BT20	2169,74	3491,05	1,61	1,44
HST578T	4478,56	5438,25	1,21	1,09
BT474	9972,45	11488,49	1,15	1,03
MDA-MB-468	9763,82	14131,12	1,45	1,29
HPV4-12	2684,36	3797,04	1,41	1,26

Figure 3.25: hsa-let-7g semi-quantitative duplex PCR results
Upper bands are GAPDH and lower bands are microRNA genes. in gel images. Fold changes are represented as colored boxes from grey to black scale with increasing fold change respectively and dashed boxes represent fold changes of loss.

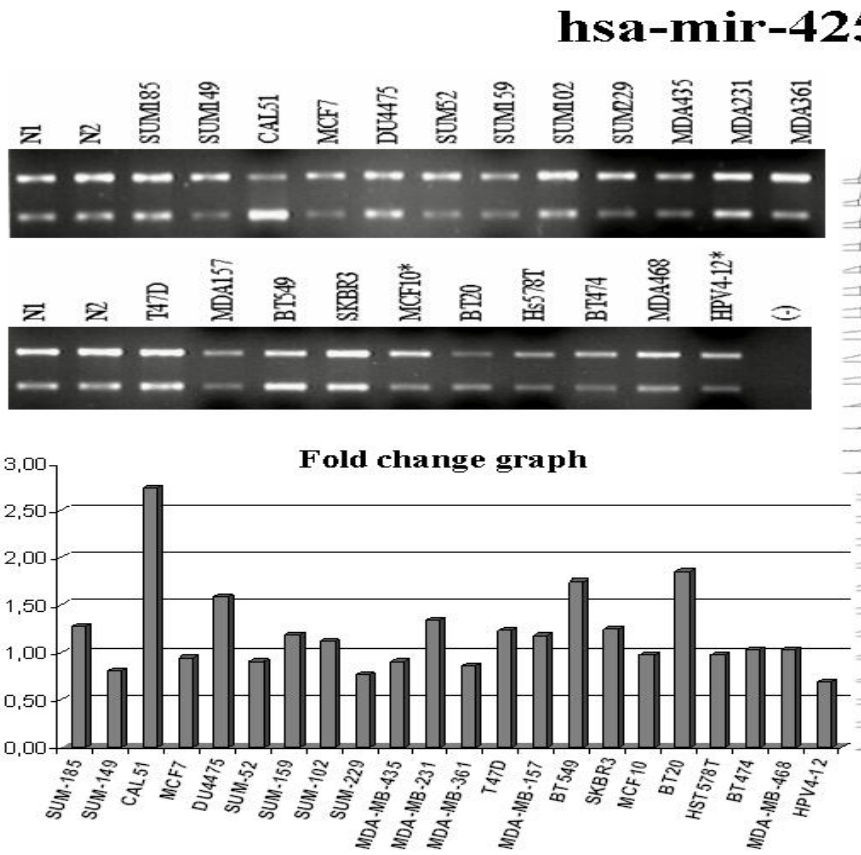

Densitometry and Fold change results

cell lines	gapdh	mir	mir/gapdh	fold change
N1	11714,86	8188,57	0,70	0,64
N2	13939,50	8070,24	0,58	
SUM-185	15998,48	13016,51	0,81	1,27
SUM-149	11998,86	6200,59	0,52	0,81
CAL51	9750,55	17039,80	1,75	2,74
MCF7	12330,19	7407,58	0,60	0,94
DU4475	14199,83	14412,83	1,02	1,59
SUM-52	14057,83	8141,24	0,58	0,91
SUM-159	11833,19	8993,23	0,76	1,19
SUM-102	16448,14	11691,19	0,71	1,11
SUM-229	11714,86	5750,93	0,49	0,77
MDA-MB-435	8780,23	5088,27	0,58	0,91
MDA-MB-231	11809,53	10129,21	0,86	1,34
MDA-MB-361	14034,17	7715,24	0,55	0,86
N1	15158,95	10646,26	0,70	0,67
N2	17663,95	11419,87	0,65	
T47D	15601,01	12948,65	0,83	1,23
MDA-MB-157	9135,89	7275,56	0,80	1,18
BT549	12746,04	15030,02	1,18	1,75
SKBR3	17111,38	14366,93	0,84	1,24
MCF10	12856,56	8435,96	0,66	0,97
BT20	5838,87	7293,98	1,25	1,85
HST578T	9504,27	6280,93	0,66	0,98
BT474	10369,97	7201,88	0,69	1,03
MDA-MB-468	12838,14	8933,28	0,70	1,03
HPV4-12	10185,78	4788,98	0,47	0,70

Figure 3.26: hsa-mir-425 semi-quantitative duplex PCR results
Upper bands are GAPDH and lower bands are microRNA genes. in gel images. Fold changes are represented as colored boxes from grey to black scale with increasing fold change respectively and dashed boxes represent fold changes of loss.

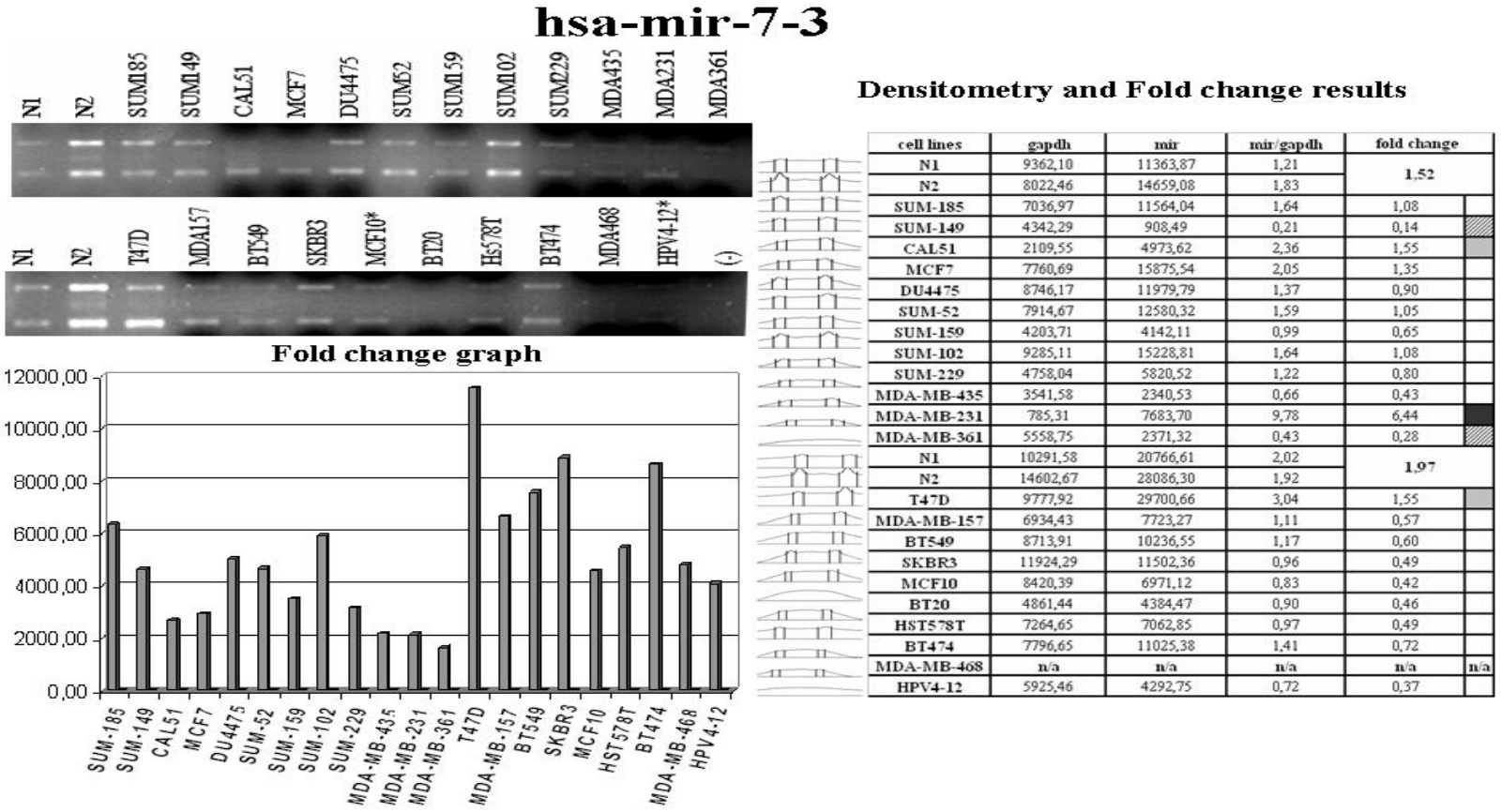

cell lines	gapdh	mir	mir/gapdh	fold change	
N1	9362,10	11363,87	1,21	1,52	
N2	8022,46	14659,08	1,83		
SUM-185	7036,97	11564,04	1,64	1,08	
SUM-149	4342,29	908,49	0,21	0,14	
CAL51	2109,55	4973,62	2,36	1,55	
MCF7	7760,69	15875,54	2,05	1,35	
DU4475	8746,17	11979,79	1,37	0,90	
SUM-52	7914,67	12580,32	1,59	1,05	
SUM-159	4203,71	4142,11	0,99	0,65	
SUM-102	9285,11	15228,81	1,64	1,08	
SUM-229	4758,04	5820,52	1,22	0,80	
MDA-MB-435	3541,58	2340,53	0,66	0,43	
MDA-MB-231	785,31	7683,70	9,78	6,44	
MDA-MB-361	5558,75	2371,32	0,43	0,28	
N1	10291,58	20766,61	2,02	1,97	
N2	14602,67	28086,30	1,92		
T47D	9777,92	29700,66	3,04	1,55	
MDA-MB-157	6934,43	7723,27	1,11	0,57	
BT549	8713,91	10236,55	1,17	0,60	
SKBR3	11924,29	11502,36	0,96	0,49	
MCF10	8420,39	6971,12	0,83	0,42	
BT20	4861,44	4384,47	0,90	0,46	
HST578T	7264,65	7062,85	0,97	0,49	
BT474	7796,65	11025,38	1,41	0,72	
MDA-MB-468	n/a	n/a	n/a	n/a	n/a
HPV4-12	5925,46	4292,75	0,72	0,37	

Figure 3.27: hsa-mir-7-3 semi-quantitative duplex PCR results
Upper bands are GAPDH and lower bands are microRNA genes. in gel images. Fold changes are represented as colored boxes from grey to black scale with increasing fold change respectively and dashed boxes represent fold changes of loss.

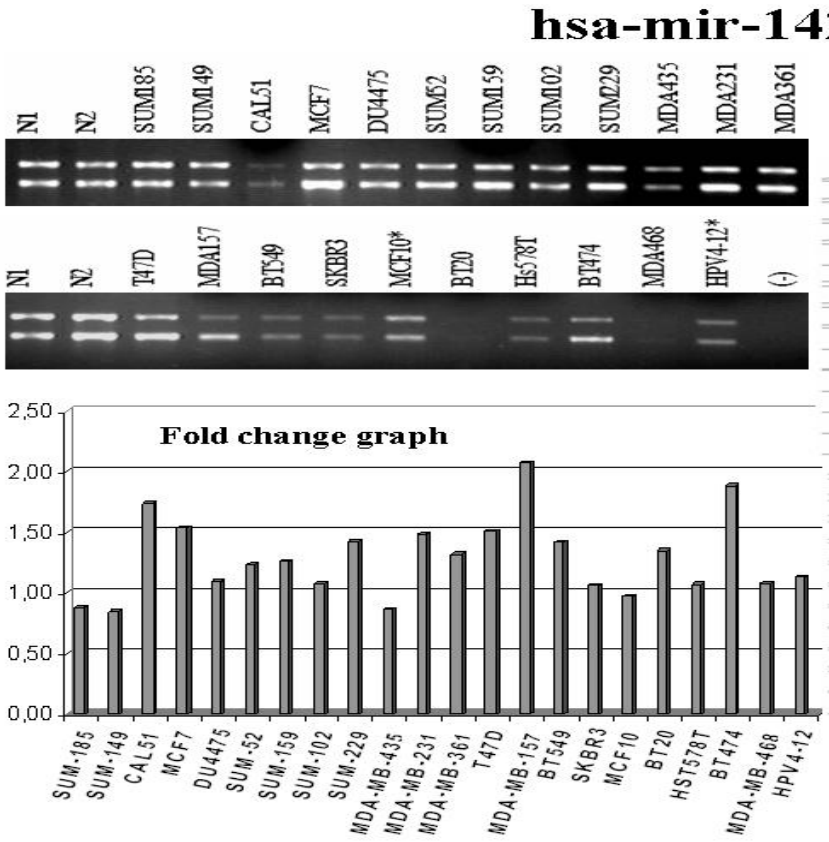

Densitometry and Fold change results

cell lines	gapdh	mir	mir/gapdh	fold change
N1	8654,33	9268,26	1,07	1,19
N2	7386,88	9802,96	1,33	
SUM-185	9901,98	10337,67	1,04	0,88
SUM-149	7545,31	7584,92	1,01	0,84
CAL51	1821,96	3762,75	2,07	1,74
MCF7	9050,41	16476,90	1,82	1,53
DU4475	8119,63	10535,71	1,30	1,09
SUM-52	8179,04	12001,20	1,47	1,23
SUM-159	10298,06	15387,68	1,49	1,26
SUM-102	5564,91	7129,43	1,28	1,08
SUM-229	7763,15	13110,22	1,69	1,42
MDA-MB-435	3822,17	3921,19	1,03	0,86
MDA-MB-231	8396,88	14753,95	1,76	1,48
MDA-MB-361	7624,53	11961,59	1,57	1,32
N1	13428,44	12262,33	0,91	0,97
N2	17054,30	17528,03	1,03	
T47D	11442,41	16726,33	1,46	1,51
MDA-MB-157	6450,02	12954,71	2,01	2,07
BT549	5028,83	6905,53	1,37	1,42
SKBR3	5375,02	5520,78	1,03	1,06
MCF10	10003,00	9401,73	0,94	0,97
BT20	2131,79	2769,50	1,30	1,34
HST578T	4864,85	5028,83	1,03	1,07
BT474	6213,16	11314,87	1,82	1,88
MDA-MB-468	1803,82	1876,70	1,04	1,07
HPV4-12	5666,55	6194,94	1,09	1,13

Figure 3.28: hsa-mir-142 semi-quantitative duplex PCR results
Upper bands are GAPDH and lower bands are microRNA genes. in gel images. Fold changes are represented as colored boxes from grey to black scale with increasing fold change respectively and dashed boxes represent fold changes of loss.

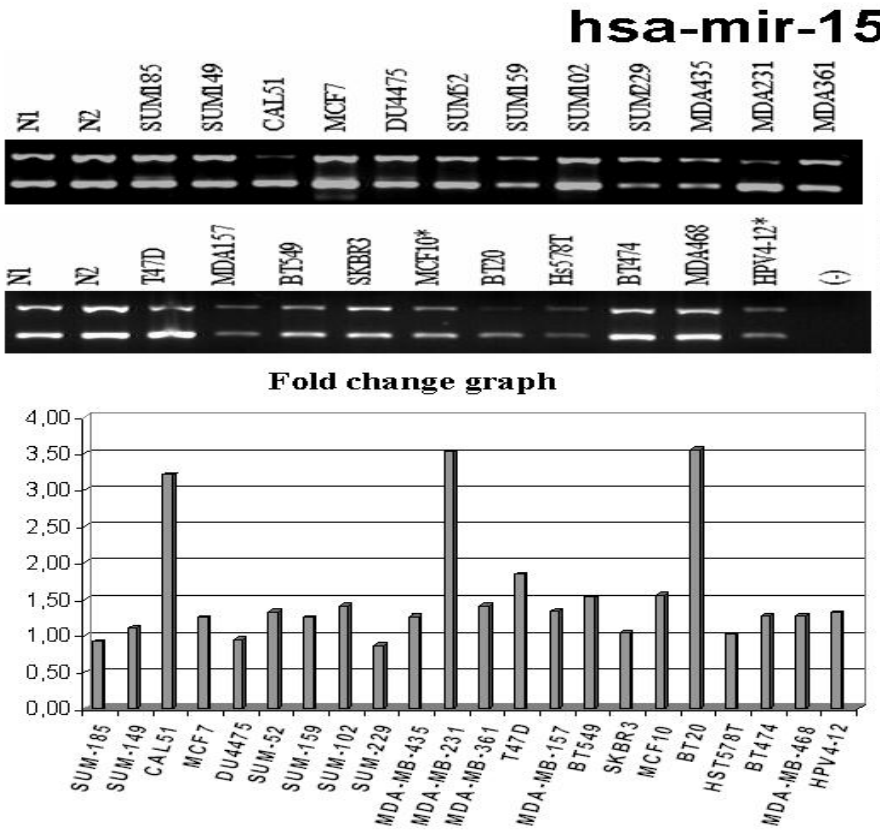

Densitometry and Fold change results

cell lines	gapdh	mir	mir/gapdh	fold change
N1	9395,71	10168,69	1,08227	1,06
N2	11354,82	11861,25	1,04460	
SUM-185	10981,65	10675,13	0,97209	0,91
SUM-149	9102,51	10728,44	1,17862	1,11
CAL51	2878,69	9822,18	3,41203	3,21
MCF7	10381,93	13873,67	1,33633	1,26
DU4475	9528,98	9662,26	1,01399	0,95
SUM-52	7836,42	11048,29	1,40986	1,33
SUM-159	5610,77	7449,93	1,32779	1,25
SUM-102	8409,50	12620,91	1,50079	1,41
SUM-229	6983,48	6437,06	0,92176	0,87
MDA-MB-435	4877,77	6543,68	1,34153	1,26
MDA-MB-231	3278,50	12274,40	3,74391	3,52
MDA-MB-361	6303,79	9475,68	1,50317	1,41
N1	7407,11	10188,49	1,37550	1,28
N2	9772,03	11631,24	1,19026	
T47D	5696,63	13475,58	2,36554	1,84
MDA-MB-157	1844,34	3153,23	1,70968	1,33
BT549	3569,69	6975,77	1,95417	1,52
SKBR3	5533,02	7377,36	1,33333	1,04
MCF10	3168,10	6321,33	1,99531	1,56
BT20	1070,91	4878,58	4,55555	3,55
HST578T	1918,71	2528,53	1,31783	1,03
BT474	6782,41	11095,79	1,63597	1,28
MDA-MB-468	6440,32	10530,59	1,63510	1,27
HPV4-12	2454,16	4149,77	1,69091	1,32

Figure 3.29: hsa-mir-15a semi-quantitative duplex PCR results
Upper bands are GAPDH and lower bands are microRNA genes. in gel images. Fold changes are represented as colored boxes from grey to black scale with increasing fold change respectively and dashed boxes represent fold changes of loss.

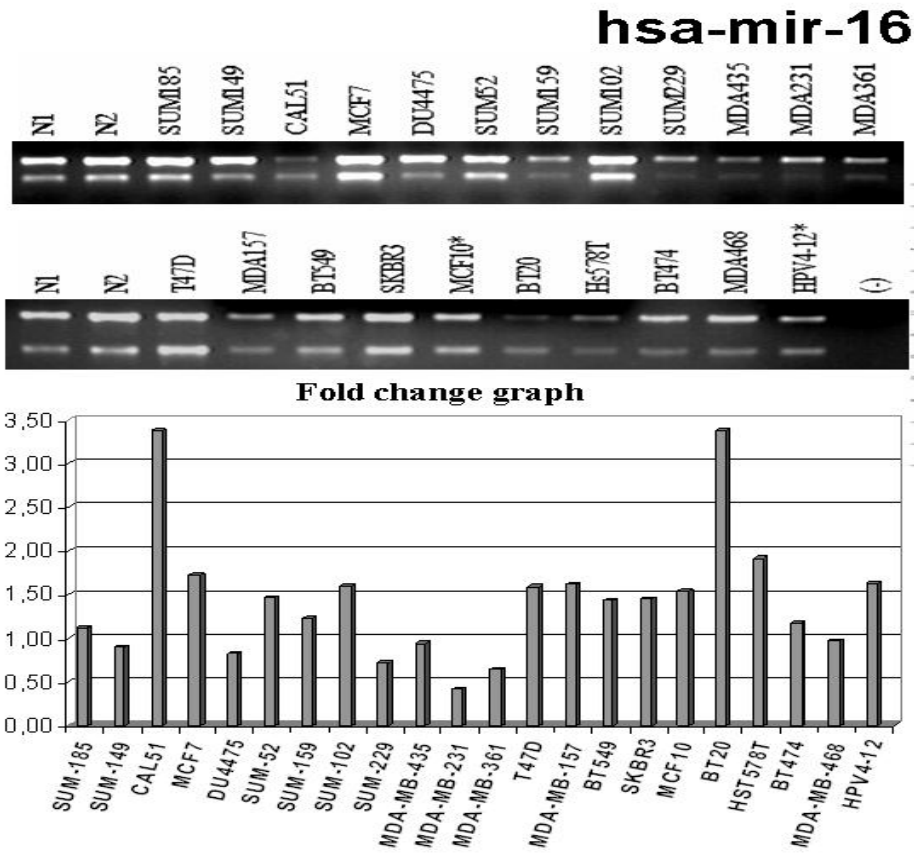

Densitometry and Fold change results

cell lines	gapdh	mir	mir/gapdh	fold change
N1	12316,11	6378,30	0,52	0,53
N2	15117,63	8263,60	0,55	
SUM-185	15822,42	9391,26	0,59	1,12
SUM-149	13514,25	6431,16	0,48	0,89
CAL51	3083,43	5532,56	1,79	3,37
MCF7	16121,95	14782,86	0,92	1,72
DU4475	14923,82	6501,64	0,44	0,82
SUM-52	13461,39	10483,67	0,78	1,46
SUM-159	8475,04	5514,94	0,65	1,22
SUM-102	16210,05	13760,92	0,85	1,60
SUM-229	6765,93	2590,08	0,38	0,72
MDA-MB-435	4017,27	2008,64	0,50	0,94
MDA-MB-231	7488,34	1673,86	0,22	0,42
MDA-MB-361	5285,89	1797,20	0,34	0,64
N1	18772,37	12971,38	0,69	0,74
N2	23146,88	18315,89	0,79	
T47D	22252,96	26113,94	1,17	1,58
MDA-MB-157	11735,11	13979,42	1,19	1,61
BT549	15976,48	16870,40	1,06	1,42
SKBR3	20255,90	21758,45	1,07	1,45
MCF10	15596,09	17764,33	1,14	1,54
BT20	5743,93	14359,81	2,50	3,37
HST578T	8520,79	12115,50	1,42	1,92
BT474	17935,50	15539,03	0,87	1,17
MDA-MB-468	20408,05	14721,19	0,72	0,97
HPV4-12	9966,28	11982,36	1,20	1,62

Figure 3.30: hsa-mir-16-1 semi-quantitative duplex PCR results
Upper bands are GAPDH and lower bands are microRNA genes. in gel images. Fold changes are represented as colored boxes from grey to black scale with increasing fold change respectively and dashed boxes represent fold changes of loss.

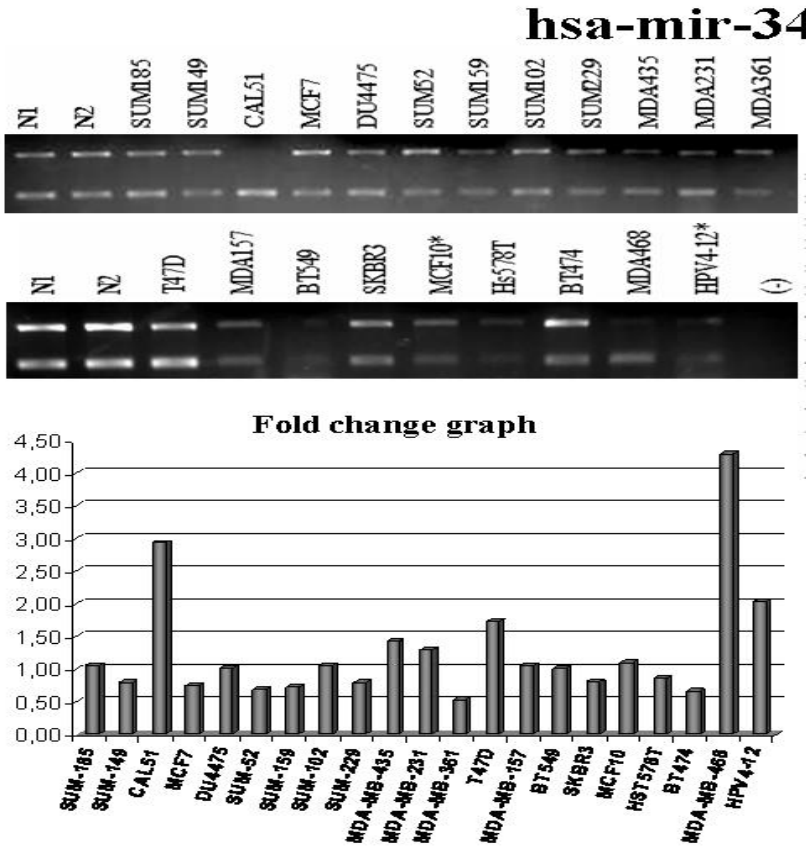

Densitometry and Fold change results

cell lines	gapdh	mir	mir/gapdh	fold change
N1	3742,29	5122,19	1,37	1,16
N2	4802,06	4581,27	0,95	
SUM-185	4415,68	5409,21	1,23	1,05
SUM-149	4216,98	3896,84	0,92	0,80
CAL51	2009,14	6855,35	3,41	2,94
MCF7	5100,11	4426,72	0,87	0,75
DU4475	3190,33	3753,33	1,18	1,01
SUM-52	4051,39	3168,25	0,78	0,67
SUM-159	3135,14	2627,33	0,84	0,72
SUM-102	3113,06	3808,53	1,22	1,05
SUM-229	3389,04	3090,98	0,91	0,79
MDA-MB-435	1556,53	2550,06	1,64	1,41
MDA-MB-231	2009,14	2991,63	1,49	1,28
MDA-MB-361	2483,82	1534,45	0,62	0,53
N1	21748,23	18665,69	0,86	0,87
N2	24304,12	21283,53	0,88	
T47D	15753,53	23576,08	1,50	1,73
MDA-MB-157	8782,94	7946,47	0,90	1,04
BT549	2586,86	2261,57	0,87	1,01
SKBR3	13786,27	9526,47	0,69	0,80
MCF10	9030,78	8535,10	0,95	1,09
HST578T	6490,39	4770,98	0,74	0,85
BT474	20369,61	11679,61	0,57	0,66
MDA-MB-468	3485,29	12996,27	3,73	4,31
HPV4-12	4058,43	7125,49	1,76	2,03

Figure 3.31: hsa-mir-34c semi-quantitative duplex PCR results
Upper bands are GAPDH and lower bands are microRNA genes. in gel images. Fold changes are represented as colored boxes from grey to black scale with increasing fold change respectively and dashed boxes represent fold changes of loss.

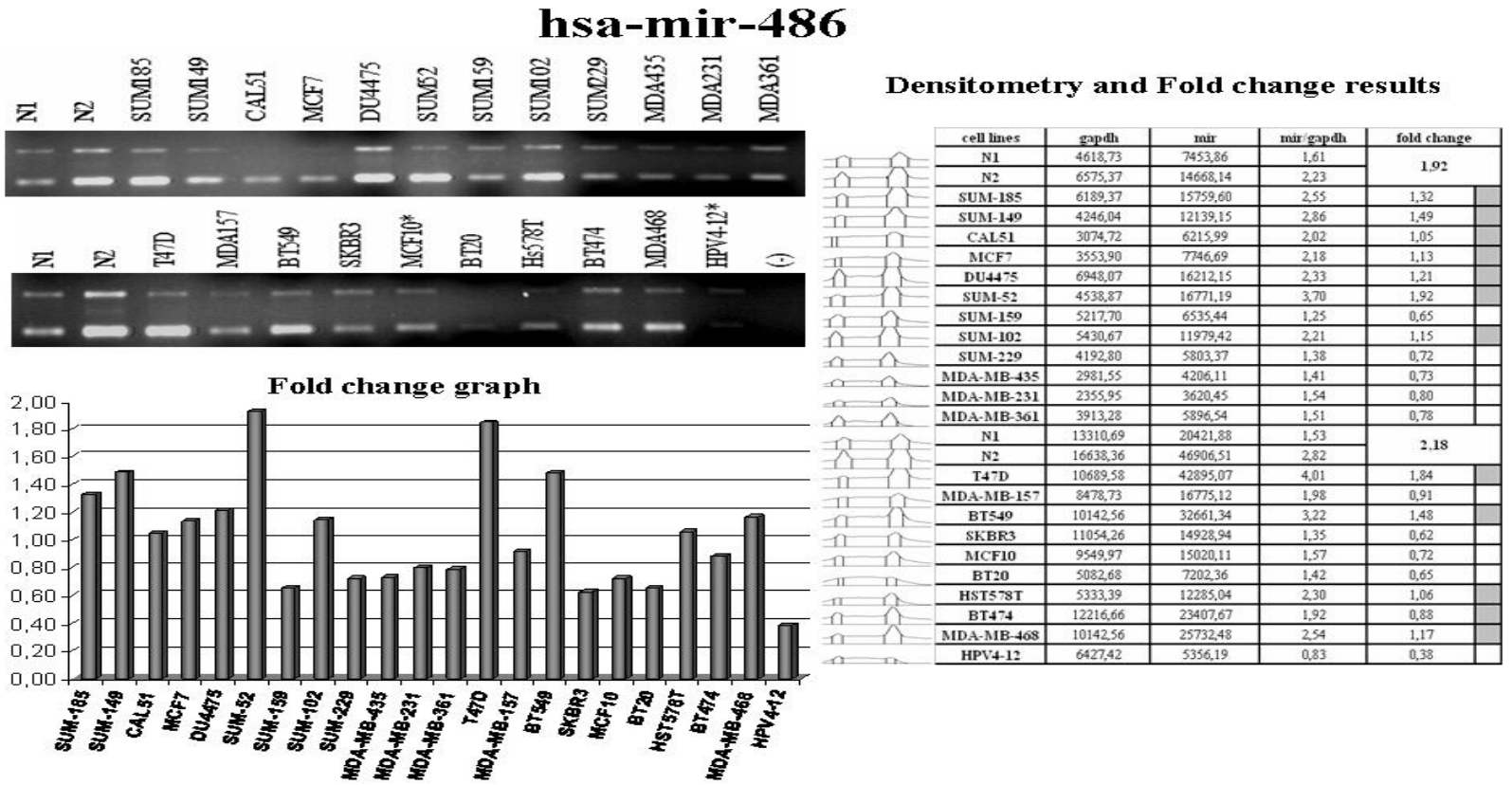

Densitometry and Fold change results

cell lines	gapdh	mir	mir/gapdh	fold change
N1	4618,73	7453,86	1,61	1,92
N2	6575,37	14668,14	2,23	
SUM-185	6189,37	15759,60	2,55	1,32
SUM-149	4246,04	12139,15	2,86	1,49
CAL51	3074,72	6215,99	2,02	1,05
MCF7	3553,90	7746,69	2,18	1,13
DU4475	6948,07	16212,15	2,33	1,21
SUM-52	4538,87	16771,19	3,70	1,92
SUM-159	5217,70	6535,44	1,25	0,65
SUM-102	5430,67	11979,42	2,21	1,15
SUM-229	4192,80	5803,37	1,38	0,72
MDA-MB-435	2981,55	4206,11	1,41	0,73
MDA-MB-231	2355,95	3620,45	1,54	0,80
MDA-MB-361	3913,28	5896,54	1,51	0,78
N1	13310,69	20421,88	1,53	2,18
N2	16638,36	46906,51	2,82	
T47D	10689,58	42895,07	4,01	1,84
MDA-MB-157	8478,73	16775,12	1,98	0,91
BT549	10142,56	32661,34	3,22	1,48
SKBR3	11054,26	14928,94	1,35	0,62
MCF10	9549,97	15020,11	1,57	0,72
BT20	5082,68	7202,36	1,42	0,65
HST578T	5333,39	12285,04	2,30	1,06
BT474	12216,66	23407,67	1,92	0,88
MDA-MB-468	10142,56	25732,48	2,54	1,17
HPV4-12	6427,42	5356,19	0,83	0,38

Figure 3.32: hsa-mir-486 semi-quantitative duplex PCR results
Upper bands are GAPDH and lower bands are microRNA genes. in gel images. Fold changes are represented as colored boxes from grey to black scale with increasing fold change respectively and dashed boxes represent fold changes of loss.

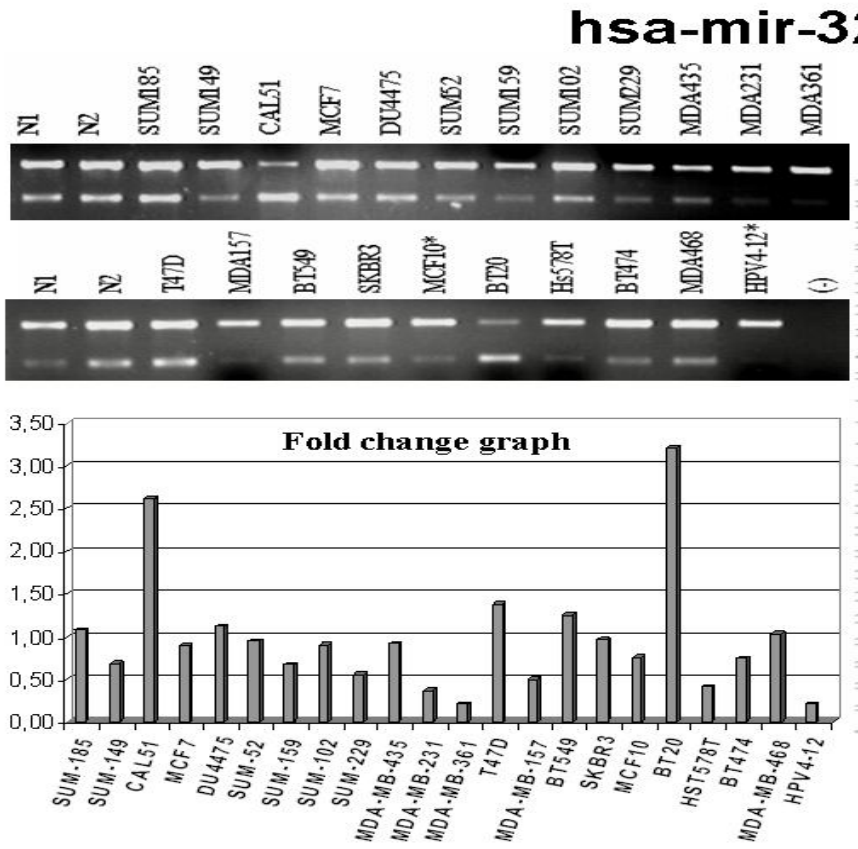

Densitometry and Fold change results

cell lines	gapdh	mir	mir/gapdh	fold change
N1	16495,55	13227,36	0,80	0,80
N2	17732,17	14198,98	0,80	
SUM-185	18328,39	15811,00	0,86	1,08
SUM-149	17467,18	9539,60	0,55	0,68
CAL51	9495,43	19874,16	2,09	2,61
MCF7	21375,77	15369,35	0,72	0,90
DU4475	17135,94	15258,94	0,89	1,11
SUM-52	17400,93	13271,52	0,76	0,95
SUM-159	13227,36	7110,53	0,54	0,67
SUM-102	17224,27	12476,56	0,72	0,90
SUM-229	12542,80	5564,77	0,44	0,55
MDA-MB-435	9362,94	6889,71	0,74	0,92
MDA-MB-231	10709,97	3157,78	0,29	0,37
MDA-MB-361	12609,05	2186,16	0,17	0,22
N1	25914,43	12034,56	0,46	0,50
N2	32520,06	17650,69	0,54	
T47D	27331,83	19068,10	0,70	1,39
MDA-MB-157	23748,21	6017,28	0,25	0,50
BT549	26155,12	16554,21	0,63	1,26
SKBR3	29605,03	14414,73	0,49	0,97
MCF10	25753,97	9814,86	0,38	0,76
BT20	14174,04	22838,93	1,61	3,20
HST578T	22277,31	4626,62	0,21	0,41
BT474	27626,01	10403,21	0,38	0,75
MDA-MB-468	26930,68	14013,58	0,52	1,03
HPV4-12	19522,74	2139,48	0,11	0,22

Figure 3.33: hsa-mir-320 semi-quantitative duplex PCR results
Upper bands are GAPDH and lower bands are microRNA genes. in gel images. Fold changes are represented as colored boxes from grey to black scale with increasing fold change respectively and dashed boxes represent fold changes of loss.

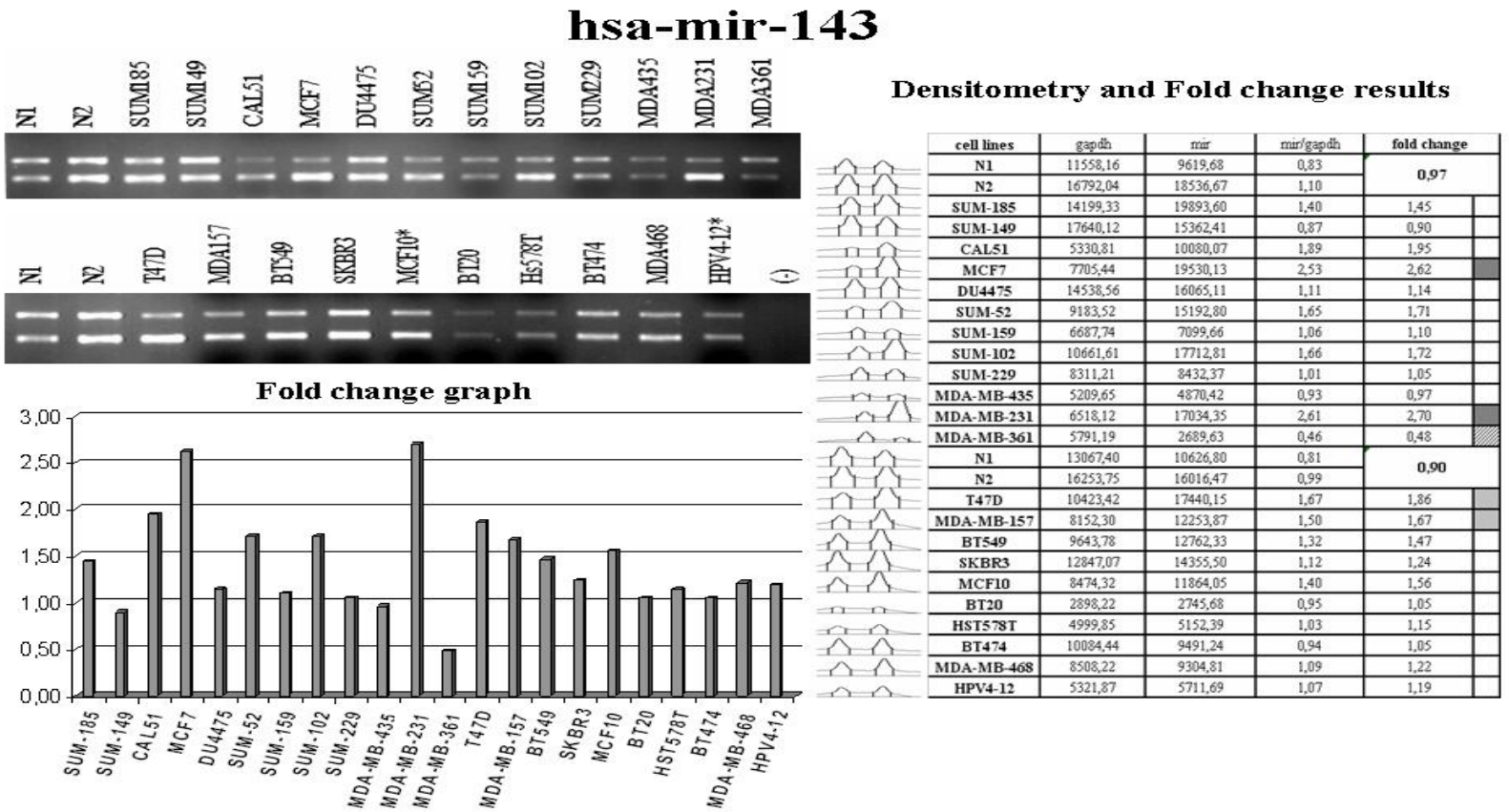

cell lines	gapdh	mir	mir/gapdh	fold change
N1	11558,16	9619,68	0,83	0,97
N2	16792,04	18536,67	1,10	
SUM-185	14199,33	19893,60	1,40	1,45
SUM-149	17640,12	15362,41	0,87	0,90
CAL51	5330,81	10080,07	1,89	1,95
MCF7	7705,44	19530,13	2,53	2,62
DU4475	14538,56	16065,11	1,11	1,14
SUM-52	9183,52	15192,80	1,65	1,71
SUM-159	6687,74	7099,66	1,06	1,10
SUM-102	10661,61	17712,81	1,66	1,72
SUM-229	8311,21	8432,37	1,01	1,05
MDA-MB-435	5209,65	4870,42	0,93	0,97
MDA-MB-231	6518,12	17034,35	2,61	2,70
MDA-MB-361	5791,19	2689,63	0,46	0,48
N1	13067,40	10626,80	0,81	0,90
N2	16253,75	16016,47	0,99	
T47D	10423,42	17440,15	1,67	1,86
MDA-MB-157	8152,30	12253,87	1,50	1,67
BT549	9643,78	12762,33	1,32	1,47
SKBR3	12847,07	14355,50	1,12	1,24
MCF10	8474,32	11864,05	1,40	1,56
BT20	2898,22	2745,68	0,95	1,05
HST578T	4999,85	5152,39	1,03	1,15
BT474	10084,44	9491,24	0,94	1,05
MDA-MB-468	8508,22	9304,81	1,09	1,22
HPV4-12	5321,87	5711,69	1,07	1,19

Figure 3.34: hsa-mir-143 semi-quantitative duplex PCR results
Upper bands are GAPDH and lower bands are microRNA genes. in gel images. Fold changes are represented as colored boxes from grey to black scale with increasing fold change respectively and dashed boxes represent fold changes of loss.

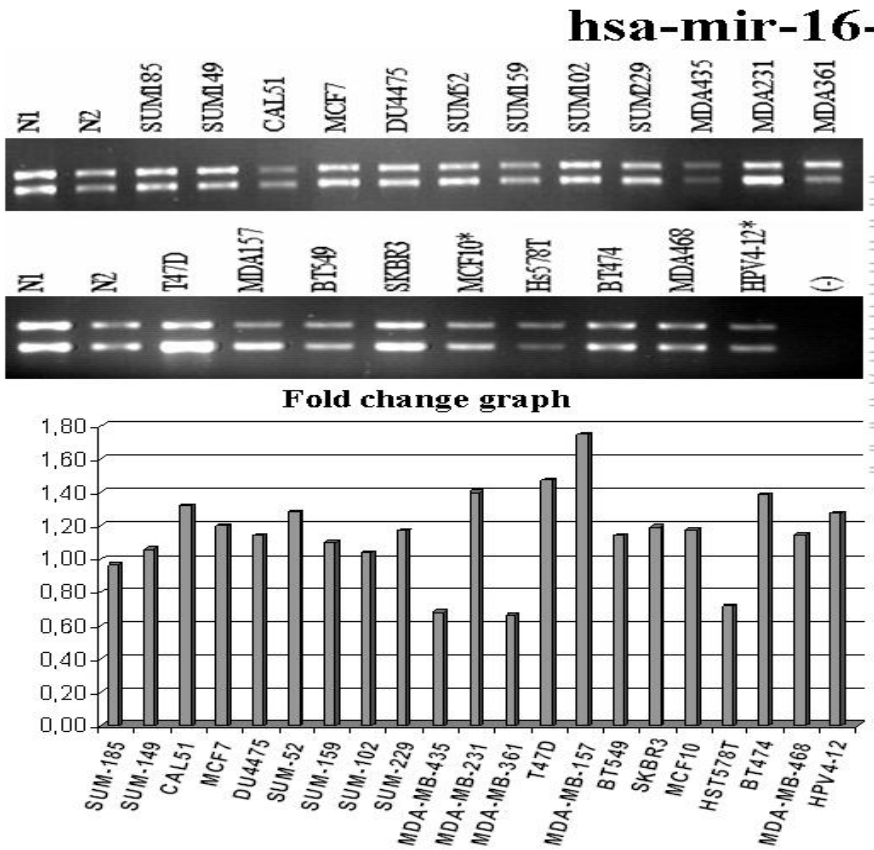

Densitometry and Fold change results

cell lines	gapdh	mir	mir/gapdh	fold change
N1	10655,63	9634,10	0,90	0,82
N2	7185,94	5266,17	0,73	
SUM-185	9493,19	7502,97	0,79	0,97
SUM-149	9634,10	8365,99	0,87	1,06
CAL51	5107,66	5530,36	1,08	1,32
MCF7	10338,60	10127,25	0,98	1,20
DU4475	10356,21	9651,71	0,93	1,14
SUM-52	9352,29	9827,83	1,05	1,28
SUM-159	7960,90	7150,72	0,90	1,10
SUM-102	10338,60	8771,08	0,85	1,04
SUM-229	8189,86	7820,00	0,95	1,17
MDA-MB-435	4297,48	2395,31	0,56	0,68
MDA-MB-231	9528,42	10937,43	1,15	1,40
MDA-MB-361	8964,82	4861,08	0,54	0,66
N1	24878,79	26832,27	1,08	1,16
N2	13719,26	16975,06	1,24	
T47D	21084,10	35948,51	1,71	1,47
MDA-MB-157	12798,66	25889,21	2,02	1,75
BT549	14168,34	18726,46	1,32	1,14
SKBR3	21825,08	30177,89	1,38	1,19
MCF10	13247,73	17985,48	1,36	1,17
HST578T	9003,97	7477,11	0,83	0,72
BT474	9857,21	15852,37	1,61	1,39
MDA-MB-468	9565,31	12686,39	1,33	1,15
HPV4-12	6915,77	10216,47	1,48	1,28

Figure 3.35: hsa-mir-16-2 semi-quantitative duplex PCR results
Upper bands are GAPDH and lower bands are microRNA genes. in gel images. Fold changes are represented as colored boxes from grey to black scale with increasing fold change respectively and dashed boxes represent fold changes of loss.

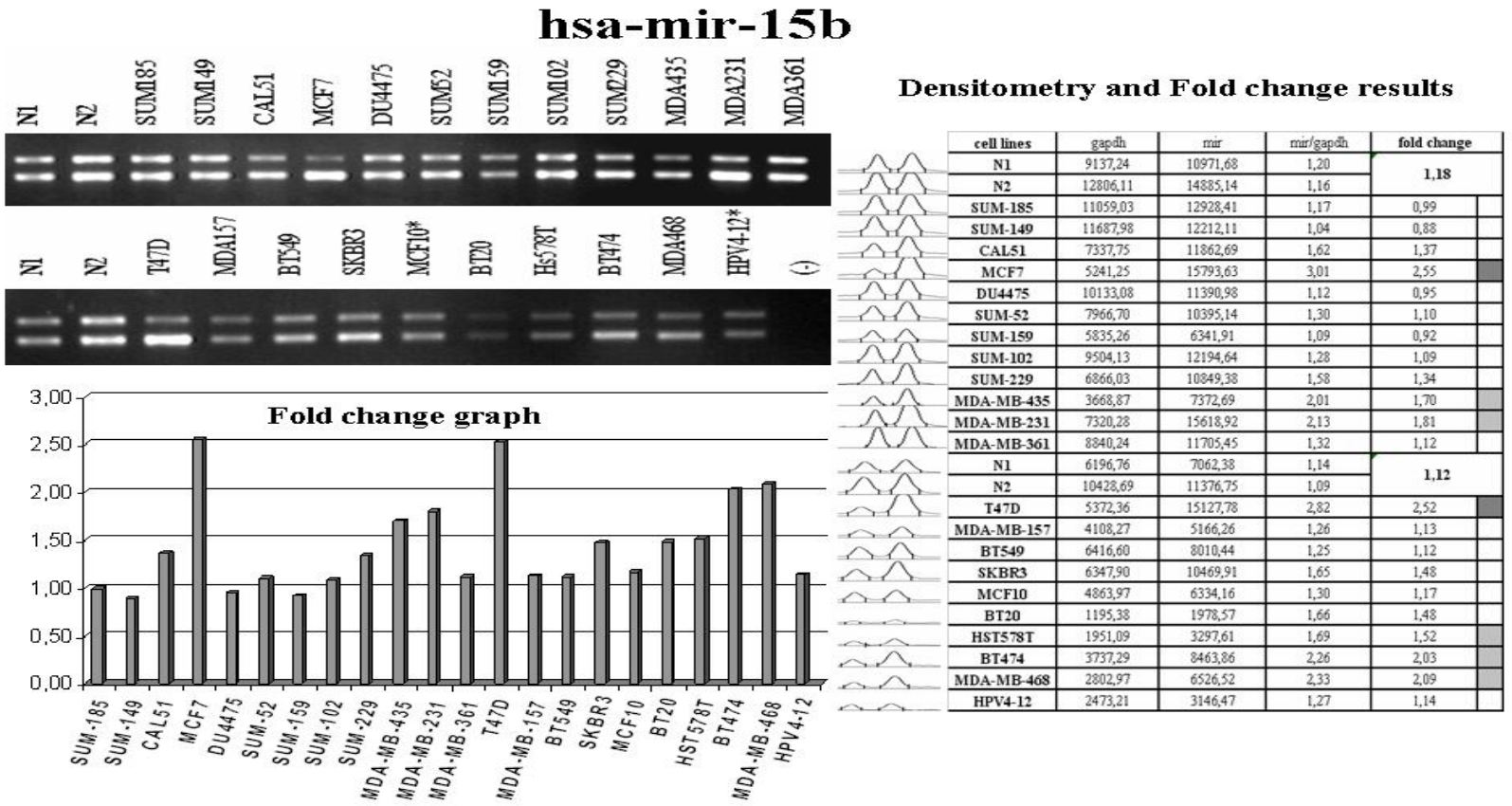

cell lines	gapdh	mir	mir/gapdh	fold change
N1	9137,24	10971,68	1,20	1,18
N2	12806,11	14885,14	1,16	
SUM-185	11059,03	12928,41	1,17	0,99
SUM-149	11687,98	12212,11	1,04	0,88
CAL51	7337,75	11862,69	1,62	1,37
MCF7	5241,25	15793,63	3,01	2,55
DU4475	10133,08	11390,98	1,12	0,95
SUM-52	7966,70	10395,14	1,30	1,10
SUM-159	5835,26	6341,91	1,09	0,92
SUM-102	9504,13	12194,64	1,28	1,09
SUM-229	6866,03	10849,38	1,58	1,34
MDA-MB-435	3668,87	7372,69	2,01	1,70
MDA-MB-231	7320,28	15618,92	2,13	1,81
MDA-MB-361	8840,24	11705,45	1,32	1,12
N1	6196,76	7062,38	1,14	1,12
N2	10428,69	11376,75	1,09	
T47D	5372,36	15127,78	2,82	2,52
MDA-MB-157	4108,27	5166,26	1,26	1,13
BT549	6416,60	8010,44	1,25	1,12
SKBR3	6347,90	10469,91	1,65	1,48
MCF10	4863,97	6334,16	1,30	1,17
BT20	1195,38	1978,57	1,66	1,48
HST578T	1951,09	3297,61	1,69	1,52
BT474	3737,29	8463,86	2,26	2,03
MDA-MB-468	2802,97	6526,52	2,33	2,09
HPV4-12	2473,21	3146,47	1,27	1,14

Figure 3.36: hsa-mir-15b semi-quantitative duplex PCR results
Upper bands are GAPDH and lower bands are microRNA genes. in gel images. Fold changes are represented as colored boxes from grey to black scale with increasing fold change respectively and dashed boxes represent fold changes of loss.

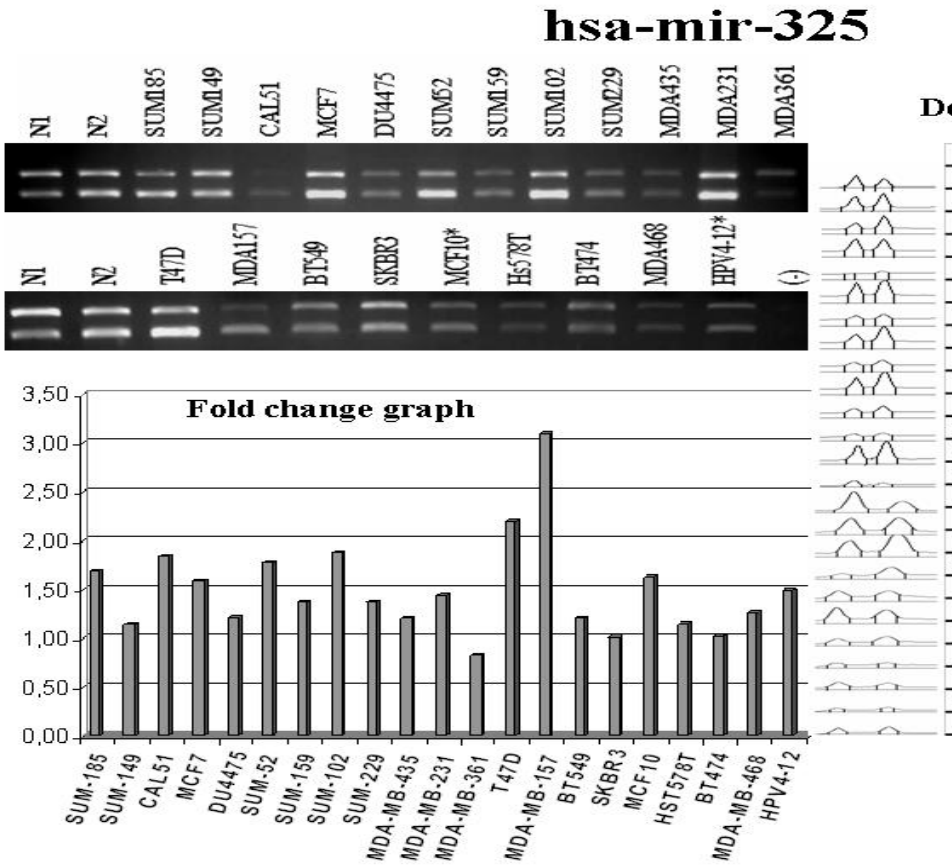

Densitometry and Fold change results

cell lines	gapdh	mir	mir/gapdh	fold change
N1	2086,02	1702,38	0,82	0,93
N2	3176,98	3344,82	1,05	
SUM-185	2253,86	3548,63	1,57	1,69
SUM-149	4064,14	4315,90	1,06	1,14
CAL51	1102,95	1894,20	1,72	1,85
MCF7	3812,38	5634,65	1,48	1,59
DU4475	2565,56	2901,24	1,13	1,22
SUM-52	3488,68	5754,53	1,65	1,77
SUM-159	2649,48	3380,79	1,28	1,37
SUM-102	3452,72	6030,27	1,75	1,88
SUM-229	2349,77	2997,15	1,28	1,37
MDA-MB-435	1918,18	2157,95	1,12	1,21
MDA-MB-231	4004,19	5346,92	1,34	1,44
MDA-MB-361	1330,74	1019,03	0,77	0,82
N1	11918,93	7485,58	0,63	0,89
N2	9736,78	11269,81	1,16	
T47D	9115,29	17843,86	1,96	2,20
MDA-MB-157	2983,18	8245,19	2,76	3,11
BT549	6284,02	6739,79	1,07	1,21
SKBR3	8493,79	7665,13	0,90	1,01
MCF10	4060,45	5897,31	1,45	1,63
HST578T	2499,80	2555,04	1,02	1,15
BT474	4129,50	3742,79	0,91	1,02
MDA-MB-468	1533,03	1726,38	1,13	1,27
HPV4-12	2458,36	3259,41	1,33	1,49

Figure 3.37: hsa-mir-325 semi-quantitative duplex PCR results
Upper bands are GAPDH and lower bands are microRNA genes. in gel images. Fold changes are represented as colored boxes from grey to black scale with increasing fold change respectively and dashed boxes represent fold changes of loss.

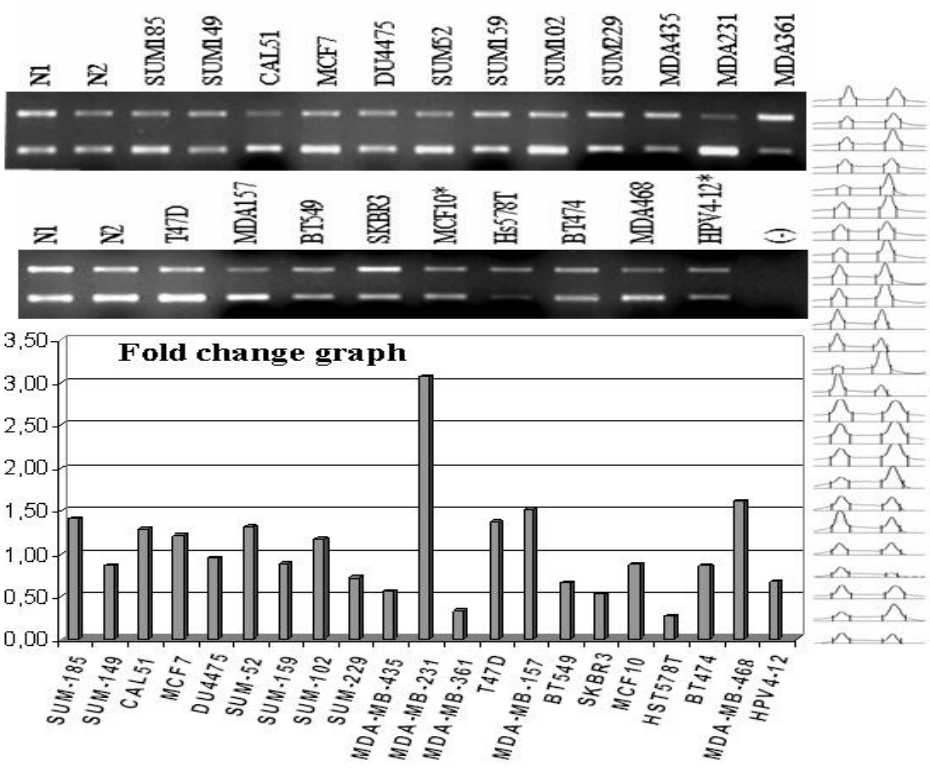

Densitometry and Fold change results

cell lines	gapdh	mir	mir/gapdh	fold change
N1	12809,24	13361,36	1,04	1,26
N2	7464,69	10976,19	1,47	
SUM-185	8701,45	15459,42	1,78	1,41
SUM-149	9606,93	10313,64	1,07	0,85
CAL51	7398,44	12036,26	1,63	1,29
MCF7	11439,97	17491,23	1,53	1,22
DU4475	11439,97	13626,38	1,19	0,95
SUM-52	10181,13	16828,69	1,65	1,32
SUM-159	12500,05	13935,57	1,11	0,89
SUM-102	12279,20	18021,27	1,47	1,17
SUM-229	11660,82	10556,58	0,91	0,72
MDA-MB-435	9960,29	7067,16	0,71	0,56
MDA-MB-231	4858,68	18705,90	3,85	3,06
MDA-MB-361	14001,82	5918,75	0,42	0,34
N1	17021,84	18335,20	1,08	1,28
N2	13617,47	20253,39	1,49	
T47D	11751,12	20685,42	1,76	1,37
MDA-MB-157	7379,01	14343,27	1,94	1,52
BT549	8865,18	7465,41	0,84	0,66
SKBR3	12736,14	8640,53	0,68	0,53
MCF10	6324,87	7102,51	1,12	0,88
HST578T	5616,34	1918,20	0,34	0,27
BT474	8467,72	9297,21	1,10	0,86
MDA-MB-468	5668,19	11699,27	2,06	1,61
HPV4-12	5650,90	4855,98	0,86	0,67

Figure 3.38: hsa-mir-384 semi-quantitative duplex PCR results
Upper bands are GAPDH and lower bands are microRNA genes. in gel images. Fold changes are represented as colored boxes from grey to black scale with increasing fold change respectively and dashed boxes represent fold changes of loss.

3.3 Expression Analysis Results

Expression analysis of microRNAs was performed for two forms of the microRNA pre-miRNA (precursor) by RT-PCR and mature miRNA (active form) by real-time RT-PCR.

3.3.1 pre-miRNA Expression Results

Both oligodT and random hexamer primers were used in cDNA synthesis although pre-microRNAs were known to have no poly-A tail but primary microRNAs have. Because pre-miRNAs are small (~70 bp), cDNA synthesis might not be efficient or not reflect the actual pre-miRNA amount in the cell. RT-PCR by oligodT and random hexamer primers in MCF7, MDA-MB-231, HeLa and normal breast tissue agarose gel image was given in Figure 3.39. HeLa cell line was used as a non-breast sample for comparison.

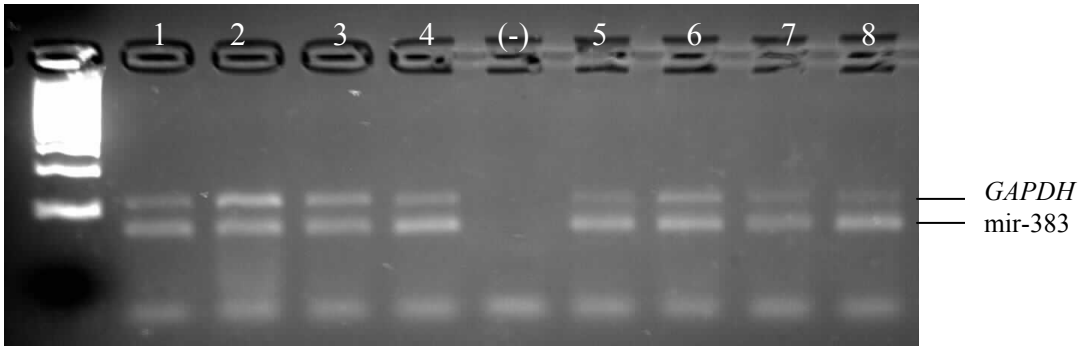

Figure 3.39: RT-PCR of hsa-mir-383 pre-miRNA in MCF7, MDA-MB-231, HeLa and normal breast tissue by using oligodT and random hexamer primers. Legend is shown in Table 3.2.

Fold changes of hsa-mir-383 in cell lines normalized to microRNA (mir)/ *GAPDH* in normal breast are shown in Table 3.2. Results showed that oligodT and random hexamer primers didn't differ and resulted in similar fold changes.

Table 3-2: Densitometry and Fold Change Results for hsa-mir-383 normalized to *GAPDH* and normal breast tissue.

	primers used in RT	cell lines	*GAPDH*	mir	*mir/GAPDH*	fold change normalized
1	oligodT	MCF7	6461,84	10515,12	1,63	0,77
2	oligodT	MDA-MB-231	19096,00	17340,40	0,91	0,43
3	oligodT	HeLa	16250,08	16662,80	1,03	0,48
4	oligodT	Normal breast	11944,24	25379,20	2,12	
5	random hexamer	MCF7	9116,80	22422,40	2,46	0,80
6	random hexamer	MDA-MB-231	14469,84	23278,64	1,61	0,52
7	random hexamer	HeLa	8155,84	13810,72	1,69	0,55
8	random hexamer	Normal breast	6092,24	18695,60	3,07	

Densitometry analysis on the RT-PCR gel image showed that hsa-mir-383 precursor expression was detected as loss (with fold changes ranging from 0.4 to 0.8) in MCF7, MDA-231, and HeLa cells compared to normal breast tissue. Analysis of precursor miRNAs (pre-miRNA) and primary transcripts (pri-miRNA) was not very accurate as differentiating them was not easy. Although primary transcript and pre-miRNA expression levels indicate expression of the mature form, it is not necessarily a direct indication of how much mature microRNA is present. Detection of mature microRNAs gives more biologically relevant results in expression levels and significance of a particular microRNA as mature forms are the active forms.

3.3.2 Mature microRNA Expression Results

Detection of mature microRNA expression is challenging with methods such as northern blotting [115], microarrays, and microRNAs are very small and require optimizations for accurate detection especially for low abundant microRNAs. Real-time RT-PCR analysis is used to detect mature microRNAs

Expression of hsa-miR-21 and hsa-miR-383 was analyzed using Taqman miRNA assay kit and compared to U6 expression. Data analysis was done using absolute quantification.

3.3.2.1 Results for RNA Isolation by Trizol Reagent versus *mir*Vana

Real time RT-PCR analysis of hsa-miR-21 in MCF7 was compared by using two different RNA isolation methods: mirVana and Trizol. *Mir*Vana microRNA isolation kit detected was more sensitive in detecting hsa-miR-21 (at Ct=18) than Trizol Reagent (Ct=19) with no very significant difference (Figures 3.40 and 3.41). This shows the accuracy and efficiency of both detection method and isolation methods. Trizol Reagent was used for further experiments as it is more cost effective.

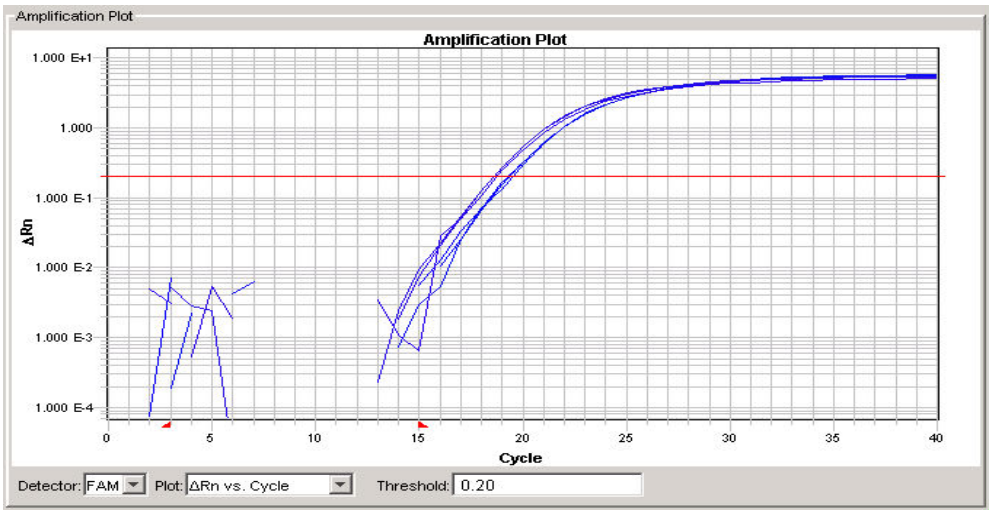

Figure 3.40: Amplification plot (Ct=18 and Ct=19) of hsa-miR-21 in MCF7
Starting amount of 10 ng and 20 ng RNA were used and isolated by *mir*Vana Isolation Kit.

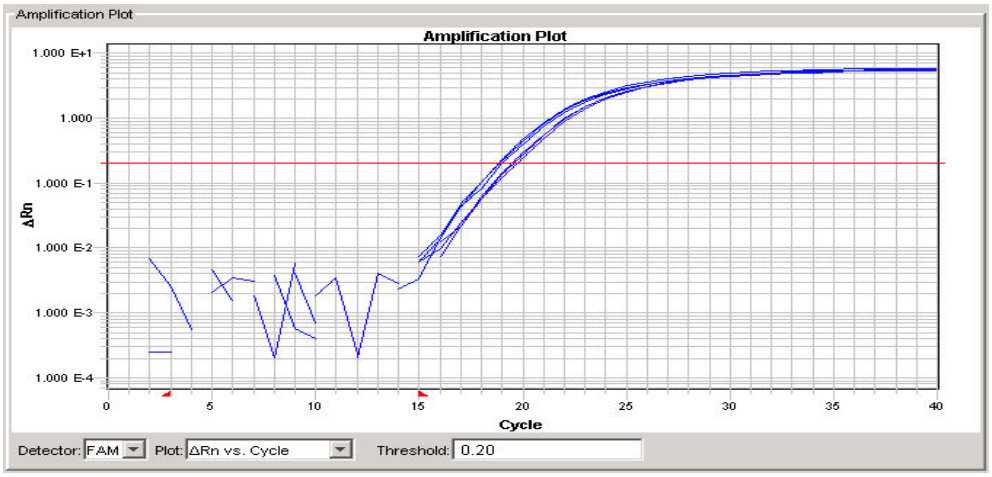

Figure 3.41: Amplification plot (Ct=19) of hsa-miR-21 in MCF7
Starting amount of 10 ng and 20 ng RNA were used and isolated by Trizol Reagent.

3.3.2.2 Real time RT-PCR Results and Absolute Quantification of U6, hsa-miR-21 and hsa-miR-383

Taqman microRNA real-time detection involved two types of data analysis: relative quantification and absolute quantification.

Relative quantification (comparative Ct method) requires an endogenous gene that is constantly expressed across the samples to normalize sample expressions according to a selected calibrator sample. Constitutive expression of selected endogenous gene was analyzed prior to the experiment. Commonly used endogenous genes are 18S rRNA, let-7a, and hsa-miR-16. Ribosomal RNA (rRNA) 18S subunit was used in some studies and found to be most stable endogenous gene in colorectal cancer samples [116]. RNU6B regulation process is similar to that of microRNAs, unlike 18S rRNA. Moreover, let-7a and hsa-mir-16 have the potential to be deregulated in cancer samples and might not be suitable endogenous genes. To keep the RT efficiency similar with microRNAs, RNU6B was used in other studies in breast cancer samples. In our study, we

decided to select RNU6B (small nuclear U6) as an endogenous gene, available in Taqman microRNA assays.

In our study, we assigned quantities of selected standard sample as 1, 0.5, 0.25, and 0.125 for cDNA dilutions no dilution (neat), 1:2, 1:4, and 1:8, respectively. Thus, the quantities detected were relative to standard sample selected but not the absolute quantity in the cell. In calculation of quantities, the average of all biological and technical replicates was used.

3.3.2.2.1 Absolute Quantification of U6 Endogenous Gene

Prior to detection of hsa-miR-21 and hsa-miR-383, U6 was tested to check its constant expression across different cancer samples. Acceptable Ct differences across samples should be 0.5-1 Ct (1-2 folds).

Quality control values (slope=-3.45 and R^2=0.95) in the standard curve indicated that the efficiency and reliability of the detection is optimal (Figure 3.42). Quantities of other cell lines were calculated by the SDS 2.0 software using this standard plot, assigning each quantity due to Ct value detected in PCR reaction.

The absolute quantification of U6, to see whether it was suitable for relative quantification, resulted in variation in expression across different cell lines. The amplification plot in Figure 3.43 shows variation of U6 expression detected in a Ct ranging from 32-35 cycles. A 3 Ct change is equal to a 6 fold difference across samples. This may be due to various genetic alterations present in each cell line. Thus, instead of using U6 in comparative quantification and normalization, absolute quantification by constructing a standard curve was used in data analysis.

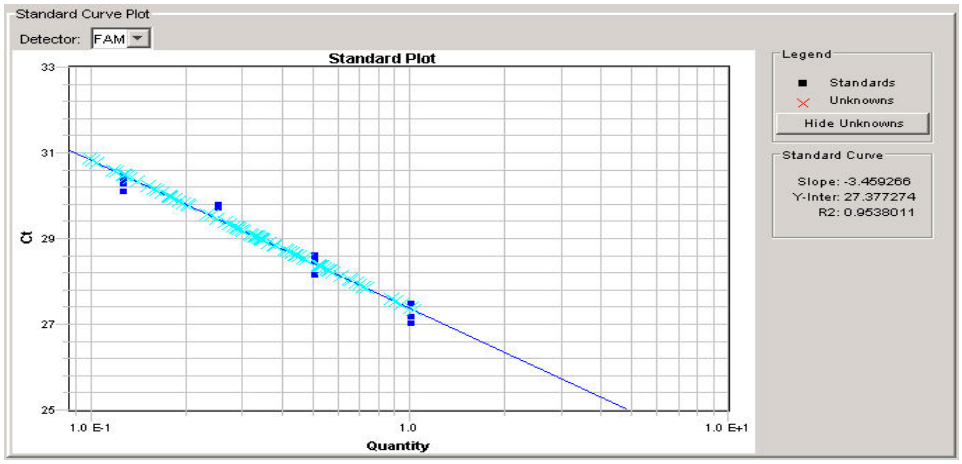

Figure 3.42: Standard Plot of U6 gene in MCF10 cell line
MCF10 was used to construct a standard curve and quantify U6 gene in other cell lines. Blue dots are different dilutions of MCF10 and replicates

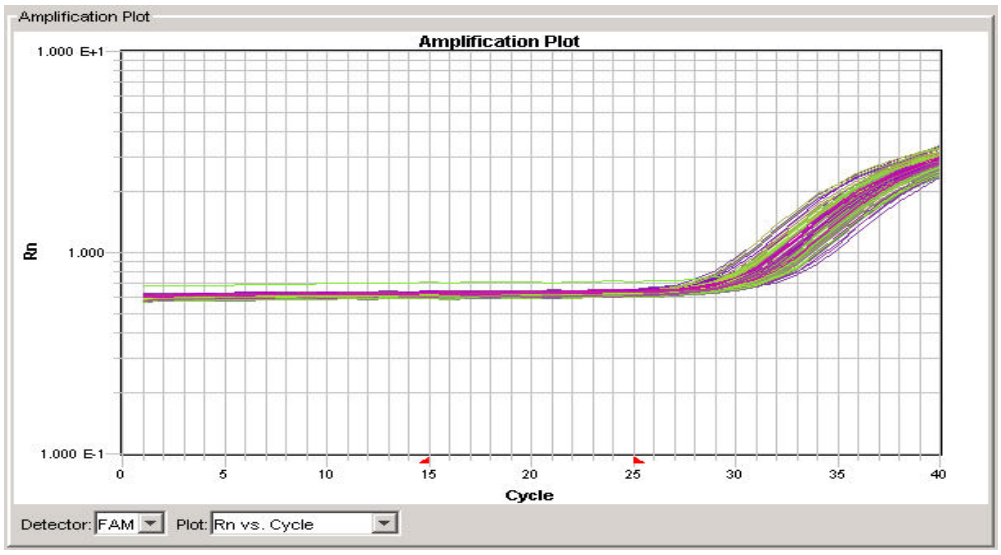

Figure 3.43: Amplification plot of U6 in all cell lines
Data is represented by different colors, Ct (at exponential state) of each sample shows variation ranging from 32-35 cycles.

The expression level variation of RNU6B among cancer cell lines and MCF10 (immortalized breast cell line) is shown in Figure 3.44. This variation was not in an acceptable range for relative quantification and normalization. Thus, absolute quantification of U6 and microRNAs were done and U6 was compared to microRNAs for each cell line, individually.

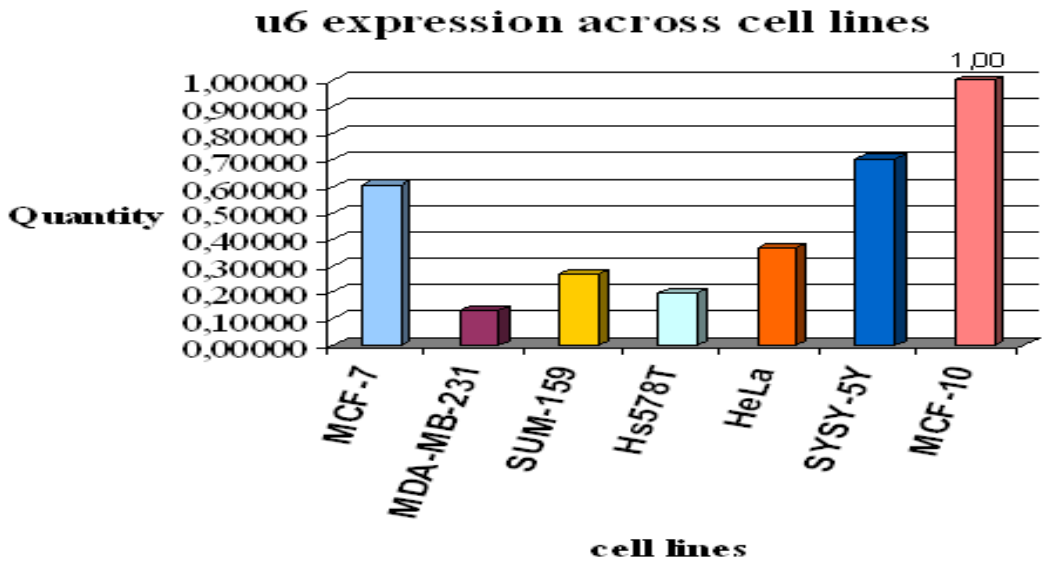

Figure 3.44: Real time RT-PCR analysis of U6 gene in all cell lines by absolute quantification

3.3.2.2.2 Absolute Quantification of hsa-miR-21

Quality control values (slope=-3.59 and R^2=0.97) in standard curve (Figure 3.45) indicated that the efficiency and reliability of the detection was optimal. MCF10 was used as standard sample. Overall amplification plot of all samples are shown (Figure 3.46).

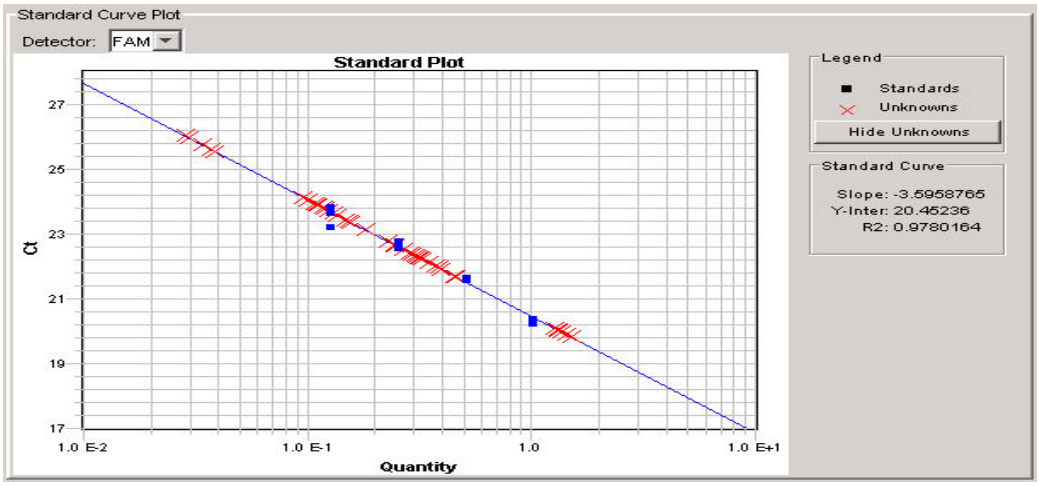

Figure 3.45: Standard Plot of hsa-miR-21 gene in MCF10 cell line
MCF10 was used to construct a standard curve and quantify hsa-miR-21 in other cell lines.

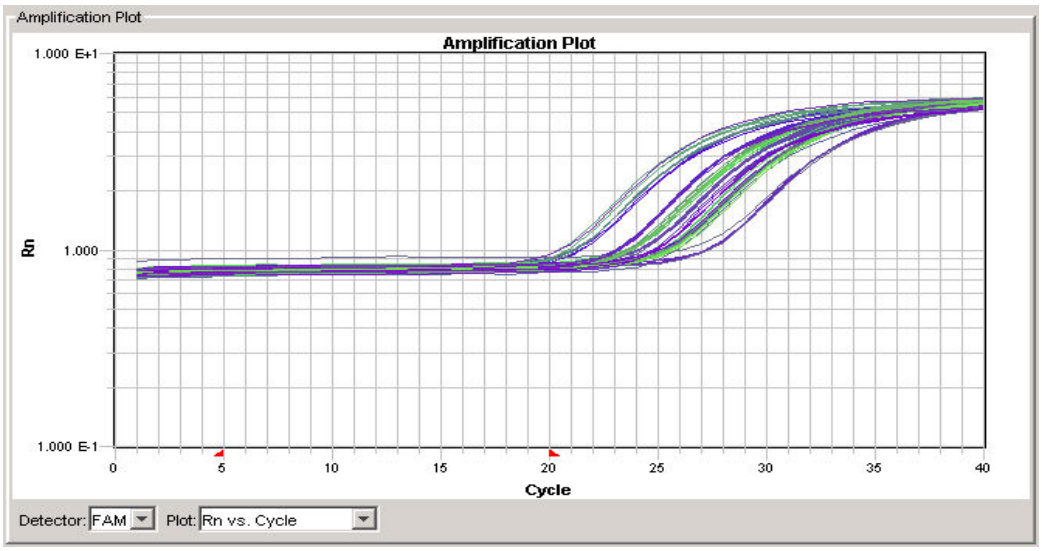

Figure 3.46: Amplification plot of hsa-miR-21 in all cell lines

Quantities calculated for hsa-mir-21 in 7 breast cancer cell lines and rat brain tissue show that hsa-mir-21 expression varies across cancer cell lines. Especially, MCF7 shows higher expression compared to other cell lines including

MCF10. However, other cell lines, MDA-MB-231, HS578T, SUM159, HeLa, and SHSY-5Y show low expression compared to MCF7 and MCF10. Also, hsa-mir-21 expression is low in SHSY-5Y (neuroblastoma cell line) and rat brain tissue (Figure 3.47).

Considering MCF10 as a representative of normal breast, expression of hsa-mir-21 was down-regulated in cancer cell lines, except MCF7, which is contrary to studies showing overexpression and oncogenic role of hsa-mir-21 in several tumors compared to normal tissues [69], [70], [71], [68]. There are no published reports on hsa-mir-21 expression in MCF10. However, it is not clear that MCF10 cell line represents real expression of a normal breast since it is derived from breast epithelial tissue that was processed through a spontaneous immortalization step

Studies on MCF10 have shown that it represents normal breast characteristics as it lacked tumorigenicity in nude mice, three- dimensional growth in collagen, hormone and growth factor induced growth in culture, and formation of dome in confluent cultures. Although cytogenetic analyses on MCF10 before immortalization process indicates a normal diploid genome, immortalized MCF10 by cultivating in low calcium concentrations was shown to exhibit minimal rearrangements and abnormal karyotype [117]. Hence, immortalization step might have caused some rearrangements in the genome as well as possible gene expression differences. Moreover, it is acceptable that cells should change some characteristics to adjust cultivation and continuous division. Continuous cultivation and passaging may have also caused small regional rearrangements in the genome even if its karyotype shows diploidy. Considering all these possibilities, it would be a biased argument to consider MCF10 as “normal breast sample”, although it is widely used as a model in studies with cancer cell lines.

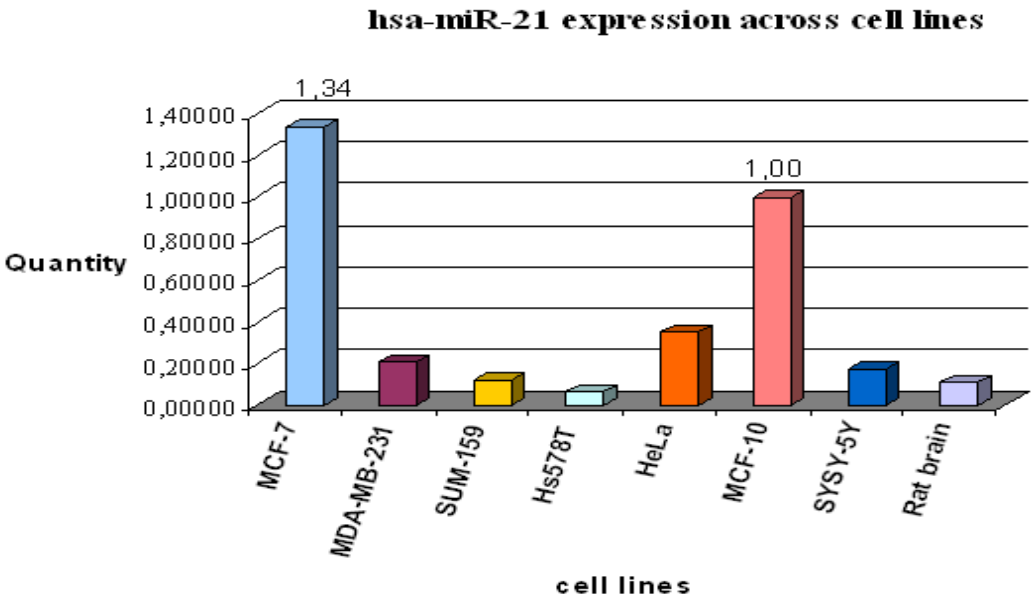

Figure 3.47: Real time RT-PCR analysis of hsa-miR-21 in cell lines by absolute quantification. MCF10 was used in standard curve and rat brain tissue was used as a control.

When we compare hsa-mir-21 expression to U6 expression within each cell line (Figure 3.48), its expression is higher in MCF7 and MDA-MB-231. MCF10 was set to equal expression as it was used in standard curve plot. SUM159 and HS578T show lower expression of hsa-mir-21 compared to U6 expression. HeLa and SHSY-5Y also showed lower expression compared to U6. These results might be due to gene expression deregulations due to cultivation and passaging of cell lines. Besides these, hsa-miR-21 expression (as well as many other microRNAs) may be dependent on complex factors such as cell type, cellular status, environmental effects or combinatorial consequence of these.

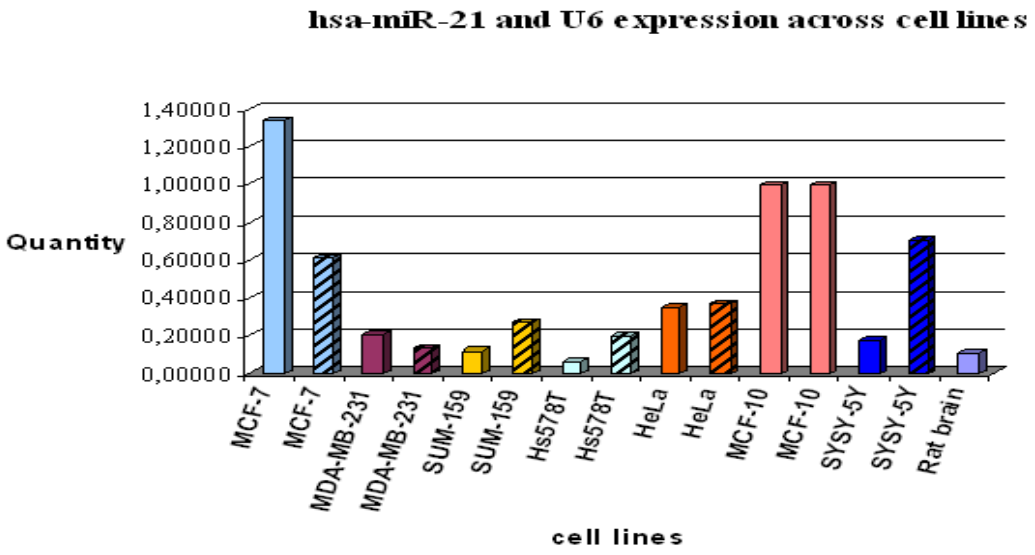

Figure 3.48: Comparison of hsa-miR-21 and U6 expression in cell lines

3.3.2.2.3 Absolute Quantification of hsa-miR-383

Quality control values (slope=-3.76 and R^2=0.96) in standard curve (Figure 3.49) indicated that the efficiency and reliability of the detection is in the optimal range. Rat brain tissue was used as standard sample as previously we detected its high expression in this tissue. Overall amplification plot of all samples are shown in Figure 3.50.

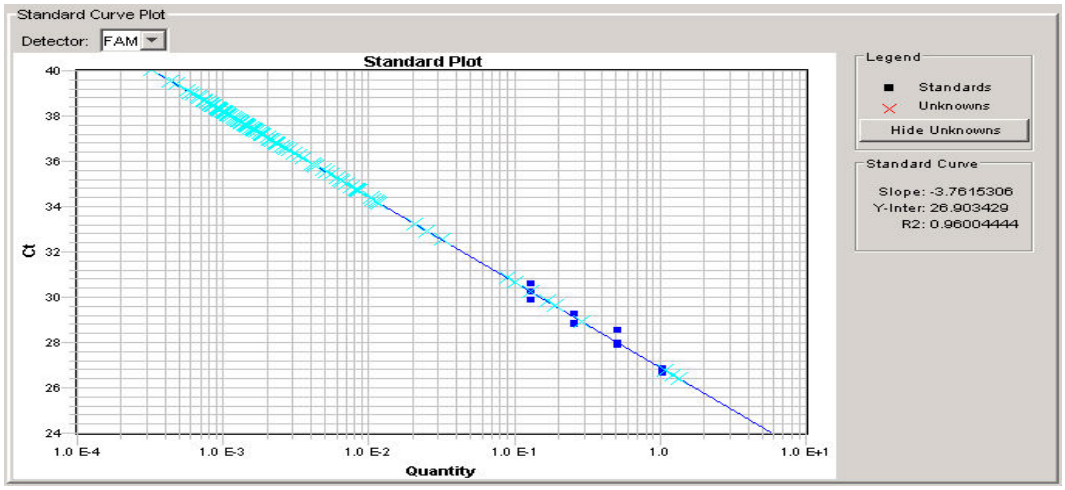

Figure 3.49: Standard plot of hsa-miR-383 in brain tissue
Rat brain tissue was used to construct a standard curve and quantify hsa-miR-21 in other cell lines.

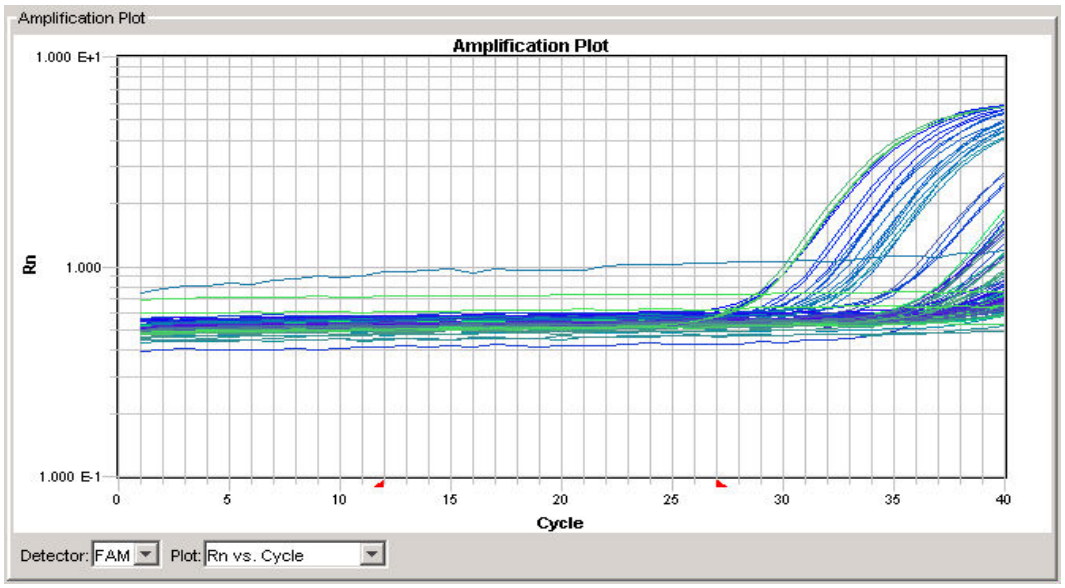

Figure 3.50: Amplification plot of hsa-miR-383 in all cell lines

Absolute quantification of hsa-miR-383 (Figure 3.51) in breast cancer cell lines showed that its expression is very low except in MDA-MB-231 and rat brain tissue where hsa-miR-383 is highly expressed. This may indicate that hsa-mir-383 is a brain specific miRNA; however, in the neuroblastoma cell line (SHSY-5Y) it is also expressed at low levels. Relatively high expression in the MDA-MB-231 cell line may suggest its cell type specific expression. MDA-MB-231 is known to be different from other cell lines as it is poorly differentiated and highly metastatic, Estrogen Receptor negative (ER-). Thus these differences may cause differential expression of some microRNAs.

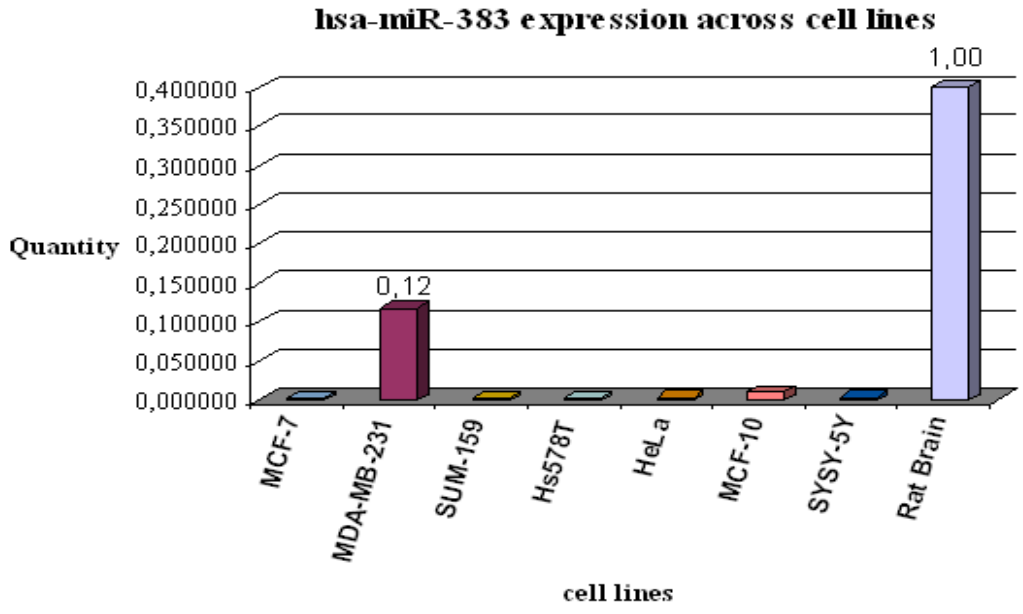

Figure 3.51: Real-time RT-PCR analysis of hsa-miR-383 in all cell lines

When we compare it with internal U6 expression, it is down-regulated in all cell lines, except MDA-MB-231 where its expression if slightly higher than U6 (Figure 3.52). It significance in MDA-MB-231 cell line should be investigated further.

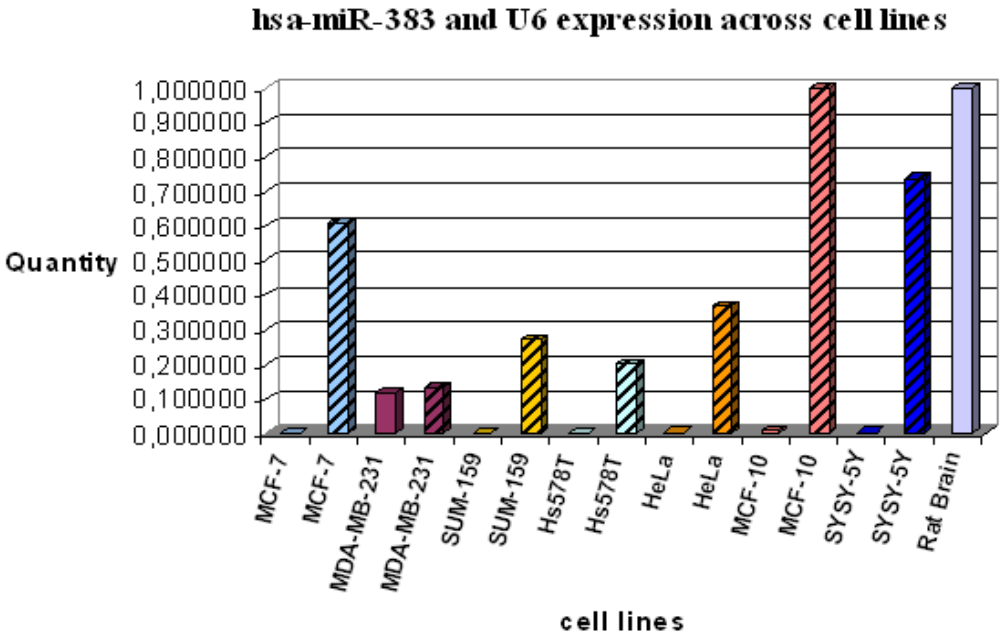

Figure 3.52: Comparison of hsa-miR-383 and U6 expression in cell lines

3.4 Potential Targets of hsa-miR-21

A search for predicted miR-21 targets in available microRNA target prediction programs (MiRanda, miRBase, TargetScan, and Pictar) resulted in a list of a thousand genes targeted by miR-21 with near-perfect complementarity to 3'UTR regions. High scoring (top of the list) targets indicated the high probability of being targeted by corresponding microRNA. Approximately 40 genes were selected from each program according to listing from high score to low score (top to bottom) within each program (Table 3.4).

Table 3-3: Predicted targets of hsa-miR-21 by 4 target prediction programs
Colored pairs are common genes targeted by different programs

MiRanda		MiRBase		TargetScan		Pictar	
NFIB	Nuclear factor I/B	PDCD4	neoplastic transformation inhibitor, apoptosis	PLAG1	Protooncogene	PLAG1	Protooncogene
CNTFR	Ciliary neurotrophic factor receptor	PELI1	Adaptor of tum necrosis factor	PURB	DNA replication and transcription	RP2	Retinitis pigmentosa
SOX5	Regulation of embryonic development, determination of cell fate	MRIP	unknown	LOC153222	Adult retina protein	ADNP	Stimulatory or inhibitoey of tumor cells
ACAT1	Acetyl-Coenzyme A acetyltransferase	GLCCI1	Glucocorticoid induced transcript 1	ARHGAP24	GTPase activating protein	LOCI153222	Adult retina protein
PCBP1	Poly(rC) binding protein, RNA binding	NFIB	nuclear factor I/B	BNC2	basonuclin	CCL1	Inflammatory process
PIK3R1	Metabolic actions of insulin	THOC7	unknown	CCL1	Inflammatory process	PIP3AP	PIP3 associated protein
SLMAP1		TSG101	Tumor susceptibility gene 101	CDC25A	oncogene	STAT3	Transcription activator, apoptosis
RECK	Reversion-inducing-cysteine-rich protein, expression is suppressed in many tumors	TGFB1	Transforming growth factor, deregulation shown in cancer	CBFP		TESK2	Testis specific kinase
PHF6	Transcriptional regulation, mental retardation	CCL1	Inflammatory process	EHD1	Endocytosis of IGFI receptors	SATB1	Homeobox 1 ,apoptosis
BRD1	Unknown	ZNF104	Zinc finger protein	ELF2	Transcription factor	SFRS8	Splicing regulatory protein
MRPL9	Helps protein synthesis within the mitochondrion	IL12A	Natural killer cell stimulatory factor	EPHA4	Nervous system	CNTFR	Ciliary neurotrophic factor receptor
PITX2	Transcription factor , development of the eye	MSH2	Homolog of mismatch repair gene, mutated in colon cancer	FASLG	apoptosis	PB1	polybromo
STAG2	Transcriptional co-activator, stromal antigen	UFC1	Ubiquitin-fold modifier conjugating enzyme	FLJ13910	Meiotic nuclear division	BRD2	Signal transduction pathway in growth control
PTGER3	digestion, nervous system, kidney reabsorption, and uterine contraction	STCH	Stress protein chaperone	GATAD2B	GATA zinc finger domain	PPARA	Peroxisome proliferator activated receptor
KCNA3	T-cell proliferation and activation	ASPN	Cartilage matrix	GPR64	G-protein coupled receptor	NTF3	Survival and differentiation of neurons
PLEKHA1	age-related maculopathy	RTN4	Neurite outgrowth inhibitor	JAG1	Tumor progression	MRPL9	Helps protein synthesis within the mitochondrion
PDCD4	neoplastic transformation inhibitor, apoptosis	KRIT1	Ankyrin repeat containing	LOC51136	unknown	ZNF367	Zinc finger protein
SKI	Sarcoma Viral oncogene	LANCL1	Peptide modifying enzyme	MRIP	unknown	MRIP	unknown
RQCD1	Tumor suppressor,retinoic acid different.	CCL20	Chemokine ligand	NFIB	Nuclear factor I/B	NPAC	unknown
NT3	3' nucleotidase	PCBP2	poly(rC) binding protein, RNA binding	PDCD4	neoplastic transformation inhibitor, apoptosis	PCBP1	poly(rC) binding protein, RNA binding
HPGD	Prostoglandin,colon cancer	SPATA5L1	Spermatogenesis associated	PELI1	Adaptor of tum necrosis factor	CASKIN	
CCL22	Chemokine,promotes bone metastasis of lung ca.	TTRAP	Tumor necrosis factor, inhibits NF-KB	PLEKHA1	age-related maculopathy	DDA3	p53 mediated growth suppression
GNG12	MAPK pathway	TSN9		PPARA	Peroxisome proliferator activated receptor	SPIN	unknown
RNPS1	mRNA survaliance	ATX2	unknown	RAB11A	Ras oncogene family member	TGFBI	Transforming growth factor, deregulation shown in cancer

SOX2	Sex determining region Y, driver of breast cancer	TEK	Endothelial tyrosine kinase	RASGRP1	Ras guanyl releasing protein	RNF103	Protein-protein-DNA interactions
MTAP	Polyamine metabolism,deficient in many cancer,MCF7, co-deleted with p16	DEPDC1	unknown	RECK	reversion-inducing-cysteine-rich protein, expression is suppressed in tumors	SKI	Sarcoma Viral oncogene
SOCS5	Suppressor of cytokine signalling	SNRPA1	Small nuclear ribonucleoprotien polypeptide	SCML2	unknown	TIMP3	Inhibitors of matrix metalloproteinases
GLCCI1	Glucocorticoid induced transcript 1	GALNT12	unknown	SKI	Sarcoma Viral oncogene	BRD1	Unknown
SATB1	Homeobox 1 ,apoptosis	PMI4		SMAD7	Block apoptosis	TAGAP	T cell activation
JAG1	Alagille syndrome, overexpressed in breast cancer	MERTK	Protooncogene tyrosine kinase	SOX5	Regulation of embryonic development, determination of cell fate	RHOB	Apotosis, tumor suppressor!!
TRPM7	Receptor potential cation channel, apoptosis	TNFRSF11B	Tumor necrosis factor receptor	TGFB1	Transforming growth factor, deregulation shown in cancer	PITX2	Transcription factor , development of the eye
TGFB1	Transforming growth factor, deregulation shown in cancer	PIK3R1	Kinase, metabolic actions of insulin	PIK3R1	Kinase, metabolic actions of insulin	PLEKHA1	age-related maculopathy
CBEP3	Neuronal	FASLG	Tumor necrosis factor, apoptosis	TAGAP	T cell activation	SMAD7	Block apoptosis
PRPF4B	Pre-mRNA processing factor	TGFBR2	Transforming growth factor	CASC4	Cancer susceptibility candidate, increased expression is related with overexpression of Her-2/neu protooncogene	NFIB	Nuclear factor I/B
EGFL5	Multiple epidermal growth factor domain			MTAP	Polyamine metabolism,deficient in many cancer,MCF7, co-deleted with p16	MATR3	Role in transcription
OSBPL1A	Intracellular lipid receptor					SOX2	Sex determining region Y, driver of breast cancer
KCNA1	Potassium channel,MCF7 cell proliferation,epilepsy					KCNA2	Potassium channel
RHOB	Apotosis, tumor suppressor					RECK	reversion-inducing-cysteine-rich protein, expression is suppressed in tumors
MBL1	Manose specific leptin, Muscle dystrophy					TRPM7	Apoptosis;neuronal death
VCL	Cell-cell junctions, Cardiomyopathy					JAG1	Tumor progression
MATR3	Role in transcription					PDCD4	neoplastic transformation inhibitor, apoptosis
PLAG1	Pleiomorphic adenoma gene, Protooncogene					SOX5	Regulation of embryonic development, determination of cell fate
MAPK10	Kinase ,neuronal apoptosis					BCL2	Blocks apoptosis

Some genes with potential important roles in cancer mechanism (role in apoptosis and kinases) were predicted more than one program such as *PIK3RI, RECK, PLEKHA1, JAG1, and TRPM7*. Among this list, *PCDC4* and *TGFBI* were predicted by all 4 programs with potential roles in cancer such as tumor suppressor or growth factor. Recently, PDCD4 (predicted by all programs) has been shown to be regulated by hsa-miR-21 in colon cancer samples [71]. BCL-2 (predicted by Pictar) has also been shown to be indirectly regulated by hsa-mir-21 in breast cancer cells. This indirect effect was observed by transfection of MCF7 cells with anti-mir-21 inhibitors which resulted in down-regulation of BCL-2 protein (anti-apoptotic) and so lead to apoptosis [69] which may indicate the regulation of a gene that regulates BCL-2 protein expression. This may explain

the complexity of microRNA targeting and predicted oncogene targets of an oncogenic microRNA.

Experimental verifications of microRNA targets predicted by these target prediction programs show that it is worth to interrogate these predicted targets experimentally. Six target genes were selected (Table 3.4) and were examined for 3' UTR sites that hsa-miR-21 binds by using target prediction programs. Almost all resulted in same target sequences (~22 bp) which is imperfect complementary. Total 40 bp of these target regions (ordered as oligos from Sigma) were cloned into 3' UTR of luciferase vector (pMIR-REPORT miRNA Expression Reporter Vector; Ambion, AM5795; Vector map is given in Figure 3.45) and sequencing results confirmed successful cloning. Future direction for this project will be the experimental validation of hsa-miR-21 targeting these sequences and down-regulate that gene having potential roles in tumorigenesis

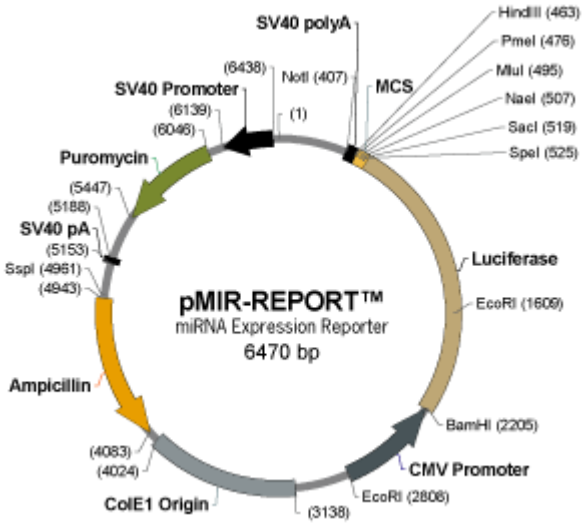

Figure 3.53: Map of PMIR-REPORT Luciferase Expression Vector

CHAPTER 4

CONCLUSION

MicroRNAs are recently discovered small non-coding RNAs that regulate protein expression and they have been found to have important roles in cellular pathways such as tumorigenesis.

The objective of this study was to investigate microRNAs mapping to reported common genomic instability regions in breast cancer.

To achieve this, first, a literature search on common reported genomic instability regions (loss or gain) in breast cancer was investigated and 18 regions were selected for further analyses. Thirty-nine microRNA genes were found to map to these regions by using databases such as UCSC Genome Browser, miRBase.

Thirty-nine DNA regions of pre-microRNAs (precursor) identified were further interrogated for confirmation of genomic instability in 20 breast cancer cell lines and 2 immortalized cell lines by using semi-quantitative duplex PCR method. Two normal DNAs were used as controls. GAPDH was co-amplified with microRNA genes and used as housekeeping gene. Densitometry analyses and fold change calculations showed that 61% (22/36) of microRNAs exhibited genomic instability (loss-less than 0.5 fold or gain-more than 2.5 folds) in at least 3 cell lines.

Among microRNAs showing significant gains, hsa-mir-383 and hsa-mir-21 were selected for further expression analysis in two stages. First, hsa-mir-383 pre-miRNA expression in MCF7, MDA-MB-231, HeLa, and normal breast was analyzed by using RT-PCR. However, this method is not very accurate in differentiating pre-miRNAs (precursor transcripts) and pri-miRNAs (primary transcripts).

Then, expression of hsa-miR-383 and hsa-miR-21 mature microRNA (active forms) expression analysis was done by using real-time RT-PCR. U6 was used as internal control to compare expression levels of microRNAs. Its expression was varying across cancer samples and, therefore, was not used in normalization. Absolute quantification of hsa-miR-383 and hsa-miR-21 showed that hsa-miR-21 is highly expressed in MCF7, MDA-231 and MCF10 compared to U6. Hsa-miR-383 was observed to be expressed in low levels except MDA-MB-231 and rat brain tissue which was used as a control tissue.

Future work will include identification of target genes of these microRNAs by using expression reporter vector systems and other confirming methods. Potential targets of hsa-mir-21 predicted by miRNA target prediction programs include many tumor suppressor and oncogenes. Further analysis of these candidate genes targeted by microRNAs will reveal significant microRNAs that involve in tumorigenesis mechanism. Thus, analyzing microRNAs and their targets will contribute to understanding functions of microRNAs and their potential to be used as biomarkers in breast cancer.

REFERENCES

1. Calin, G.A., et al., *Human microRNA genes are frequently located at fragile sites and genomic regions involved in cancers.* Proc Natl Acad Sci U S A, 2004. **101**(9): p. 2999-3004.
2. . *The rising burden of cancer in the developing world.* Ann Oncol, 2006. **17 Suppl 8**: p. viii15-viii23.
3. *Bibliography. Current world literature. Breast cancer.* Curr Opin Obstet Gynecol, 2007. **19**(1): p. 93-102.
4. Kops, G.J., B.A. Weaver, and D.W. Cleveland, *On the road to cancer: aneuploidy and the mitotic checkpoint.* Nat Rev Cancer, 2005. **5**(10): p. 773-85.
5. Teng, D.H., et al., *Mutation analyses of 268 candidate genes in human tumor cell lines.* Genomics, 2001. **74**(3): p. 352-64.
6. Schafer, R., et al., *Functional transcriptomics: An experimental basis for understanding the systems biology for cancer cells.* Adv Enzyme Regul, 2007. **47**: p. 41-62.
7. Yoon, H., et al., *Gene expression profiling of isogenic cells with different TP53 gene dosage reveals numerous genes that are affected by TP53 dosage and identifies CSPG2 as a direct target of p53.* Proc Natl Acad Sci U S A, 2002. **99**(24): p. 15632-7.
8. Hanahan, D. and R.A. Weinberg, *The hallmarks of cancer.* Cell, 2000. **100**(1): p. 57-70.
9. Boehm, J.S. and W.C. Hahn, *Cancer genetics: Finding the right mix.* Eur J Hum Genet, 2005. **13**(10): p. 1099-100.
10. Kytola, S., et al., *Chromosomal alterations in 15 breast cancer cell lines by comparative genomic hybridization and spectral karyotyping.* Genes Chromosomes Cancer, 2000. **28**(3): p. 308-17.
11. Pellman, D., *Cell biology: aneuploidy and cancer.* Nature, 2007. **446**(7131): p. 38-9.
12. Fridlyand, J., et al., *Breast tumor copy number aberration phenotypes and genomic instability.* BMC Cancer, 2006. **6**: p. 96.
13. Kishimoto, M., et al., *Mutations and deletions of the CBP gene in human lung cancer.* Clin Cancer Res, 2005. **11**(2 Pt 1): p. 512-9.
14. Loo, L.W., et al., *Array comparative genomic hybridization analysis of genomic alterations in breast cancer subtypes.* Cancer Res, 2004. **64**(23): p. 8541-9.
15. Wang, Z.C., et al., *Loss of heterozygosity and its correlation with expression profiles in subclasses of invasive breast cancers.* Cancer Res, 2004. **64**(1): p. 64-71.

16. Cox, C., et al., *A survey of homozygous deletions in human cancer genomes.* Proc Natl Acad Sci U S A, 2005. **102**(12): p. 4542-7.
17. Parkin, D.M., et al., *Global cancer statistics, 2002.* CA Cancer J Clin, 2005. **55**(2): p. 74-108.
18. Senchenko, V.N., et al., *Discovery of frequent homozygous deletions in chromosome 3p21.3 LUCA and AP20 regions in renal, lung and breast carcinomas.* Oncogene, 2004. **23**(34): p. 5719-28.
19. Maser, R.S., et al., *Chromosomally unstable mouse tumours have genomic alterations similar to diverse human cancers.* Nature, 2007. **447**(7147): p. 966-71.
20. Li, J., et al., *Functional characterization of the candidate tumor suppressor gene NPRL2/G21 located in 3p21.3C.* Cancer Res, 2004. **64**(18): p. 6438-43.
21. Forozan, F., et al., *Comparative genomic hybridization analysis of 38 breast cancer cell lines: a basis for interpreting complementary DNA microarray data.* Cancer Res, 2000. **60**(16): p. 4519-25.
22. Levy, A., U.C. Dang, and R. Bookstein, *High-density screen of human tumor cell lines for homozygous deletions of loci on chromosome arm 8p.* Genes Chromosomes Cancer, 1999. **24**(1): p. 42-7.
23. Yin, X.L., J.C. Pang, and H.K. Ng, *Identification of a region of homozygous deletion on 8p22-23.1 in medulloblastoma.* Oncogene, 2002. **21**(9): p. 1461-8.
24. Ryu, B., et al., *Frequent germline deletion polymorphism of chromosomal region 8p12-p21 identified as a recurrent homozygous deletion in human tumors.* Genomics, 2001. **72**(1): p. 108-12.
25. Ray, M.E., et al., *Genomic and expression analysis of the 8p11-12 amplicon in human breast cancer cell lines.* Cancer Res, 2004. **64**(1): p. 40-7.
26. Aubele, M., et al., *Chromosomal imbalances are associated with metastasis-free survival in breast cancer patients.* Anal Cell Pathol, 2002. **24**(2-3): p. 77-87.
27. Davidson, J.M., et al., *Molecular cytogenetic analysis of breast cancer cell lines.* Br J Cancer, 2000. **83**(10): p. 1309-17.
28. Shadeo, A. and W.L. Lam, *Comprehensive copy number profiles of breast cancer cell model genomes.* Breast Cancer Res, 2006. **8**(1): p. R9.
29. Zhao, X., et al., *An integrated view of copy number and allelic alterations in the cancer genome using single nucleotide polymorphism arrays.* Cancer Res, 2004. **64**(9): p. 3060-71.
30. Lee, R.C., R.L. Feinbaum, and V. Ambros, *The C. elegans heterochronic gene lin-4 encodes small RNAs with antisense complementarity to lin-14.* Cell, 1993. **75**(5): p. 843-54.

31. Kusenda, B., et al., *MicroRNA biogenesis, functionality and cancer relevance.* Biomed Pap Med Fac Univ Palacky Olomouc Czech Repub, 2006. **150**(2): p. 205-15.
32. Pasquinelli, A.E., et al., *Conservation of the sequence and temporal expression of let-7 heterochronic regulatory RNA.* Nature, 2000. **408**(6808): p. 86-9.
33. Lagos-Quintana, M., et al., *Identification of novel genes coding for small expressed RNAs.* Science, 2001. **294**(5543): p. 853-8.
34. Jay, C., et al., *miRNA profiling for diagnosis and prognosis of human cancer.* DNA Cell Biol, 2007. **26**(5): p. 293-300.
35. Aravin, A. and T. Tuschl, *Identification and characterization of small RNAs involved in RNA silencing.* FEBS Lett, 2005. **579**(26): p. 5830-40.
36. Griffiths-Jones, S., et al., *miRBase: microRNA sequences, targets and gene nomenclature.* Nucleic Acids Res, 2006. **34**(Database issue): p. D140-4.
37. Cai, X., C.H. Hagedorn, and B.R. Cullen, *Human microRNAs are processed from capped, polyadenylated transcripts that can also function as mRNAs.* Rna, 2004. **10**(12): p. 1957-66.
38. Grey, F., et al., *Identification and characterization of human cytomegalovirus-encoded microRNAs.* J Virol, 2005. **79**(18): p. 12095-9.
39. Pfeffer, S., et al., *Identification of virus-encoded microRNAs.* Science, 2004. **304**(5671): p. 734-6.
40. Lee, Y., et al., *MicroRNA genes are transcribed by RNA polymerase II.* Embo J, 2004. **23**(20): p. 4051-60.
41. Bartel, D.P., *MicroRNAs: genomics, biogenesis, mechanism, and function.* Cell, 2004. **116**(2): p. 281-97.
42. Murchison, E.P. and G.J. Hannon, *miRNAs on the move: miRNA biogenesis and the RNAi machinery.* Curr Opin Cell Biol, 2004. **16**(3): p. 223-9.
43. Lee, Y., et al., *MicroRNA maturation: stepwise processing and subcellular localization.* Embo J, 2002. **21**(17): p. 4663-70.
44. Hammond, S.M., et al., *Argonaute2, a link between genetic and biochemical analyses of RNAi.* Science, 2001. **293**(5532): p. 1146-50.
45. Sempere, L.F., et al., *Expression profiling of mammalian microRNAs uncovers a subset of brain-expressed microRNAs with possible roles in murine and human neuronal differentiation.* Genome Biol, 2004. **5**(3): p. R13.
46. Ambros, V., *microRNAs: tiny regulators with great potential.* Cell, 2001. **107**(7): p. 823-6.
47. Ambros, V., *MicroRNA pathways in flies and worms: growth, death, fat, stress, and timing.* Cell, 2003. **113**(6): p. 673-6.

48. Chen, C.Z. and H.F. Lodish, *MicroRNAs as regulators of mammalian hematopoiesis.* Semin Immunol, 2005. **17**(2): p. 155-65.
49. Enright, A.J., et al., *MicroRNA targets in Drosophila.* Genome Biol, 2003. **5**(1): p. R1.
50. Lewis, B.P., C.B. Burge, and D.P. Bartel, *Conserved seed pairing, often flanked by adenosines, indicates that thousands of human genes are microRNA targets.* Cell, 2005. **120**(1): p. 15-20.
51. Harfe, B.D., *MicroRNAs in vertebrate development.* Curr Opin Genet Dev, 2005. **15**(4): p. 410-5.
52. Doench, J.G. and P.A. Sharp, *Specificity of microRNA target selection in translational repression.* Genes Dev, 2004. **18**(5): p. 504-11.
53. He, L. and G.J. Hannon, *MicroRNAs: small RNAs with a big role in gene regulation.* Nat Rev Genet, 2004. **5**(7): p. 522-31.
54. Lytle, J.R., T.A. Yario, and J.A. Steitz, *Target mRNAs are repressed as efficiently by microRNA-binding sites in the 5′ UTR as in the 3′ UTR.* Proc Natl Acad Sci U S A, 2007. **104**(23): p. 9667-72.
55. Millar, A.A. and P.M. Waterhouse, *Plant and animal microRNAs: similarities and differences.* Funct Integr Genomics, 2005. **5**(3): p. 129-35.
56. Mallory, A.C. and H. Vaucheret, *Functions of microRNAs and related small RNAs in plants.* Nat Genet, 2006. **38 Suppl**: p. S31-6.
57. Yu, Z., T. Raabe, and N.B. Hecht, *MicroRNA Mirn122a reduces expression of the posttranscriptionally regulated germ cell transition protein 2 (Tnp2) messenger RNA (mRNA) by mRNA cleavage.* Biol Reprod, 2005. **73**(3): p. 427-33.
58. Moss, E.G., R.C. Lee, and V. Ambros, *The cold shock domain protein LIN-28 controls developmental timing in C. elegans and is regulated by the lin-4 RNA.* Cell, 1997. **88**(5): p. 637-46.
59. Wu, L. and J.G. Belasco, *Micro-RNA regulation of the mammalian lin-28 gene during neuronal differentiation of embryonal carcinoma cells.* Mol Cell Biol, 2005. **25**(21): p. 9198-208.
60. Wu, L., J. Fan, and J.G. Belasco, *MicroRNAs direct rapid deadenylation of mRNA.* Proc Natl Acad Sci U S A, 2006. **103**(11): p. 4034-9.
61. Lim, L.P., et al., *Microarray analysis shows that some microRNAs downregulate large numbers of target mRNAs.* Nature, 2005. **433**(7027): p. 769-73.
62. Wakiyama, M., et al., *Let-7 microRNA-mediated mRNA deadenylation and translational repression in a mammalian cell-free system.* Genes Dev, 2007. **21**(15): p. 1857-62.
63. Dalmay, T. and D.R. Edwards, *MicroRNAs and the hallmarks of cancer.* Oncogene, 2006. **25**(46): p. 6170-5.

64. Lamy, P., et al., *Are microRNAs located in genomic regions associated with cancer?* Br J Cancer, 2006. **95**(10): p. 1415-8.
65. Chen, C.Z., et al., *MicroRNAs modulate hematopoietic lineage differentiation.* Science, 2004. **303**(5654): p. 83-6.
66. He, L., et al., *A microRNA polycistron as a potential human oncogene.* Nature, 2005. **435**(7043): p. 828-33.
67. Lu, J., et al., *MicroRNA expression profiles classify human cancers.* Nature, 2005. **435**(7043): p. 834-8.
68. Chan, J.A., A.M. Krichevsky, and K.S. Kosik, *MicroRNA-21 is an antiapoptotic factor in human glioblastoma cells.* Cancer Res, 2005. **65**(14): p. 6029-33.
69. Si, M.L., et al., *miR-21-mediated tumor growth.* Oncogene, 2007. **26**(19): p. 2799-803.
70. Zhu, S., et al., *MicroRNA-21 targets the tumor suppressor gene tropomyosin 1 (TPM1).* J Biol Chem, 2007. **282**(19): p. 14328-36.
71. Asangani, I.A., et al., *MicroRNA-21 (miR-21) post-transcriptionally downregulates tumor suppressor Pdcd4 and stimulates invasion, intravasation and metastasis in colorectal cancer.* Oncogene, 2007.
72. Cimmino, A., et al., *miR-15 and miR-16 induce apoptosis by targeting BCL2.* Proc Natl Acad Sci U S A, 2005. **102**(39): p. 13944-9.
73. Johnson, S.M., et al., *RAS is regulated by the let-7 microRNA family.* Cell, 2005. **120**(5): p. 635-47.
74. O'Donnell, K.A., et al., *c-Myc-regulated microRNAs modulate E2F1 expression.* Nature, 2005. **435**(7043): p. 839-43.
75. Esquela-Kerscher, A. and F.J. Slack, *Oncomirs - microRNAs with a role in cancer.* Nat Rev Cancer, 2006. **6**(4): p. 259-69.
76. Lewis, B.P., et al., *Prediction of mammalian microRNA targets.* Cell, 2003. **115**(7): p. 787-98.
77. Bommer, G.T., et al., *p53-mediated activation of miRNA34 candidate tumor-suppressor genes.* Curr Biol, 2007. **17**(15): p. 1298-307.
78. Zhang, L., et al., *microRNAs exhibit high frequency genomic alterations in human cancer.* Proc Natl Acad Sci U S A, 2006. **103**(24): p. 9136-41.
79. Iorio, M.V., et al., *MicroRNA gene expression deregulation in human breast cancer.* Cancer Res, 2005. **65**(16): p. 7065-70.
80. Krek, A., et al., *Combinatorial microRNA target predictions.* Nat Genet, 2005. **37**(5): p. 495-500.
81. Maitra, A., et al., *Molecular abnormalities associated with secretory carcinomas of the breast.* Hum Pathol, 1999. **30**(12): p. 1435-40.

82. Lerebours, F., et al., *Evidence of chromosome regions and gene involvement in inflammatory breast cancer.* Int J Cancer, 2002. **102**(6): p. 618-22.
83. Buchhagen, D.L., L. Qiu, and P. Etkind, *Homozygous deletion, rearrangement and hypermethylation implicate chromosome region 3p14.3-3p21.3 in sporadic breast-cancer development.* Int J Cancer, 1994. **57**(4): p. 473-9.
84. Pierga, J.Y., et al., *Microarray-based comparative genomic hybridisation of breast cancer patients receiving neoadjuvant chemotherapy.* Br J Cancer, 2007. **96**(2): p. 341-51.
85. Johannsdottir, H.K., et al., *Chromosome 5 imbalance mapping in breast tumors from BRCA1 and BRCA2 mutation carriers and sporadic breast tumors.* Int J Cancer, 2006. **119**(5): p. 1052-60.
86. Charafe-Jauffret, E., et al., *Loss of heterozygosity at microsatellite markers from region p11-21 of chromosome 8 in microdissected breast tumor but not in peritumoral cells.* Int J Oncol, 2002. **21**(5): p. 989-96.
87. Rummukainen, J., et al., *Aberrations of chromosome 8 in 16 breast cancer cell lines by comparative genomic hybridization, fluorescence in situ hybridization, and spectral karyotyping.* Cancer Genet Cytogenet, 2001. **126**(1): p. 1-7.
88. Bhattacharya, N., et al., *Three discrete areas within the chromosomal 8p21.3-23 region are associated with the development of breast carcinoma of Indian patients.* Exp Mol Pathol, 2004. **76**(3): p. 264-71.
89. Shen, K.L., et al., *Microsatellite alterations on human chromosome 11 in in situ and invasive breast cancer: a microdissection microsatellite analysis and correlation with p53, ER (estrogen receptor), and PR (progesterone receptor) protein immunoreactivity.* J Surg Oncol, 2000. **74**(2): p. 100-7.
90. Nagahata, T., et al., *Correlation of allelic losses and clinicopathological factors in 504 primary breast cancers.* Breast Cancer, 2002. **9**(3): p. 208-15.
91. Ferti-Passantonopoulou, A., A.D. Panani, and S. Raptis, *Preferential involvement of 11q23-24 and 11p15 in breast cancer.* Cancer Genet Cytogenet, 1991. **51**(2): p. 183-8.
92. Chen, C., et al., *An 800-kb region of deletion at 13q14 in human prostate and other carcinomas.* Genomics, 2001. **77**(3): p. 135-44.
93. Dahlen, A., et al., *Clustering of deletions on chromosome 13 in benign and low-malignant lipomatous tumors.* Int J Cancer, 2003. **103**(5): p. 616-23.
94. De Marchis, L., et al., *Candidate target genes for loss of heterozygosity on human chromosome 17q21.* Br J Cancer, 2004. **90**(12): p. 2384-9.

95. Orsetti, B., et al., *17q21-q25 aberrations in breast cancer: combined allelotyping and CGH analysis reveals 5 regions of allelic imbalance among which two correspond to DNA amplification.* Oncogene, 1999. **18**(46): p. 6262-70.

96. Saito, H., et al., *Detailed deletion mapping of chromosome 17q in ovarian and breast cancers: 2-cM region on 17q21.3 often and commonly deleted in tumors.* Cancer Res, 1993. **53**(14): p. 3382-5.

97. Silva, J.M., et al., *Abnormal frequencies of alleles in polymorphic markers of the 17q21 region is associated with breast cancer.* Cancer Lett, 1999. **138**(1-2): p. 209-15.

98. Yang, T.L., et al., *High-resolution 19p13.2-13.3 allelotyping of breast carcinomas demonstrates frequent loss of heterozygosity.* Genes Chromosomes Cancer, 2004. **41**(3): p. 250-6.

99. Oesterreich, S., et al., *High rates of loss of heterozygosity on chromosome 19p13 in human breast cancer.* Br J Cancer, 2001. **84**(4): p. 493-8.

100. Ohgaki, K., et al., *Mapping of a new target region of allelic loss to a 6-cM interval at 21q21 in primary breast cancers.* Genes Chromosomes Cancer, 1998. **23**(3): p. 244-7.

101. Xie, D., et al., *Discovery of over-expressed genes and genetic alterations in breast cancer cells using a combination of suppression subtractive hybridization, multiplex FISH and comparative genomic hybridization.* Int J Oncol, 2002. **21**(3): p. 499-507.

102. Weber-Mangal, S., et al., *Breast cancer in young women (< or = 35 years): Genomic aberrations detected by comparative genomic hybridization.* Int J Cancer, 2003. **107**(4): p. 583-92.

103. Blegen, H., et al., *DNA amplifications and aneuploidy, high proliferative activity and impaired cell cycle control characterize breast carcinomas with poor prognosis.* Anal Cell Pathol, 2003. **25**(3): p. 103-14.

104. Cingoz, S., et al., *DNA copy number changes detected by comparative genomic hybridization and their association with clinicopathologic parameters in breast tumors.* Cancer Genet Cytogenet, 2003. **145**(2): p. 108-14.

105. Gelsi-Boyer, V., et al., *Comprehensive profiling of 8p11-12 amplification in breast cancer.* Mol Cancer Res, 2005. **3**(12): p. 655-67.

106. Hwang, E.S., et al., *Patterns of chromosomal alterations in breast ductal carcinoma in situ.* Clin Cancer Res, 2004. **10**(15): p. 5160-7.

107. Guan, X.Y., et al., *Identification of cryptic sites of DNA sequence amplification in human breast cancer by chromosome microdissection.* Nat Genet, 1994. **8**(2): p. 155-61.

108. Andersen, C.L., et al., *High-throughput copy number analysis of 17q23 in 3520 tissue specimens by fluorescence in situ hybridization to tissue microarrays.* Am J Pathol, 2002. **161**(1): p. 73-9.

109. Barlund, M., et al., *Increased copy number at 17q22-q24 by CGH in breast cancer is due to high-level amplification of two separate regions.* Genes Chromosomes Cancer, 1997. **20**(4): p. 372-6.
110. Wu, G., et al., *Structural analysis of the 17q22-23 amplicon identifies several independent targets of amplification in breast cancer cell lines and tumors.* Cancer Res, 2001. **61**(13): p. 4951-5.
111. Parssinen, J., et al., *High-level amplification at 17q23 leads to coordinated overexpression of multiple adjacent genes in breast cancer.* Br J Cancer, 2007. **96**(8): p. 1258-64.
112. Gunther, K., et al., *Differences in genetic alterations between primary lobular and ductal breast cancers detected by comparative genomic hybridization.* J Pathol, 2001. **193**(1): p. 40-7.
113. James, L.A., et al., *Comparative genomic hybridisation of ductal carcinoma in situ of the breast: identification of regions of DNA amplification and deletion in common with invasive breast carcinoma.* Oncogene, 1997. **14**(9): p. 1059-65.
114. Barlund, M., et al., *Multiple genes at 17q23 undergo amplification and overexpression in breast cancer.* Cancer Res, 2000. **60**(19): p. 5340-4.
115. Lim, L.P., et al., *The microRNAs of Caenorhabditis elegans.* Genes Dev, 2003. **17**(8): p. 991-1008.
116. Bandres, E., et al., *Identification by Real-time PCR of 13 mature microRNAs differentially expressed in colorectal cancer and non-tumoral tissues.* Mol Cancer, 2006. **5**: p. 29.
117. Soule, H.D., et al., *Isolation and characterization of a spontaneously immortalized human breast epithelial cell line, MCF-10.* Cancer Res, 1990. **50**(18): p. 6075-86.

APPENDIX A

MAMMALIAN CELL CULTURE MEDIUM

Table A-1. Composition of Cell Culture Medium

Component	End conc.	MCF7	HS578T	MDA-MB-231	SUM159	MCF10	HeLa	SHSY-5Y
DMEM	-	+	+	+	-	-	+	+
Ham's F12 Nutrient mix	-	-	-	-	+	-	-	-
Leibovitz's media	-	-	-	+	-	-	-	-
Horse Serum	5%	-	-	-	-	+	-	-
Insulin (5 mg/ml)	10 μg/ml	-	-	-	-	+	-	-
EGF (100 ug/ml in DMEM)	20 ng/ml	-	-	-	-	+	-	-
Cholera Toxin (1 mg/ml in dH_2O)	100 ng/ml	-	-	-	-	+	-	-
Hydrocortisone (50 ug/ml)	0.5 μg/ml	-	-	-	-	+	-	-
L-Glu (200 mM)	1%	+	+	+	+	+	+	+
Penicillin / Streptomycin (10 mg/ml)	1%	+	+	+	+	-	+	+

APPENDIX B

PRIMERS AND PCR OPTIMIZATION CONDITIONS

Table B-1. Pre-miRNA microRNA DNA Specific Primers and Product Sizes

microRNAs	**primer sequences (5' → 3')**	**product sizes**
mir-let7a2-F	ATAGGGAGAAAAGGCCTGGA	238 bp
mir-let7a2-R	ATGGCCCAAATAGGTGACAG	
mir-135a1-R	GAAGAAGTGCCTGCAAGAGC	169 bp
mir-135a1-F	CTGTCCTGCCTCCTTTTGAG	
mir-15a-R	ATTCTTTAGGCGCGAATGTG	203 bp
mir-15a-F	TACGTGCTGCTAAGGCACTG	
mir-34b-R	CAGGCATCTTCTCTCGAAGG	335 bp
mir-34b-F	CAGCTACGCGTGTTGTGC	
mir-let7g-R	AGCCTCTGCTGTGAGGATGT	238 bp
mir-let7g-F	GGTTTCCCAGAGATGAGCAG	
mir-138-1-F	AGCAGCACAAAGGCATCTCT	210 bp
mir-138-1-R	CTCTGTGACGGGTGTAGCTG	
mir-100-R	GTCACAGCCCCAAAAGAGAG	231 bp
mir-100-F	AGGTCTCCTTCCTCCACCTC	
mir-320-R	GGGACTGGGCCACAGTATTT	238 bp
mir-320-F	GAGGCGAATCCTCACATTG	
mir-425-F	CCACCCCCATTCCTTTTAAT	247 bp
mir-425-R	CAGGTCATGCACCTTCAGAAT	
mir124a-1 F	TTGCATCTCTAAGCCCCTGT	201 bp

mir-124a1-R	TCTACCCACCCCTCTTCCTT	
mir-7-3-R	CCGAGTGGAAGCGATTCTT	236 bp
mir-7-3-F	CAGGTGAGAAGGAGGAGCTG	
mir-16-1-R	CCATATTGTGCTGCCTCAAA	248 bp
mir-16-1-F	TGAAAAAGACTATCAATAAAACTGAAAA	
mir-34c-F	TTGAGCTCCAACTCAACCAA	191 bp
mir-34c-R	GATGCACAGGCAGCTCATT	
mir-125b-1-F	ACCAAATTTCCAGGATGCAA	171 bp
mir-125b-1-R	CGAACAGAAATTGCCTGTCA	
mir-191-F	AAGTATGTCTGGGGGTCAGG	245 bp
mir-191-R	ACAACCTACTCCCGGGTCTT	
mir-383-F	AGTCCACCAAATGCAGTTCC	176 bp
mir-383-R	ACTTCAGAATCTCCCCGTCA	
mir-486-F	CCTGGGGTGTGAATGGTAAC	217 bp
mir-486-R	ATCTCCAGCAGGTGTGTGTG	
mir198F	GCCGGAGGTTAAACATGAAA	391 bp
mir198R	CCCAGCCTACCAATATGCTC	
mir384F	TGGCCAGTTAGCATCTTGAA	238 bp
mir384R	TCAGGCCTGCAGAAATAGTG	
mir325F	TCCTTTTCACCCCTCAACAC	280 bp
mir325R	GGATTCAAGTCCACAGAACCA	
mir145F	GGCTGGATGCAGAAGAGAAC	258 bp
mir145R	CAGGGACAGCCTTCTTCTTG	
mir143F	CCCTCTAACACCCCTTCTCC	276 bp
mir143R	AACTTCCCCAGCATCACAAG	
mir125b2F	TCGTCGTGATTACTCAGCTCAT	262 bp
mir125b2R	CAGGGATCAGCTGGAAGAAG	
mir10bF	TAATAAAGCCGCCATCCTTG	395 bp
mir10bR	CTGGCTATTCCGAAGAAACG	

mir361F	GGAGCTCAACCATACCAGGA	317 bp
mir361R	TTGGGCATATGTGACCATCA	
mir15bF	AGAACGGCCTGCAGAGATAA	388 bp
mir15bR	CGTGCTGCTAGAGTGGAACA	
mir16-2F	TGTTCGTTTTATGTTTGGATGA	391 bp
mir16-2R	AGTGGTTCCACCAAGTAAGTCA	
mir103-2F	CCCTAGGGAGGAATCCAGAG	236 bp
mir103-2R	AGCCATAAGCTGCACCAACT	
mir152 F	AAGGTCCACAGCTGGTTCTG	243 bp
mir152 R	CAGGGATCAGCTGGAAGAAG	
mir92-1F	CCATGCAAAACTGACTGTGG	199 bp
mir92-1R	CAGTGGAAGTCGAAATCTTCAG	
mir20aF	CGATGTAGAATCTGCCTGGTC	203 bp
mir20aR	GGATGCAAACCTGCAAAACT	
mir17 F	CCCCATTAGGGATTATGCTG	254 bp
mir17 R	CCTGCACTTTAAAGCCCAACT	
mir 18a F	GGCACTTGTAGCATTATGGTGA	247 bp
mir 18a R	TGCAAAACTAACAGAGGACTGC	
mir 19a F	TGCCCTAAGTGCTCCTTCTG	244 bp
mir 19a R	CCAGGCAGATTCTACATCGAC	
mir 19b-1F	GCCCAATCAAACTGTCCTGT	173 bp
mir 19b-1R	ACCGATCCCAACCTGTGTAG	
mir 21 F	CCATTGGGATGTTTTTGATTG	478 bp
Mir 21 R	TCCATAAAATCCTCCCTCCA	
mir142 F	CAGGGTTCCACATGTCCAG	479 bp
mir 142 R	CTGAGTCACCGCCCACAAG	
mir301F	CTCATTTAGACAAACCATAACAACTT	499 bp
mir 301R	CATCAATAAGCAACATCACTTTGA	
mir 633 F	AGGACTGGGTTTGAGTCCTG	284 bp

mir 633 R	TTAGACATTCCTCCTGGTGAA	
GAPDH (644) F	TGCCTTCTTGCCTCTTGTCT	644 bp
GAPDH (644) R	CTGCAAATGAGCCTACAGCA	
*GAPDH*_F(472bp)	TGCCTTCTTGCCTCTTGTCT	472 bp
*GAPDH*_R(472 bp)	TTGATTTTGGAGGGATCTCG	

Table B-2. Semi-quantitative Duplex PCR Optimization Conditions

microRNAs	***GAPDH*:miR primer amounts**	***GAPDH* conc.**	**miR conc.**	**Tm**	**Cycle #**
hsa-mir-10b	3µl/3µl	100%	100%	59°C	28
hsa-mir-138-1	3µl/3µl	100%	100%	59°C	28
hsa-mir-425	3µl/3µl	100%	100%	58°C	28
hsa-mir-191	3µl/3µl	100%	100%	63°C	28
hsa-let7g	3µl/2µl	100%	100%	58°C	28
hsa-mir-135a1	3µl/3µl	100%	100%	58°C	28
hsa-mir-198	3µl/3µl	100%	100%	58°C	28
hsa-mir-15b	3µl/3µl	100%	100%	58°C	28
hsa-mir-16-2	3µl/3µl	100%	100%	58°C	28
hsa-mir-143	3µl/3µl	100%	100%	58°C	28
hsa-mir-145	3µl/3µl	100%	100%	58°C	28
hsa-mir-383	3µl/3µl	100%	100%	58°C	28
hsa-mir-320	3µl/3µl	100%	100%	58-60°C	29
hsa-mir-486	3µl/2µl	100%	100%	63°C	28
hsa-mir-34c	3µl/3µl	100%	100%	58°C	28
hsa-mir-125b1	3µl/2µl	100%	100%	58°C	28
hsa-let7a-2	3µl/3µl	100%	100%	60°C	28
hsa-mir-100	3µl/3µl	100%	50%	56°C	28
hsa-mir-16-1	3µl/3µl	100%	100%	59°C	29
hsa-mir-15a	3µl/2.5µl	200%	100%	58°C	30
hsa-mir-17	2µl/3µl	50%	100%	58°C	28
hsa-mir-18a	3µl/3µl	150%	100%	56°C	28
hsa-mir-19a	3µl/3µl	100%	100%	59°C	28
hsa-mir-20a	2µl/3µl	100%	50%	58°C	28
hsa-mir-19b-1	3µl/3µl	100%	100%	59°C	28
hsa-mir-92-1	3µl/3µl	50%	100%	56°C	28
hsa-mir-152	3µl/3µl	50%	100%	58°C	28
hsa-mir-142	3µl/3µl	100%	100%	59°C	28

hsa-mir-301	3µl/3µl	100%	100%	58°C	28
hsa-mir-21	3µl/3µl	100%	100%	59°C	27
hsa-mir-633	3µl/3µl	100%	100%	59°C	27
hsa-mir-7-3	3µl/1,5µl	100%	100%	63°C	28
hsa-mir-103-2	3µl/3µl	100%	100%	59°C	27
hsa-mir-125b-2	3µl/3µl	100%	100%	59°C	28
hsa-mir-384	3µl/3µl	100%	100%	59°C	28
hsa-mir-325	3µl/3µl	100%	100%	59°C	27
hsa-mir-361	3µl/3µl	100%	100%	58°C	28

Table B-3. pre-microRNA cDNA Specific Primers

Primers	**Sequences 5'→3'**
*GAPDH (*115bp)_F	TATGACAACGAATTTGGCTAC
*GAPDH (*115bp)_R	TCTCTCTTCCTCTTGTGCTCT
hsa-mir-633cDNA_F	CTCTGTTTCTTTATTGCGGTAG
hsa-mir-633cDNA_R	CCTCACAACAATTTTATTGTGG
hsa-mir-145cDNA_F	CACCTTGTCCTCACGGT
hsa-mir-145cDNA_R	AGAACAGTATTTCCAGGAATCC
hsa-mir-383cDNA_F	CTCCTCAGATCAGAAGGTGAT
hsa-mir-383cDNA_R	CTCTTTCTGACCAGGCAGT
hsa-mir-361cDNA_F	GGTGCTTATCAGAATCTCCAG
hsa-mir-361cDNA_R	GCAAATCAGAATCACACCTG
hsa-mir-21cDNA_F	TGTCGGGTAGCTTATCAGACT
hsa-mir-21cDNA_R	TCAGACAGCCCATCGAC
hsa-mir-486cDNA_F	GTATCCTGTACTGAGCTGCC
hsa-mir-486cDNA_R	CATCCTGTACTGAGCTGCC

APPENDIX C

BUFERS AND SOLUTIONS

10X TBE (Tris Borate) Buffer -1L

Tris-base	108 g
Boric acid	55 g
0.5M EDTA (pH: 8.0)	40 ml

The volume was completed to 1 L with dH_2O.

1X TE (Tris-EDTA) Buffer -1 L

Tris.HCl 10 mM

EDTA 1 mM

The volume was completed to 1 L with dH_2O.

DNA Loading Dye (6X)

Xylene Cyanol	0.025 g
Bromophenol Blue	0.010 g
Glycerol (60%)	5 ml
dH_2O	5 ml